



Swansea University
Prifysgol Abertawe



Swansea University E-Theses

The tensile properties of polymeric liquids.

Brad, Rhodri

How to cite:

Brad, Rhodri (2008) *The tensile properties of polymeric liquids..* thesis, Swansea University.
<http://cronfa.swan.ac.uk/Record/cronfa42332>

Use policy:

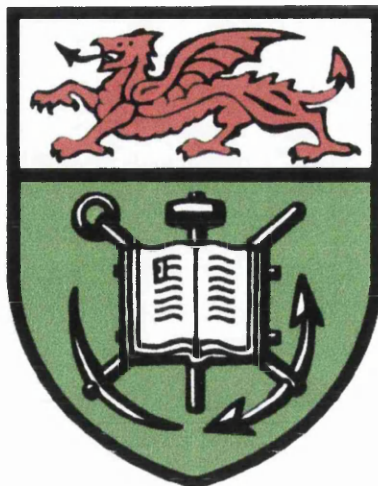
This item is brought to you by Swansea University. Any person downloading material is agreeing to abide by the terms of the repository licence: copies of full text items may be used or reproduced in any format or medium, without prior permission for personal research or study, educational or non-commercial purposes only. The copyright for any work remains with the original author unless otherwise specified. The full-text must not be sold in any format or medium without the formal permission of the copyright holder. Permission for multiple reproductions should be obtained from the original author.

Authors are personally responsible for adhering to copyright and publisher restrictions when uploading content to the repository.

Please link to the metadata record in the Swansea University repository, Cronfa (link given in the citation reference above.)

<http://www.swansea.ac.uk/library/researchsupport/ris-support/>

**The Tensile Properties
of
Polymeric Liquids**



BY

Rhodri Brad

MSc (U.W. Aberystwyth)

Thesis submitted to the University of Wales
in partial fulfillment of the requirements for the
Degree of Philosophiae Doctor

Department of Chemical Engineering,

University of Wales, Swansea

July 2008

ProQuest Number: 10798040

All rights reserved

INFORMATION TO ALL USERS

The quality of this reproduction is dependent upon the quality of the copy submitted.

In the unlikely event that the author did not send a complete manuscript and there are missing pages, these will be noted. Also, if material had to be removed, a note will indicate the deletion.



ProQuest 10798040

Published by ProQuest LLC (2018). Copyright of the Dissertation is held by the Author.

All rights reserved.

This work is protected against unauthorized copying under Title 17, United States Code
Microform Edition © ProQuest LLC.

ProQuest LLC.
789 East Eisenhower Parkway
P.O. Box 1346
Ann Arbor, MI 48106 – 1346

CERTIFICATE OF ORIGINALITY

This thesis is submitted to the University of Wales, Swansea, under the supervision of Professor P.R. Williams in the Department of Chemical Engineering, University of Wales, Swansea, in candidature for the degree of Doctor of Philosophy. The material in this thesis is the original work of the author except where acknowledgement to other authors is expressly made.

Signed,

.....

Rhodri Brad

(Candidate)

Signed,

.....

Professor P.R. Williams

(Supervisor)

Date: 24/07/08.....

*To my family
especially my wife Jean*

ACKNOWLEDGEMENTS

I would like to thank my academic supervisor Professor P. R. Williams for his ideas, help and support throughout this project.

I am indebted to all the academic and technical staff within the department of Chemical Engineering for their assistance and advice. Special thanks go to Dr. Matthew Barrow, Dr. Dale Rogers, Dr. Al-Hussany and Dr. Alex Lubansky for whose friendship, help and encouragement have made this PhD both enjoyable and rewarding.

I would also like to thank E.P.S.R.C and AVECIA, for their financial support during this research programme.

Finally, thanks go to my wife who has endured with me whilst writing my thesis.

SUMMARY

The work reported in this Thesis reports on studies of the tensile strength of polymeric liquids by two experimental techniques, namely the Bullet-Piston (B-P) technique and a Capillary Break-up Extensional Rheometer (CaBER). The motivation for this work lies in the fact that although many associations exist between the cavitation properties of fluids and their extensional flow properties, these associations have never been systematically investigated due to a lack of an appropriate cavitation technique. The work presented in this thesis addresses this, using two custom-built instruments (a filament stretching device and a dynamic stressing technique for cavitation studies). Together, these were used to investigate the appropriate rheological and cavitation characteristics of a range of fluids including model polymer solutions. In experiments in which samples of degassed, deionised water are subjected to dynamic stressing by pulses of tension, the pulse reflection technique allows the rate of development of tension in the liquid, $\dot{\Omega}_r$, to be varied in a systematic manner, in order to investigate its influence on the resulting measurement of the liquid's 'effective' tensile strength, F_c . Results are reported for a range of stressing rates, $\dot{\Omega}_r, \approx 0.19\text{bar}/\mu\text{s} \leq \dot{\Omega}_r \leq 0.77\text{bar}/\mu\text{s}$. These experiments, which are the first of their kind to be reported on water, show an approximately four-fold increase of F_c at the highest stressing rate, this value being 224bar (for $\dot{\Omega}_r = 0.77\text{bar}/\mu\text{s}$) compared to 59bar (for $\dot{\Omega}_r = 0.187\text{bar}/\mu\text{s}$). The present work has resolved a longstanding anomaly concerning the role of polymeric additives in determining the cavitation thresholds of dilute aqueous polymer solutions. For the first time it is shown that with increasing molecular weight there is an increased effective tensile strength of the solution. However, the results reveal that increasing polymer concentration results in a stress saturation level in terms of effective tensile strength. This work is also the first to relate cavitation failure of a fluid and its extensional properties in terms of two appropriately chosen stress parameters; and to report the relationship between these stress parameters on the basis of an experimental study involving two different techniques over a range of stress rates and a wide range of polymer concentration and molecular weight. Despite differences in the magnitudes of the tensile stress parameters, both techniques show that the relevant parameter increases with polymer concentration and molecular weight, but that such stress levels become effectively saturated at essentially the same levels of concentration and molecular weight. This information has never previously been available. As a result of the work reported in this thesis it may now be possible to conduct fluid breakup measurements in extensional flow experiments in order to ascertain the likely levels of cavitation threshold stress for dilute aqueous polymer solutions.

CONTENTS

DECLARATION	
STATEMENT	
CERTIFICATE OF ORIGINALITY	
ACKOWLEDEMENTS	
SUMMARY	
CONTENTS	
NOMENCLATURE	

CHAPTER 1 – Introduction and Literature Review

1.1	Introduction	2
1.2	Experimental techniques for the measurement of liquid tensile strength	6
1.3	Rheological properties of polymeric liquids	10
1.4	Cavitation and filamentation	12
	1.4.1 Nucleation theory	15
	1.4.2 Cavitation in flowing liquids	19
	1.4.3 Cavitation in confined spaces	22
	1.4.4 Some processes involving cavitation	22
1.5	Extensional flows	27
	1.5.1 Filament stretching rheometry	29

CHAPTER 2 - Materials and Bullet-Piston Technique

2.1	Introduction	36
2.2	Materials	36
2.3	Bullet-piston apparatus	37
	2.3.1 Operation	43
	2.3.2 Typical results	43

2.4	Bubble dynamics	45
2.4.1	Nonlinear oscillations	48
2.4.2	Mass-diffusion effects	49
2.4.3	Cavitation and vapour bubbles	50
2.4.4	Spherical bubbles in non-Newtonian fluids	56

CHAPTER 3 – Tensile Properties of Water

3.1	Introduction	61
3.2	Dynamic testing of purified water	63
3.2.1	The effect of stressing rate on the tensile strength measurements of deionised water	67
3.3	Discussion	74
3.4	Conclusions	76

CHAPTER 4 – Tensile Properties of Polymeric Liquids

4.1	Introduction	80
4.2	Polyethylene glycol solutions	83
4.2.1	Tensile strength results	84
4.3	Effect of stressing rate on polymer solutions	98
4.4	PAA results	100
4.5	Results and discussion	102

CHAPTER 5 – Extension Rheology

5.1	Introduction	105
5.2	Capillary Break-up Extensional Rheometer	106
5.3	Operation	108

5.4	Results	114
5.5	Summary	124
 <i>CHAPTER 6 – CONCLUSIONS AND RECOMMENDATIONS FOR FUTURE WORK</i>		 128
 REFERENCES		 133
 APPENDIX A – Additional Pressure-tension cycles		 153
 APPENDIX B – Additional filament breakup images		 167

NOMENCLATURE

$\dot{\Omega}_f$	Stressing Rate
F_c	Effective Tensile Strength
τ_E	Extensional Stress
ρ	Fluid density
σ	Surface Tension
η_0	Zero-shear viscosity
μ	Shear viscosity
ε	Strain
g	Gravitational constant
R	Bubble Radius
T	Temperature
T_R	Trouton ratio
t	Time
p_v	Liquids vapour pressure
D_{mid}	Mid filament diameter

CHAPTER 1

Introduction and Literature Review

Chapter 1

Introduction and Literature Review

1.1 Introduction

Mesoscale-thickness liquid films experience rapid deformation between separating surfaces in many industrial processes such as lubrication, coating and peeling. In the case of fluid mechanical machinery these separating surfaces are usually solid, whereas in biomechanics they may be flexible surfaces, such as biological membranes. In printing processes involving ink films (McPhee (1997)) or coating flows involving films of liquid adhesives (Gent et al. (1985)), rapidly-stretching liquid filaments may form - possibly as a consequence of cavitation film-splitting. Such filaments are responsible for 'linting' and 'picking' problems in printing, while their break-up leads to unwanted droplet deposition. The 'tack' of such a film is the maximum tensile stress (or 'negative pressure') which it can withstand before splitting (Zang et al. (1991)).

Attempts to quantify tack usually rely upon direct measurements involving pressure transducers, but there is no satisfactory method of calibrating such transducers in terms of the often significant levels of dynamic negative pressure which arise. Such measurements may be further compromised by an elastic de-cohesion of the fluid from the transducer's surface. Moreover, the concept of 'negative pressure' is not particularly useful in this context as it is more pertinent to consider the state of stress experienced by the fluid; to understand this it is necessary to know the flow field (Brennen (1995)). The latter requirement imposes stringent experimental demands,

chief among which is the necessity of imaging and recording meso-scale events with sub-millisecond resolution in the case of filament stretching; and sub-microsecond resolution in the case of cavitation phenomena. Cavitation of a fluid film may occur under the high tensile stresses developed in the rapid separation of surfaces and can result in loss of machine performance, or have damaging consequences (Trevena (1987)). Surface damage in high speed microelectromechanical systems devices has been attributed to the cavitation of perfluoropolyether (PFPE) lubricant films (Spikes, 2000).

Due to the high deformation rates and short timescales which typify meso-scale film-splitting phenomena, significant viscoelastic effects may be anticipated. One of the few studies in this area suggests that an observed delay in the cavitation of viscoelastic fluids may be due to the development of normal stresses while other claimed viscoelastic effects include a significant displacement of the point of cavitation from the centre of contact (where film thickness is a minimum) and enhanced film thicknesses (Coyle (1984)). Despite the potential scientific and technological significance of these findings, the effect of viscoelasticity has not been widely studied in micron-scale film-splitting phenomena and very little is known about its influence in sub-micron situations. A crucial factor is the initial film thickness (which in many processes may be sub-micron). Even ostensibly low rates of surface separation may provoke the high rates of fluid deformation needed to induce the mechanical breakdown of a fluid film if its initial thickness is sufficiently small (Carvalho 1996).

An improved understanding of the tensile properties of process fluids such as polymeric liquids is extremely valuable in a diverse range of industries including the automotive, printing and food industries.

Within these industries substantial negative pressures are developed within many flow situations. Once the pressure reaches a critical value for each fluid - its effective tensile strength - the fluid 'breaks up'; driven by a mechanism known as cavitation. The term 'cavitation' refers to the formation of cavities (or cavitation 'bubbles') in a liquid when it experiences tension (Trevena, 1987; Joseph, 1998). If the tension exceeds the liquid's cavitation threshold (or effective tensile strength, F_c) the liquid changes irreversibly into a two-phase system of liquid and a mixture of vapour and dissolved gas (Brennen, 1995). The cavitation of liquid films is an important aspect of lubrication (Dowson & Taylor, 1979) and printing (Zang *et al*, 1991), processes which often involve meso-scale (0.1-10 μm) thickness films undergoing rapid deformation between separating surfaces. In fluid mechanical machinery these are usually solid whereas in biomechanics surfaces such as biological membranes are flexible. The 'cracking' of knuckle joints has been attributed to cavitation within meso-scale lubricating films of synovial fluid (Unsworth *et al*, 1971).

In coating processes, cavitation film-splitting may result in the formation of rapidly-stretching filaments, whose breakup leads to unwanted droplet deposition. Filament formation is also a feature of coating flows involving adhesive films (Lakrout *et al*, 1999) but descriptions of the process are still largely qualitative, commonly invoking the term 'tack' (Braithwaite & McKinley, 1999; Zosel, 1998). The tack of an ink film is primarily connected with the tensile forces developed in film-splitting (Strasburger,

1958), the function of cavitation being to limit the forces of separation of surfaces joined by a tacky liquid (Banks & Mill, 1953). By definition, the tack of an ink film is the maximum tensile stress (or 'negative pressure') which it can withstand before splitting (Zang *et al*, 1991).

Due to the high deformation rates which typify many meso-scale cavitation phenomena, significant viscoelastic effects may be anticipated. One such effect is a delay in the cavitation of viscoelastic liquids in micron-sized gaps, due to the development of normal stresses (Ouibrahim *et al*, 1996). Other claimed viscoelastic effects include a displacement of the point of cavitation from the centre of contact (where film thickness is a minimum) and enhanced film thicknesses (Narumi & Hasegawa, 1986). Although little is known about the influence of viscoelasticity in *sub*-micron liquid film cavitation, the initial film thickness has been identified as a crucial factor: for sufficiently thin films, even ostensibly low rates of surface separation may provoke the high rates of fluid deformation necessary to generate enough tension (through viscous forces) to result in cavitation (Joseph, 1998). In ultra-thin films of water, cavitation may occur spontaneously due to the antipathy between the liquid and hydrophobic surfaces between which it is confined (Christenson & Claesson, 1988).

The development of the stress being applied to the fluid is an important factor (Trevena 1987) and the range of stressing rate varies extensively within industrial applications. The oil in an engine bearing may experience shear rates in the magnitude of 10^7 s^{-1} while the shear rate associated with rubbing or applying a cream as well as roll-coating of inks could be in the order of 10^4 s^{-1} . Other techniques which allow

surface tension and gravity to control the kinematics of a flow may only experience shear rates in the magnitude of 10^{-2} s^{-1} .

In many manufacturing situations such as, the spinning of synthetic fibres for clothing, the moulding of plastic bottles and in the production of paints, inks and motor oils, polymers are important components.

There are many rheological experiments that can determine different aspects of a polymeric fluid. Shear, oscillatory and extensional rheometers are all used to characterise different aspects of a fluid, however these experiments are not sufficient to explain all the industrial problems with fluid arising from filament break-up, hence a study into the tensile properties of fluids is essential to describe these additional parameters.

1.2 Experimental techniques for the measurement of liquid tensile strength

The methods used to generate tension within a liquid fall into two main categories, depending upon the rate of stress development. In ‘static’ stressing, tension develops gradually (over seconds, or more), dynamic techniques involve timescales which are typically in the microsecond to millisecond range.

Early studies of liquids under (quasi-static) tension were conducted by Berthelot in 1850 and various forms of his apparatus are still used (Trevena 1987). Typically it consists of a sealed cylindrical tube, almost completely filled with liquid. On heating,

the liquid expands until it completely fills the tube. On cooling the tube, the liquid adheres to its walls and due to differential rates of contraction between tube and liquid, tension sets in until the liquid ruptures. Berthelot obtained breaking tensions of *ca.* 50 Bar for water in a glass tube while Henderson and Speedy (1980) reported values of *ca.* 130 Bar in their modified version of the apparatus which exploited the Bourdon effect to measure pressures directly.

Briggs (1950) employed a centrifugal method to apply a static tension to a liquid using a Z-shaped capillary tube containing liquid. The tube, which was open at both ends, rotated about its centre, the plane of the Z remaining horizontal. The maximum tension sustained was calculated from the maximum rotational speed attained without causing rupture of the liquid. Briggs' results for water varied between 20 Bar at 1⁰ C, rising to 277 Bar at 10⁰ C and falling to 220 Bar at 50⁰ C.

In Apfel's (1970) work, a small, filtered sample of ether was suspended in an inert 'host' liquid. The two liquids being immiscible, the sample 'droplet' container was the host liquid thus the possibility of nuclei for bubble growth at the container walls was eliminated. The droplet, suspended in the host liquid (glycerine), was stressed acoustically at the resonant frequency of the entire system and at temperatures well above the normal boiling points of the liquids. At a particular combination of superheating and acoustic stress, the droplet reached its ultimate tensile strength and vaporised. The results agreed well with homogenous nucleation theory, suggesting that cavitation occurred within the droplet, not at the liquid-liquid interface.

The reflection of a pressure wave as tension from a suitable boundary has been exploited in dynamic stressing, such as in measurements of F_c in 'bullet-piston' (B-P) experiments (Davies *et al* 1955). In that work, a vertical steel tube, closed at its ends with steel pistons was filled with a liquid and a compression pulse was generated in the liquid by firing a bullet at the lower piston. Degassed distilled water was found incapable of sustaining a tension greater than 10 Bar. Later B-P work involving free surfaces gave values of 8.5 Bar for ordinary tap water and 15 Bar for degassed deionised water (Trevena 1987). Kedrinskii *et al* (1995) have described an x-ray imaging system which was used to investigate the structure of the cavitating zone produced by the reflection of pressure waves at the free surface of water.

Wilson *et al* (1975) detonated an explosive charge below the surface of a liquid and obtained high-speed photographs of the spray dome formed above the original undisturbed free surface. From measurements of the initial spray dome velocity, F_c was estimated to be 8.0 Bar for 'ordinary water'. Williams and Williams (2000) have shown that the anomalously low values of F_c recorded in some work involving pulse reflection at a free surface are due to inadequate transducer response, and low data sampling rates.

Dynamic stressing work often involves ultrasound, which subjects a liquid to compression and rarefaction during its positive and negative half-cycles, respectively. Using focussed ultrasound, Willard (1953) found that water could withstand tensions of 70 Bar until a suitable nucleus appeared at the focus of the wave. Using a 42.9 kHz ultrasound wave, Greenspan and Tschiegg (1967) found that clean water could sustain tensions of 160 Bar for periods as long as a minute at 30 °C, and even higher (*ca.* 210

Bar) for a few seconds. Galloway (1954) also reported ultrasonic thresholds as high as 200 Bar for water, for similar sound frequencies. Coleman *et al* (1995) have studied the cavitation threshold of human tissue exposed to pulsed ultrasound in clinical lithotripsy (see Barnett and Kossoff (1998) for a survey of issues involving cavitation in biomedical applications of ultrasound, including diagnostic techniques).

Maris and Balibar (2000) have reported the ultrasonic stressing of liquid helium, in which laser light scattered by bubbles at the acoustic focus was detected by a photomultiplier. This work involves an 'electron bubble'- a spherical cavity from which helium atoms are excluded when an electron is injected into helium. The bubble forms due to the repulsion of the electron by helium. If the pressure is zero, such a bubble has a radius of around 190 nm; and at around -2 Bar, it grows without limit.

It is interesting to compare the tensile strength of other liquids when measured statically and dynamically: usually, the higher the rate of stressing, the higher the value of F_c obtained (Temperley and Trevena 1987). In glycerol, differences in F_c may be explained in terms of different stressing rates. Bull (1956) found a tensile strength of 60 Bar while Carlson and Henry (1973) reported 600 Bar and in both experiments, cavitation occurred in the body of the liquid but the rate of stressing was 10^4 times lower in Bull's work than in Carlson and Henry's. Similar findings have been reported for mercury, in which Briggs (1953) was unable to generate static tensions greater than 425 Bar but Carlson (1975) found that tensile failure occurred at a tension of 19 kBar, at a stressing rate of *ca.* 10^6 Bar/ms. At a lower rate (1 Bar/ms),

Williams *et al.* (1998a) found a limit for F_c of *ca.* 3 kBar. In this respect mercury follows the trend observed in glycerol and water.

Spark discharge techniques have proved valuable in studies of bubble dynamics, such as in the work reported by Chahine (1979). Gibson and Blake (1982) have studied large spark-generated bubbles in a free-fall apparatus designed to remove buoyancy effects. In common with spark discharge work, the generation of bubbles by pulsed-laser also involves intense local heating and vaporization of the liquid. Its advantage over the spark technique is that high-voltage electrodes do not intrude into the liquid and thus disruption of the bubble motion is avoided. Brujan (1998) has reported the size of bubbles produced in laser induced cavitation and its relation to the pulse duration. In a CMC solution, the smallest size of the spherical bubbles produced using a Nd:YAG laser, with a pulse duration of 8 ns was 0.22 mm, but the maximum radius is reduced by decreasing the pulse duration. Vogel *et al* (1994) found that the smallest value of the maximum bubble radius produced by a 30 psi pulse in water is about 0.04 mm. Vogel *et al* (1989, 1996) and Tomita and Shima (1990) have reported optical and acoustic studies of laser-produced bubbles, including studies of shock wave emission and bubble generation by picosecond and nanosecond optical breakdown in water.

1.3 Rheological properties of polymeric liquids

Rheology is the study of fluids that do not follow the constitutive equation associated with Newtonian fluids and has been defined as is the study of ‘flow and deformation of matter’ (Bingham, 1929). In many flow situations the fluids are subjected to both shear and extensional deformation. Fluids exhibit a resistance to shearing of the fluid

known as its shear viscosity and the resistance to the extensional deformation of the fluid is known as the extensional viscosity. A brief description of shear and extensional characterisation will follow.

By considering a thin layer of liquid between two parallel plates, a set distance apart, dy , we can define the shear stresses applied to a liquid. The upper plate is subjected to a horizontal force, F_s , which moves at a velocity dV_x , whilst the bottom plate remains fixed.

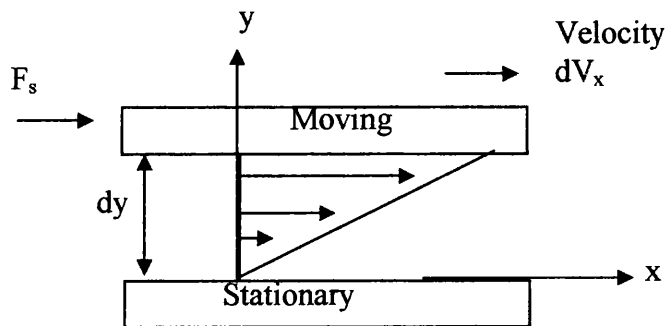


Figure 1.1 Development of shear stress

The force per unit area that is required to produce motion is referred to as shear stress, σ_s ,

$$\sigma_s = F_s/A \quad [1.1]$$

Since the bottom plate is stationary shearing of the material is caused, as hypothetical layers of the liquid retard the flow of an adjacent layer. The velocity gradient in the direction normal to the flow is known as the shear rate, given by

$$\dot{g} = dv_x / dy \quad [1.2]$$

Newton's postulate in these terms can be simply expressed as the doubling of the shear stress doubles the shear rate,

$$\sigma = \eta \dot{\gamma} \quad [1.3]$$

In this equation we can note that there is an additional coefficient, that is the shear viscosity which overcomes the 'lack of slipperiness' as mentioned by Newton. Hence the rearrangement of this gives a simple definition for shear viscosity.

$$\eta = \sigma / \dot{\gamma} \quad [1.4]$$

This equation is only held for what is known as a Newtonian fluid, water being a good example of this. However many liquids exhibit non-Newtonian behaviour, that is they exhibit a non-linear dependence of shear stress on shear rate.

1.4 Cavitation and filamentation

Cavitation is the dynamic process of the formation and subsequent collapse of bubbles in a liquid when it experiences negative pressure (or 'tension') (Trevena (1987), Joseph (1995)). Cavitation occurs when the tension exceeds a certain critical value; the liquid changes irreversibly into a two-phase system of liquid and a mixture of vapour and dissolved gas, the latter appearing as cavitation bubbles. It is the critical value of localised tension that leads to the rupture of the liquid which is known as the liquid's effective tensile strength, F_c . For some liquids, substantial negative pressures can be supported before rupture (Brennan 1995).

Euler had predicted what we now call cavitation as early as 1754 where he stated 'But when it should happen that this quantity [the absolute pressure] will be negative somewhere inside the pipe, then the water would desert the inner wall of the pipe and create a void in space' (Euler 1754). It was however the occurrence of cavitation in hydraulic machinery that first prompted considerable research into this subject, and particular interest has been placed on the characteristic erosion-like patterns of damage which are found to occur at the lining surfaces of machinery in contact with cavitating liquids. This phenomenon, known as 'cavitation damage' was first noted by Barnaby and Thornycroft, in the case of fast-steam boats which failed to meet their expected design speed (Trevena (1987), Thornycroft and Barnaby (1895)). The damage found near these regions was ascribed to the violent collapse of the bubbles at the blade surfaces as they moved to regions of higher pressure. Thornycroft and Barnaby (1895) described the problems with the design of one particular destroyer, H.M.S. Daring. This was nearly 150 years after Euler had first described this problem. Cavitation occurs when the pressure on the forward face of the propeller blade becomes low enough that vapour bubbles form and the water boils. The collapsing of the vapour bubbles might at first seem trivial, but it can be a very violent event which can result in the erosion and pitting of the propeller surface. As well as cavitation being a major source of propeller damage, vibration, noise and loss of performance are also attributed to this phenomenon. Cavitation can be caused by nicks on the leading blades, since trapped air bubbles within these pits can grow under negative pressure and cavitate. Since cavitation can cause these pits it is a progressive problem with more cavitation damage likely to happen later.

The ability of liquids to withstand negative pressure or tension, is very similar to the more familiar property exhibited by solids and is a manifestation of the elasticity of a liquid (Brennen 1995). Much cavitation research has been stimulated by the erosion of solid surfaces in the near vicinity of collapsing cavities but it is also an important factor in the life of plants and animals (Tyree 1997; Smith 1991), including humans (Unsworth *et al* 1971).

Whereas gas-filled bubbles expand by diffusion from the liquid (or by pressure reduction, or temperature rise), in the case of predominantly vaporous bubbles a reduction of pressure may cause an ‘explosive’ vaporisation of the liquid into the bubble. The formation of bubbles (or their growth from preexisting nuclei) during the negative part of the acoustic cycle in an alternating pressure field is called ‘*acoustic cavitation*’. Subsequently, under positive acoustic pressure, the growth of the bubble slows and eventually it begins to collapse. The behaviour of such a bubble depends on factors such as the amplitude of the acoustic pressure, the ambient pressure in the liquid, the frequency and duty cycle of the pressure wave, the liquid’s characteristics (such as its viscosity) and the presence of any dissolved gases (Leighton 1994). In ‘*resonant cavitation*’ the acoustic wave frequency is equal to the resonant frequency of the bubble. In ‘*stable cavitation*’ the bubble’s growth rate during the acoustic rarefaction phase is equivalent to its contraction rate during the compression phase: such bubbles may oscillate around a mean radius for many acoustic cycles whereas ‘*transient cavitation*’ exists for only a few cavity cycles, during which time they grow several times larger than their initial size. Their eventual collapse may produce extreme intracavity temperatures and pressures. Transient cavitation provides the relatively violent activity usually required in processes such as industrial ultrasonic

cleaning, the dispersion of solid particles in liquids, depolymerization and cell disruption and the destruction of microbes.

The formation of stable bubbles implies an absence of rectified diffusion, the process by which bubbles in an oscillating pressure field grow more during expansion than they shrink during contraction, due to unequal diffusion of gases and vapor from the bulk liquid phase into the bubble. Other acoustic cavitation phenomena are bubble coalescence and the production of ‘cavitation streamers’. The latter involve a line of bubbles along a path in a sound field, their collective motion resulting from the effects of radiation pressure and mutual Bjerknes forces. Flows over solid surfaces can involve individual travelling bubbles (*‘travelling cavitation’*) in which bubbles are continuously shed, to collapse and rebound in regions of higher pressure.

1.4.1 Nucleation theory

Cavitation is not necessarily a consequence of pressure reduction to the liquid’s vapour pressure, p_v , which is the equilibrium pressure, at a specified temperature, of the liquid’s vapour in contact with an existing free surface. In a homogeneous liquid, cavitation requires a stress sufficiently large to rupture the liquid and this stress represents the tensile strength, F_c , of the liquid at that temperature.

Theory predicts that vapour bubbles will only form in pure liquids as a result of very large tensions, some 1.3 – 1.4 kBar in the case of water (Fisher 1948), although a somewhat higher figure (*ca.* 1.9 kBar) results from an interpretation of the thermodynamic properties of stretched water known as the stability limit conjecture

(Speedy 1982). Experiments involving small quantities of pure water have produced tensions close to the homogeneous nucleation limit of 1.3 kBar (Zheng *et al.* 1991). As large tensions are not commonly observed, the idea of bubble nucleation and its manifestation as the effective tensile strength of a liquid has been introduced.

In some treatments, nuclei represent ‘holes’ in the liquid which grow into macroscopic bubbles (Frenckel 1955) but heterogeneous nucleation may involve microscopic impurities such as ‘motes’ of dirt, or dust. An energy barrier against nucleation arises because the liquid-gas transition is discontinuous and the interface between the two phases has a finite energy per unit area – the surface tension, σ . Thus bubble formation has an energy cost of $4\pi R^2\sigma$. The energy of the system also contains the work of the negative pressure over its volume, so that the total energy cost of forming the bubble is (Maris and Balibar 2000):

$$\Delta E = 4\pi R^2\sigma + \frac{4\pi}{3}R^3F$$

At negative pressures, this energy has a maximum for a critical radius $R_c = 2\sigma/|P|$.

The liquid pressure, p , exterior to a bubble of radius R , will be related to the interior pressure, p_B , by:

$$p_B - p = 2\sigma/R$$

where σ is the surface tension. If the temperature, T , is uniform and the bubble contains only vapour, then the interior pressure, p_B , will be the saturated vapour pressure, $p_V(T)$. However, the exterior liquid pressure, $p = p_V - 2\sigma/R$, must be less than p_V in order to produce equilibrium conditions. Consequently, if the exterior liquid pressure is maintained at a constant value just slightly less than $p_V - 2\sigma/R$, the

bubble grows, R will increase the excess pressure causing the growth and rupture occurs. It follows that if the maximum size of the cavity is R_c (the 'critical' radius), then F_c will be given by:

$$F_c = 2\sigma / R_c$$

For some finite tension the liquid stretches without limit. The pressure at which that happens is called the spinodal limit, at which the compressibility is infinite and there is no barrier to nucleation. For small tensions the energy barrier is large and a pure liquid may sustain tension for a prolonged period. In this condition it is in a metastable state and inhabits the region between the spinodal and the coexistence curve where liquid and vapour coexist. The spinodal parabola meets the coexistence curve at the critical point but otherwise is separated from it by a finite distance.

The presence of dissolved gas would appear to be an obvious factor in reducing F_c . Several studies have found that as the gas content is reduced, cavitation thresholds increase. Galloway (1954) found that the highest attainable acoustic pressure ranged from 1 - 200 Bar as the air content of water was reduced from a saturation of 100% to 0.05%. However, for carefully cleaned liquids, Greenspan and Tschiegg (1967) found no dependence on gas content for slightly undersaturated liquids. Apfel's (1970) model for the stabilization of gas pockets in conical crevices has shown that this lack of dependence on gas content is the case for sufficiently small, imperfectly wetted impurities, whereas a large dependence on gas saturation results if the liquid contains large impurities.

Kuper and Trevena (1952) estimate that the reduction for water saturated with air at 1 Bar would be less than 0.5%. Their theory involved a small, free, spherical cavity in

the liquid acting as a nucleus for bubble growth to macroscopic size under tension. Such a bubble would rapidly dissolve, whereas larger bubbles would rise up through the liquid. The necessary mechanism by which gas bubbles may be stabilised and remain available as nuclei was proposed by Fox and Herzfeld (1954) who suggested that a 'skin' (possibly organic) might exist around gas bubbles thereby inhibiting the diffusion of gas across the boundary. The phenomenon of rectified diffusion suggests that diffusion at the bubble boundary is not heavily inhibited (Crum 1980). The mechanism of stabilisation has been attributed to surface-active substances which, in being absorbed onto the bubble's surface give rise to an elastic skin (Hayward 1970). The model by which spherical gas bubbles become stabilised against diffusion by membranes of surface-active materials, is known as the varying-permeability (VP) model. Ordinarily, VP membranes are gas permeable but become effectively impermeable when subjected to compressions exceeding 8 Bar. Holographic studies show that cavitation nuclei of 1 μm to 1 mm exist in water and the nuclei number density distribution function varies from 10^9 to 10^{15} m^{-4} (Gates and Bacon 1978). For a survey of VP model work see Yount (1997).

Stabilised nuclei may also exist in cracks on the surfaces of microscopic particles ('motes') in a liquid (Harvey 1944). Under tension, the trapped gas pocket grows until, at a critical tension, the cavity detaches from the crevice. If the surface is hydrophobic, such a nucleus might persist for an appreciable period of time, providing a nucleus for bubble growth. In the case of motes with hydrophilic surfaces, failure of the liquid may occur at a location other than the mote. Brownian motion could keep a small mote in suspension almost indefinitely. For sufficiently large hydrophobic crevices, the critical factors governing the value of F_c are the liquid's gas content and

its stress history (Apfel 1970). Akulichev (1994) has reported a study of cavitation nuclei and thresholds of acoustic cavitation in ocean water. For sea water, F_c grows with water depth. In the upper sea water layer, the most characteristic nuclei are gas bubbles whose concentration increases with increasing sea roughness and wind speed. Evans and Walder (1969) suggest that gas micronuclei are present *in vivo* within the human body and that their production is related to impulsive internal stress resulting from muscular movement (see also Harvey 1951).

The greatest effort in cavitation research has involved the study of bubble dynamics, a preponderance of attention deriving from the association between collapsing bubbles and instances of damage to solid surfaces in their vicinity. The term ‘cavitation damage’ is widely used to describe this phenomenon. An early attempt to explain it was made by Lord Rayleigh (1917), whose seminal analysis of the behaviour of an isolated spherical void collapsing in an incompressible liquid still serves as the starting point of many studies. Rayleigh’s results are considered in detail later but an important conclusion is that as the collapse nears completion, the pressure inside the liquid becomes indefinitely large. It is this mechanism, albeit extensively modified, which has led to the association of bubble collapse with cavitation damage.

1.4.2 Cavitation in flowing liquids

Cavitation can be induced in liquids by flow over submerged bodies, or in vortices. Many flows induce the periodic formation and collapse of a ‘cloud’ of bubbles (*‘cloud cavitation’*). In flow about a blunt body a sudden transition often occurs from

travelling cavitation to the formation of a single vapour-filled wake known as a ‘fully developed-’ or ‘attached-cavity’. The vapour-filled separation zone formed on hydrofoils or propeller blades is known as ‘sheet cavitation’ whereas its counterpart in pumps is termed ‘blade cavitation’. This proliferation of terms is confusing but all describe the same large-scale cavitation structure (Brennen 1995). ‘*Supercavitation*’, in which a moving object is enveloped by a large bubble, has military application in high speed underwater munitions (Miller 1995).

In the cavitation of submerged jets, the cavitation number is defined as,

$$\sigma = \frac{p_r - p_v}{\frac{1}{2} \rho V_j^2}$$

with p_r the pressure in the reservoir where the jet is discharging and V_j the bulk velocity of the jet. A decrease in pressure from a non cavitating situation until cavitation is reached, or an increase in pressure from a cavitating situation until the non cavitating conditions are achieved, provide the inception, σ_i , or desinent, σ_d , cavitation numbers respectively. Extensive literature exists on underwater jet cavitation, much of it provoked by interest in the turbulent drag reduction associated with dilute solutions of high molecular weight polymers (Acosta and Parkin 1975). Several studies, such as those of Hoyt (1976), report that cavitation is either delayed or unaffected in such fluids and that major changes seem to be associated with a modified free-shear layer structure but there is little, if any, contribution from the fluid properties on inception. When cavitation is well developed, the cavities are larger and have smoother surfaces than their counterparts in the Newtonian solvent. These

observations are related to the delayed departure from sphericity and instability of single bubbles in polymer solutions.

In flow around blunt bodies, major changes appear to be correlated with the early occurrence of laminar to turbulent transition in drag reducing polymer solutions, without significant contribution from bubble dynamics. In separated flows, such as jets and wakes, cavitation occurs in the low pressure regions of the vortices developing in the free shear layers. In tip-vortex flow situations with homogeneous polymer solutions, non-Newtonian effects seem to enhance the occurrence of cavitation, while, in pure water and polymer solutions there is a systematic cavitation inhibition. In confined vortex flow in homogeneous solutions, the results show either cavitation enhancement or inhibition (see Fruman 1999).

Joseph (1995) has studied cavitation inception in terms of a comparison of the cavitation threshold at each point in a liquid sample with the principal stresses present and emphasises from this, that for liquids in motion, cavitation criteria must be based not on the pressure but on the stress. A cavitation bubble will open in the direction of maximum tension in principal coordinates and an important point which emerges is that a liquid can cavitate as a result of experiencing a shear deformation, the resulting cavity being pulled open by tension in the direction defined by principal stresses.

Kezios and Schowalter (1986) have studied the effect of a controlled shear flow on the deformation of laser-generated bubbles.

1.4.3 Cavitation in confined spaces

Few studies have examined cavitation in thin films, such as disk-lubricant films under high shear forces. Chen *et al* (1992) used a surface-force apparatus technique to observe, at the nanoscopic level, the growth and disappearance of vapour cavities between two moving solid surfaces. As the relative separation velocity of the surfaces increased they deformed elasto-hydrodynamically, becoming pointed in regions corresponding to negative pressure in the liquid and vapour cavities formed once the relative velocity of the surfaces exceeded a critical value. The sudden nucleation and growth of a cavity in a thin liquid film was claimed to be more violent than its collapse. Ouibrahim *et al.* (1996) have studied flows of water and a viscoelastic fluid in micron size gaps. They found that the initiation of cavitation was delayed in the polymer solution and speculate that the effect is due to normal stress development in the elongational flow.

1.4.4 Some processes involving cavitation

Sonochemistry relies on the use of ultrasound for invoking acoustic cavitation, which initiates reactions, changes reaction pathways or increases reaction rates and/or yields. Sonochemistry occurs when ultrasound induces 'true' chemical effects on the reaction system, such as the formation of reaction-accelerating free radicals. Two theories exist to explain the chemical effects due to cavitation. The former involves the idea that high (localised) temperatures and pressures may be associated with cavitation while the latter invokes an electrical charge on the bubble's surface (Thompson and Doraiswamy 1999). Intense ultrasound fields can result in sonoluminescence and also

possible free radical recombination. Sonochemiluminescence involves light emission in which radicals, produced by cavitation, react with solutes that chemiluminesce.

In lubrication, subambient pressures may occur in the divergent section of wedge-shaped oil films in bearings, giving rise to gaseous or vaporous cavitation (Braun and Hendricks 1984). Cavitation has been associated with bearing damage in internal combustion engines, but cavitation does not necessarily have a deleterious effect upon the load-carrying capacity of fluid-film bearings. If the film does not rupture, then the load capacity is zero since the convergent and divergent regions of the film make equal and opposite contributions. Gas release ensures that the pressure in the divergent section remains close to the saturation pressure, with a net force normal to the surfaces. In this case the load-carrying capacity results from film rupture (Dowson and Taylor 1979). Berker *et al* (1995) have reported the effects of polymer additives on flow in dynamically loaded journal bearings and concluded that their role in reducing wear may be associated with some mitigating effects of viscoelasticity on cavitation.

The ability of liquids to sustain tension is an important factor in the survival of plants, in which the cohesion-tension (C-T) theory explains water transport (Tyree 1997).

The C-T theory assumes that water, when confined in small tubes with wettable walls such as xylem elements, can sustain a tension ranging from 3 to 30 MPa. The liquid forms a continuous system in the water-saturated cell walls, from the evaporating surfaces of the leaves to the absorbing surfaces of the roots. During evaporation, the reduction in water potential at the surfaces causes movement of water out of the xylem, with water loss producing tension in the xylem sap that is transmitted

throughout the continuous water columns to the roots. The C-T theory has been questioned repeatedly and is currently the subject of considerable debate.

The acoustic production of liquid droplets has been ascribed to an interaction between hydrodynamic instabilities involving surface waves and sub-surficial cavitation of a liquid (Boguslavskii and Eknadiosyants 1969). This interaction is thought to induce the generation of surface ‘spray’ phenomena subsequent to underwater explosions in which spray droplet formation involves layers of vapor which are ‘sandwiched’ between layers of liquid (Trevena 1987). It is the putative ability of these vapor layers, formed by cavitation, to reflect incident compressional waves as tension which is crucial to explaining the production of droplets. The need for further research in this area has been identified in a U.S. National Research Council report which notes that ultrasonic atomisation “*seems to involve acoustic cavitation but is poorly understood*” (Prosperetti 1996).

The tensile strength of a liquid is relevant to printing processes which involve the ‘tack’ of an ink - the maximum tensile stress developed in the splitting of ink films at a printing nip exit, where the ink is subjected to an extensional flow in the direction normal to the roller surfaces (Zang *et al* 1991). Banks and Mill (1953) proposed that tack is a consequence of cavitation and of the drop in hydrostatic pressure at the nip exit, and so is independent of the liquid. Zang *et al.* (1991) conclude that tack is primarily determined by polymer content, which suggests that extensional, not shear, viscosity properties govern film splitting.

In many industries an interesting parameter is that of tack, however it has many different definitions depending on the procedure the fluid is going through. Zang et al. (1991) defined 'tack' to be the maximum tensile strength of a liquid. In the ink and coating industry the tack of an ink is connected with the forces developed in the splitting of ink films near the nip exit, where the ink is subjected to an extensional flow in the direction normal to the roller surfaces. In the region of the nip exit, tension develops within the liquid, this tension increases until the tension reaches the critical tension for the sample and the ink film splits. Cavitation film-splitting results in the formation of filaments, which on break-up cause unwanted droplet deposition and hence lower the printing quality. McPhee (1997) describes the film splitting procedure in six steps, shown in figure 1.2: 1. At a critical negative pressure, cavities or bubbles are formed (cavitation). 2. As the cavities move away from the exit they expand and become interconnected forming filaments. 3. The filaments are stretched as rollers separate. 4. At a critical point, the filament ruptures. 5. Following rupture, the filament ends recoil. 6. The recoiled filaments cause satellite drops and other detrimental effects. It is clearly evident that one of the causes of detrimental printing is that of cavitation within the ink, caused due to the negative pressure that the liquid experiences on exit of the roller. It is one of the purposes of this thesis to investigate the cavitation threshold of polymeric liquids used in the ink and coating industry to study this phenomena.

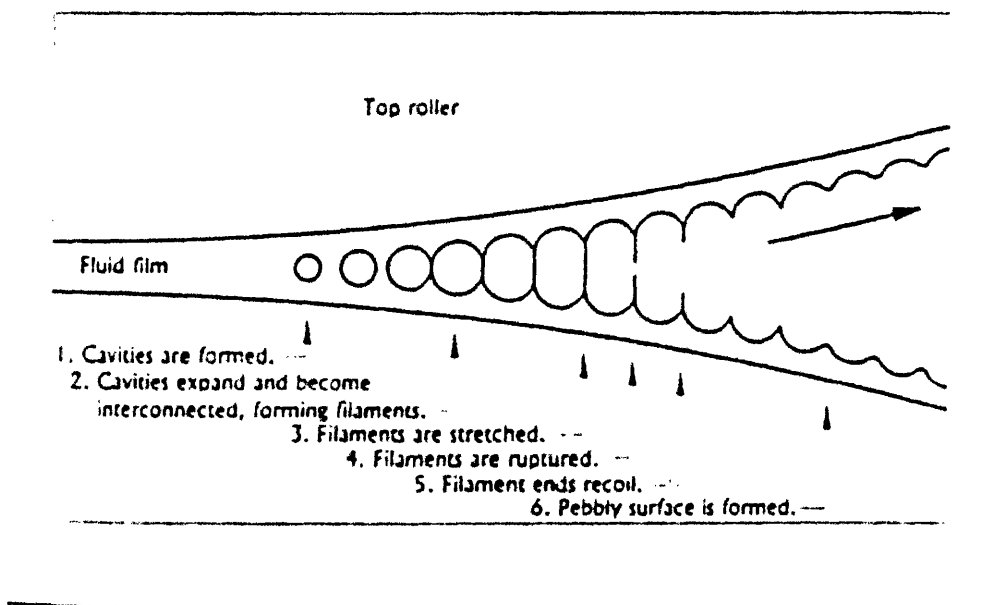


Figure 1.2 Process of Film Splitting (McPhee 1997)

Filament formation is a feature of coating flows involving pressure sensitive adhesives, but descriptions of the process are as yet qualitative (Zosel (1998)). Zang et al (1991) describe tack as one of the most important characteristics of an ink, affecting the runnability and printability of inks. An excessive ‘tack’ can cause the ink to remove fibres or coating particles from the paper during the printing process. Banks and Mill (1953) proposed that tack is a consequence of cavitation and of the drop in hydrostatic pressure at the nip exit and so is independent of the liquid. However Zang et al. (1991) conclude that tack is primarily determined by polymer content and suggest that extensional, not shear, properties of the fluid govern film-splitting. It is therefore appropriate to examine the extensional nature of fluid flows to further our understanding of tack.

1.5 Extensional flows

Examples of extensional flows abound in the process industries, in situations such as fibre-spinning, lubrication, spraying, atomisation and anti-misting, coating and printing. The lack of adequate rheological information concerning extensional flows of mobile (i.e. low viscosity) fluids, is a significant impediment to the development of process simulation. The requisite information involves the extensional viscosity, η_E , the significance of which is that it may be several orders-of-magnitude higher than the corresponding shear viscosity in elastic liquids (Petrie (1979)).

Measurements of the extensional flow properties of 'mobile' fluids are acknowledged to be difficult. A US National Research Council survey of progress in non-Newtonian Fluid Mechanics has concluded that "*the measurement of extensional stresses of mobile fluids is a major outstanding problem; and this measurement is essential for determining the predictive power of constitutive equations for flows which are closely related to many important processing situations*" (Sridhar (1990)). In the case of mobile fluids, the generation of a purely extensional flow is considered virtually impossible and workers have resorted to the generation of flows with a high extensional component (Coyle (1984)). Perhaps the best known approach involves a filament stretching device wherein a sample is held between two plates which move apart at controlled rates, the upper plate being attached to a load measuring device. This technique provides a transient extensional viscosity growth function as the Hencky strain ϵ increases but is restricted to low deformation rates ($< 100 \text{ s}^{-1}$) and only provides meaningful data for fluids of high extensional viscosity. Furthermore, at

large ϵ the filaments suffer elastic decohesion from the plates, rendering the determination of elongational stress, σ_e , unreliable (McPhee 1997).

A major advancement in determining the transient extensional viscosity was devised by Matta and Tytus in 1990. They developed an extensional rheometrical device to obtain such information on both Newtonian and non-Newtonian viscoelastic fluids, known as the falling mass rheometer. This simple device consisted of two cylindrical plates in between which was placed a sample fluid, the bottom plate was then allowed to fall under the influence of gravity. A nearly pure extensional flow is generated during the stretching process. High speed photography of the extensional flow is used to deduce the liquid deformation rate and ligament stress. These values help determine the elongational viscosity, which give comparable results to the Trouton ratio for Newtonian liquids, the testing of viscoelastic media indicated that the extensional viscosity is significantly greater than Newtonian liquids with the same shear viscosity. Modifications to this technique were presented by Matthew Barrow (2000), these modifications include, due to advancement in photographic techniques, the high speed camera system being replaced by a digital recording system. This new digital imaging means that there is less error in the measurement of the fluid during the stretching process. It was also shown that error crept into the falling mass technique when highly viscous fluids were used, with the base cylinder tilting during its fall. Modifications to this base cylinder and to the retaining shelf were implemented to overcome these issues and successful results of this were presented by Matthew Barrow (2000).

1.5.1 Filament stretching rheometry

The design of filament stretching rheometers followed the work of Matta and Tytus (1990) with the attempt to create a purely extensional (elongational) flow by placing a small sample of the test fluid in between two circular endplates and moving them apart so that the gap increases exponentially in time. This device known as the filament stretching rheometer came about to overcome the issues raised by Sridhar (1990) where a test fluid had been experimentally analysed by differing extensional rheometers with a wide variety of results. A comprehensive review of filament stretching rheometry has recently been published by McKinley and Sridhar (2002). The first design in this form was implemented by Tirtaatmadja and Sridhar (1991, 1993). They implemented an exponential displacement profile of the endplates with the tensile force of the filament, $F_p(t)$ and the mid point diameter of the filament, $D_{mid}(t)$ were measured in time. The mid point of the diameter can be measured by different techniques such as laser micrometers, wire gauges or by analysing high speed photographic images of the extended filament. This method can look at the whole profile of the filament but does not give as good results. A basic sketch of the device is shown in figure 2, the original dimensions of the filament being length, L_0 , and width D_0 . These two measurements give us an initial aspect ratio $\Lambda_0=L_0/(D_0/2)$. The initial aspect ratio of the filament has been shown to affect the initial transient response of the tensile forces within the filament Spiegelberg (1996)).

In extensional devices the material function that normally is to be obtained is the transient extensional viscosity as a function of time, this is defined as,

$$\bar{\eta}(t, \dot{\epsilon}_0) \equiv \frac{[\tau_{zz}(t) - \tau_{rr}(t)]}{\dot{\epsilon}_0}$$

where $\dot{\epsilon}_0$ is the axial elongation rate. By balancing the forces within the filament, we can relate the transient extensional viscosity to measurable quantities such as the force exerted on the endplate and the diameter of the filament. The value for the force on the endplate is adjusted to include the affects of surface tension and gravity. The Trouton ratio is a non-dimensional form, with the ratio of the transient extensional viscosity with the zero-shear-rate viscosity, η_0 . This can be written in the form,

$$T_r \frac{\bar{\eta}(t, \dot{\epsilon}_0)}{\eta_0} = \frac{[\tau_{zz}(t) - \tau_{rr}(t)]}{\eta_0 \dot{\epsilon}_0} = \frac{F_p}{\pi \left(\frac{D_{mid}(t)}{2}\right)^2 \eta_0 \dot{\epsilon}_0}$$

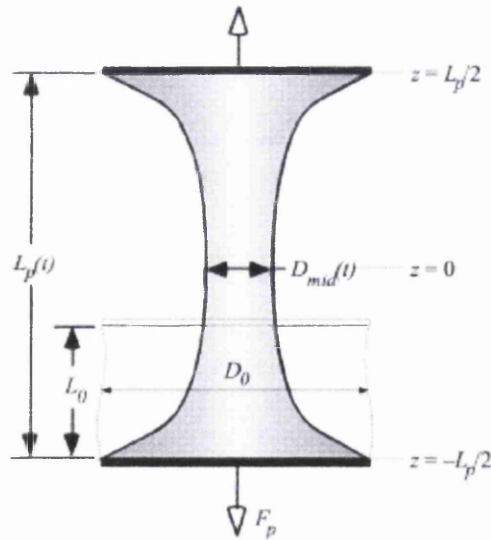


Fig. 1.3 Diagram of filament stretching rheometer (McKinley et al. 1999)

The first models used to describe the filament stretch assumed a perfectly uniform radial decrease; in practice this was established not to be the case due to the no-slip

criterion imposed by the endplates. A trial and error experiment produced an endplate profile that would result in the mid-filament diameter to decrease exponentially (Tirtaatmadja (1993)). A 'velocity compensation algorithm' was designed to achieve such a mid-diameter profile, the analysis was also used to predict the effect of the initial aspect ratio on the transient stress growth in the filament.

There are three main sections to the flow within filament stretching rheometers, firstly the filament is elongated with the radius of the filament decreasing exponentially, secondly the fluid undergoes stress relaxation where the tensile stress in the filament relax and the radius of the filament remains almost constant, and the final section of the flow is the breakup of the filament this is caused when the capillary pressure and gravitational stresses become dominant. It was very clear even from these early experiments that there was an additional shearing component to the flow near the end plates due to the no-slip boundary conditions. This instability within the flow has been experimentally investigated by Spiegelberg et al. (1996) and numerically by Yau and McKinley (1998).

A recent thesis by Welsh (2000) developed a stability region of stretching flows and can be used to determine useful limits of initial parameters for the filament stretching rheometer. This work also focused on the fingering instability that appears during the stretching process, the radial cross-section of the filament near the endplates loses its symmetry and fibrils are formed. The formation of fibrils during filament stretching is very closely related to the peeling and failing of adhesives as has been discussed with respect to roll coating. Welsh also ascertained that the results for extensional viscosity measurements from the filament stretching rheometer should not be sensitive to the

changes in the initial aspect ratio, but that the total work of adhesion is sensitive to such changes.

Computational Rheometry and numerical analyses have been used in filament stretching Rheometry to confirm that true homogeneous uniaxial elongation can be achieved. One of the main theories used is that of the lubrication theory, also used for describing the flow in many roll coating analyses, along with different constitutive models. Yau et al. (1998) have shown axial profiles for transient uniaxial elongation of fluid filaments with three different constitutive equations, namely Newtonian, Oldroyd-B and Giesekus models. Spiegelberg et al (1996) showed that for Newtonian fluids and small initial aspect ratios the liquid bridge can be approximated by the lubrication theory.

Another theory that is commonly used in the literature is the slender-body theory, in this theory the filament is taken as a one-dimensional system. The model can be assumed to be one-dimensional for the majority of the filaments history since the endplate separation, $L_p(t)$, causes rapid decreasing of the mid-filament diameter $D_{mid}(t)$. However near the endplates two-dimensional shearing arises due to the axial curvature and no-slip boundary conditions imposed there; hence this approximation does not capture these kinematics. It has been noted that the axial curvature is negligible for aspect ratios less than or equal to one. Yau et al (1998) have shown that a good approximation to the overall flow is still generated by the use of the slender body experiment.

Some of the failing mechanisms in polymeric liquids have been reviewed by Malkin and Petrie (1997). The ‘necking’ and filament failure during the transient uniaxial elongation of viscoelastic fluid samples in extensional rheometers has been analysed by McKinley (1998). As the filament is stretched a viscoelastic fluid undergoes molecular relaxation, the limit of this relaxation results in filament failure. The energy gained before this breakup is stored elastically and the Considéré criterion is used to calculate the Hencky strain before failure. Their work looks at constitutive conditions for branched polymer melts such as the Doi-Edwards and the Pom-Pom models. These numerical calculations predict the onset of necking and suggest the possibility of determining the optimal operating conditions for strong uniaxial extensional flows. Recent work by Anna et al (2001) looked at the comparison of filament stretching rheometers across different laboratories and shows that there is good relationship with results for the Trouton ratio and hence shows it to be a reliable method of measuring the response of viscoelastic fluids.

The CaBER experiment has been used by many different workers on the extensional properties of polymeric systems, including Rodd et al. (2005), Anna and McKinley (2000) and Wunderlich et al. (2000).

The surface tension of the liquid filament is one of the main parameters that ‘holds’ the filament together before rupture. The extensional stress on the filament can be given by,

$$\tau_E = \frac{2\sigma}{D_{mid}}$$

where D_{mid} is the diameter of the filament just prior to break-up.

From the foregoing work, described above, it is evident that many important associations exist between the cavitation properties of fluids (in terms of their response and ultimate failure under imposed tensile stresses) and their extensional flow properties. These associations require careful consideration in relation to the behaviour of fluids in industrial processes (such as those outlined above) in which cavitation and filamentation may both result from the generation and application of tension in flow settings. What is also evident however is that no appropriate systematic experimental study has been conducted which enables the relationship between cavitation properties (such as cavitation resistance or tensile strength) and extensional flow properties to be explored and elucidated. The principal reason underlying the lack of such a study is that, until now, no appropriate cavitation technique has been identified or applied in this area. The work presented in this thesis addresses this situation by introducing two custom-built instruments (a filament stretching device for extensional flow work and a dynamic stressing shock tube technique for cavitation studies). Together, these instruments are used herein to investigate the appropriate rheological and cavitation characteristics of a range of fluids including model polymer solutions. The results, which are described in later chapters, are the first to be reported for such a study and present a new experimental basis for assessing the performance of low shear viscosity, non-Newtonian fluids in high strain rate / high (tensile) stressing rate regimes.

CHAPTER 2

Materials and Bullet-Piston Technique

Chapter 2

Materials and Bullet-Piston Technique

2.1 Introduction

The investigation into the tensile properties of polymeric solutions has been conducted within this thesis by the means of two main dynamic stressing experiments: the modified bullet-piston (B-P) technique and a Capillary Break-up Extensional Rheometer (CaBER). The first of which, the bullet-piston technique, will be discussed in this chapter with subsequent chapters 3 and 4 discussing results obtained via this method on water and polymeric solutions respectively. The CaBER experiment will be discussed in more detail in Chapter 5 alongside the results obtained on the same polymeric samples as for the B-P technique in chapter 4.

2.2 Materials

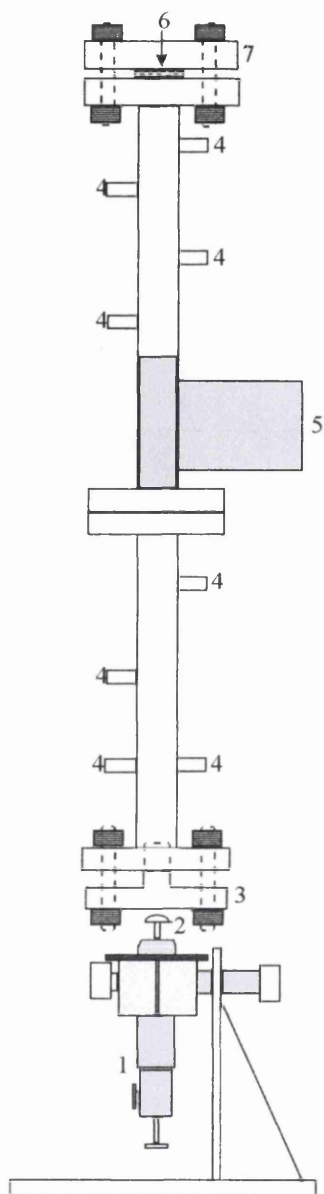
Polyethylene glycol (PEG) is a hydrophilic non-ionic polymer used in many biological and industrial applications. PEG is a non-toxic polymer and is used in the cosmetic, pharmaceutical and food industries. It is most commonly used as a binding agent in gels and pastes and to alter the shear characteristics of a fluid such as ink. In ink-jet printing about 5% of the ink is made of up of polymers which are used to increase the shear viscosity of the ink to around 10 centipoise, measured over a range of 10-500 s⁻¹.

The polymers used were obtained from Fisher (1500 and 6000 Mw) and Sigma-Aldrich (600, 10000 and 20000 Mw). PEG is soluble in water and for these experiments was dissolved in purified water and mixed with a rotational mixer for 8-16 hours to ensure complete solubility.

PEG is commonly used within industry and especially in the printing industry. The effects on the shear characteristics with increased polymer concentration are known but an extensive study into the tensile properties of these fluids has yet to be completed. This thesis will show a systematic testing of PEG over a range of Molecular weights and concentration.

2.3 Bullet-piston apparatus

The current bullet-piston apparatus, is based on the instrument described by Williams and Williams (2000), and consists of a cylindrical stainless steel tube of length 1.4 m and an internal diameter of 0.0243 m with the lower end closed by a piston. A schematic figure and picture are shown below (figures 2.1 & 2.2). The piston's base surface is coupled to the bolt of a cartridge driven stun-gun (Shelby and Volkes, UK, 'Magnum' model 7000) which on impact generates a pressure pulse in a column of liquid within the tube. The upper steel flange permits connection of the tube to a high pressure steam line, a vacuum line (-1 Bar) and a regulated pressure line which is connected to an oxygen-free nitrogen supply and a pressure gauge (PSITronix, USA).



- 1 Magnum model 7000
cattle stun gun
- 2 Mushroom-headed cosh
- 3 Steel piston
- 4 Transducer ports
- 5 Support arm
- 6 Sealing gasket
- 7 Sealing flange

Figure 2.1. Schematic of bullet-piston apparatus

The tube is locked to restraining lugs and is supported by a steel arm, which absorbs some of the pressure applied to the system, on a counter-weighted aluminium stand.

When the stun-gun is fired in operational procedure the piston is forced upwards (relative to the tube) by the movement of the cosh, this generates a compression pulse in the liquid. A typical pressure pulse generated would last for around 300 μs , with a rise time to peak amplitude in the order of 50-100 μs .

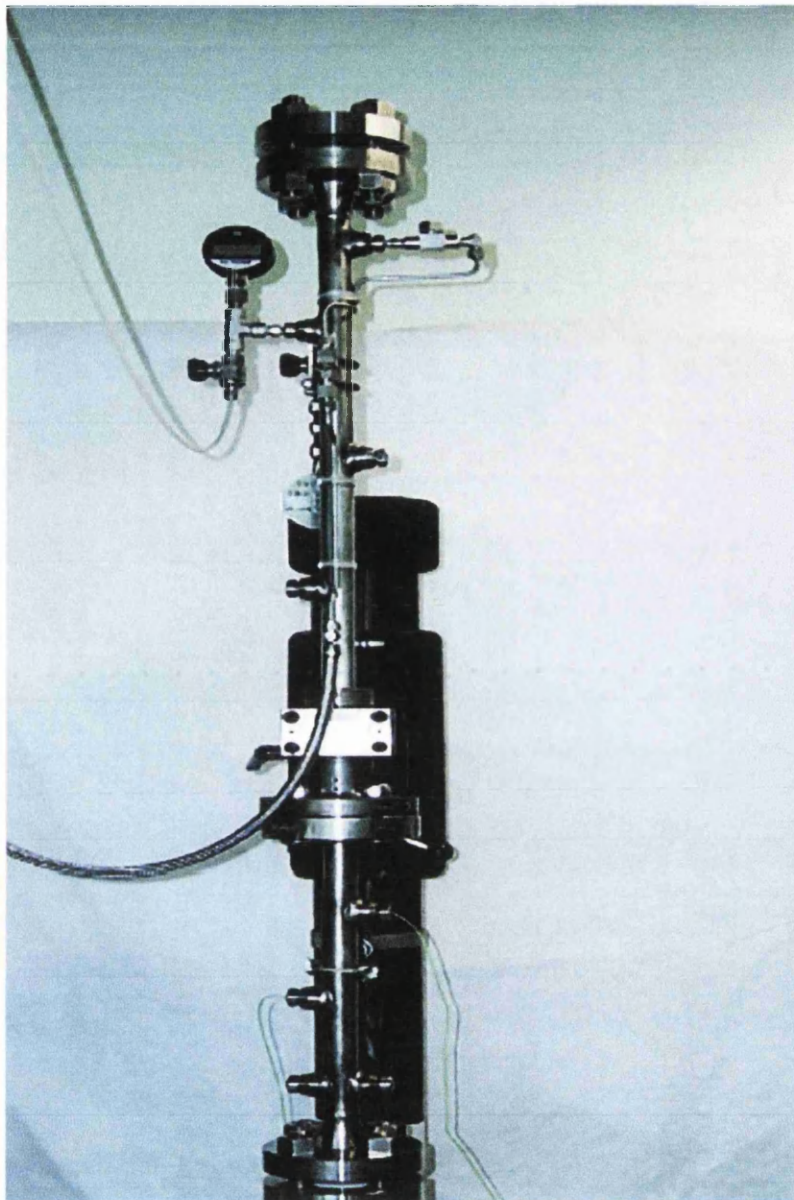


Figure 2.2 The B-P apparatus

The pressure transducers used in the current tube arrest apparatus are Kistler type 603B (Kistler Ltd, Switzerland). These transducers have a dynamic pressure range of up to 200 Bar, with a rise time of ca. 1 μ s and a natural frequency of > 400 kHz. The measuring element in construction has a built-in stability against both thermal and mechanical shocks. When the pressure is transmitted through the silicone oil fitting,

shocks are reduced before reaching the measuring cell. Shocks of 1 kg are easily absorbed. These pressure transducers change pressure into an electrical signal by deforming a diaphragm manufactured from monocrystalline silicon, the pressure being exerted on one side.



Figure 2.3 Image of pressure transducer Kistler 603B

The pressure transducers are mounted within the walls of the tubes (#4 in figure 2.1). The output voltages of the transducers were recorded by a high speed acquisition system (Microlink 4000; BioData Uk Ltd) specifically designed for the capture of rapid transient signals. The transducer output voltage was sampled at 1 MHz by a 12-bit analogue to digital converter with an 8 MB memory buffer. The pressure records were transferred to a PC-AT microcomputer for analysis using signal processing software (DADiSP; DSP Corp., USA).

To ensure that there is no metal-to-metal connection during this experiment we position a high density rubber disc at the base of the lower piston fixed by an adhesive, this ensures that no damage to the apparatus can occur. Also a plastic ‘O’-

ring is used around the piston to ensure the bottom flange does not directly hit the static upper flange.

Temperature control on the rig was achieved by the combination of a heating coil and a refrigeration unit. The refrigeration unit consists of a TAE M10 water cooler (M.T.A. SRL, Italy) connected to a double copper coil (OD 5 mm) tightly wound around the steel tube of the B-P apparatus. Coolant liquid is then circulated around the coil, this liquid being Go Therm AF200 (Linde, UK) which contains 1,2 propanediol, enabling a temperature range of -15°C to room temperature (25°C). Heating tape (100W/m at 230 V) is also used for the temperature control to obtain temperature up to 135°C (see figure 2.4). This tape is closely wrapped around the cooling coils on the B-P apparatus. The operating temperatures for this apparatus are therefore between -15°C and 115°C . To provide insulation and heating efficiency the heating and cooling tapes are surrounded by Armourflex lagging (IPS Ltd., UK). The temperature measurements were made by the use of thermocouples, (Jenway, UK), at the tubes inner surface. The temperature was recorded at different heights over the liquid column within the tube and minimal variation was observed.

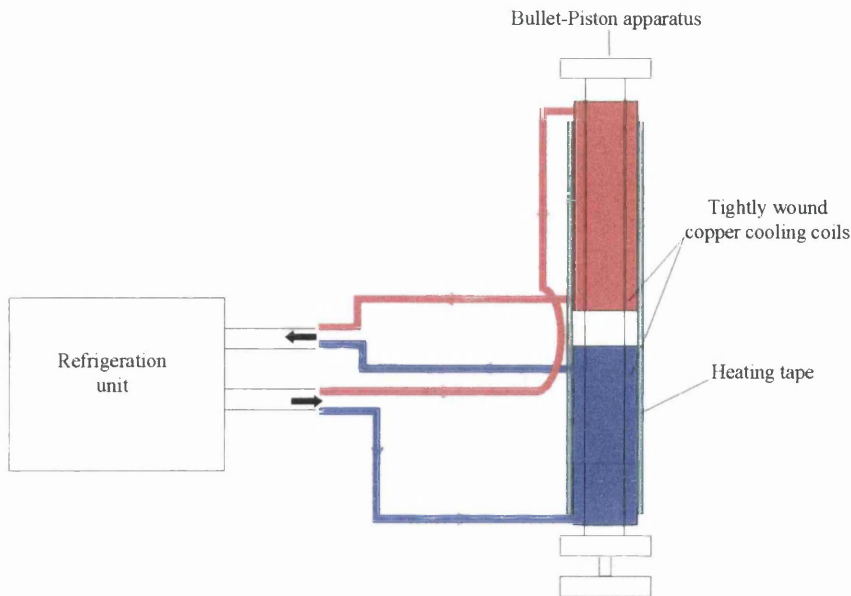


Figure 2.4 Schematic of heating/cooling system.

For cleaning purposes the upper steel flange connects the tube to a high pressure steam line. The lower flange can incorporate a steam condensation system and a liquid drain point. Prior to experiments, superheated (110°C) steam is blown through the tube, ensuring that all oil particles are removed from the walls of the tube. Cleaning of the tube is also done by the use of domestic cleaning products and a soft brush pushed up and down the inside of the steel tube, with subsequent steam to take away the cleaning products. When the sample is changed the steel plugs, which are screwed into the transducer ports in the walls, are removed, checked, inspected and then returned or replaced. The walls of the open tube are then allowed to dry by applying heat up to 100°C . Following this procedure the tube was allowed to cool prior to being refilled to the required depth with a fresh sample of the test liquid. The sample is kept in situ for 90 minutes prior to the first measurement and 30 minutes in between each subsequent measurement to allow the sample to rest. The upper flange is also connected to a vacuum line and a regulated pressure line, the latter being connected to an oxygen-free nitrogen supply and a pressure gauge. This part of the

apparatus allows a recorded increased static pressure to be applied over the liquid sample.

2.3.1 Operation

Within the modified B-P apparatus a pressure pulse is generated by the bullet striking the piston. This piston is forced upwards generating the pressure pulse through the liquid sample within the tube. At the top of the liquid column the pressure pulse is reflected. As the pressure pulse returns as tension, the liquid is pulled downward to the bottom of the tube and it eventually ruptures due to it being unable to sustain the tension, and cavitation bubbles are formed. Due to the compression of the liquid these cavitation bubbles collapse. This in turn emits a pressure wave to the surroundings and is again reflected as a tension pulse from the base of the tube, causing the bubble to grow under this tension. This process repeats itself with the bubble growth and subsequent collapse until the energy is dissipated into the surroundings.

2.3.2 Typical results

A typical pressure record is shown in figure 2.4, which shows the typical features of a pressure pulse, and is measured with a Kistler 603B dynamic pressure transducer. The incident pressure pulse, generated by the lower piston being pushed into the liquid column by the resultant action of the stun-gun, is represented by feature '1' in figure 2.5. This is immediately followed by a pulse of tension, feature '2', from the reflection of the incident pressure pulse at the free surface. This cycle '1-2' is referred to as the 'primary' pressure-tension cycle with the following cycles ('3-4', '5-6', etc.)

known as the ‘secondary’ cycles. The presence of these subsequent cycles has been attributed, within dynamic stressing experiments, to cavitation activity within the liquid column. (Williams et al. 2002, 2003).

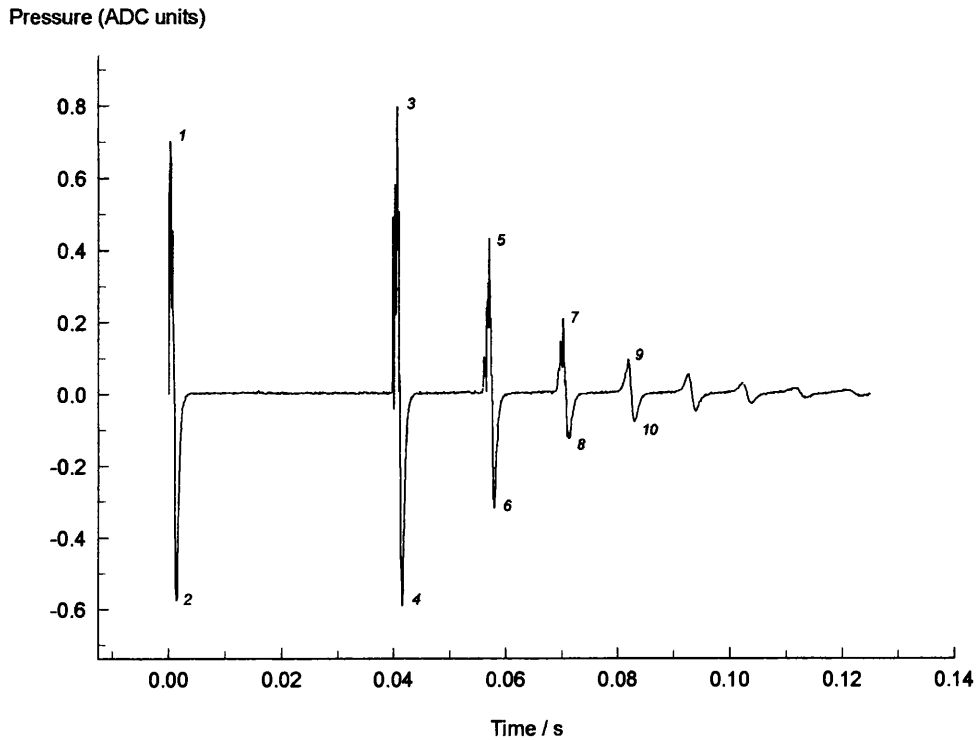


Figure 2.5 A typical pressure record showing the primary (‘1-2’) and secondary pressure cycles (‘3-4’, ‘5-6’, etc.)

The B-P method used involves regulating a static pressure, P_s , in the space above the liquid column. This static pressure is increased gradually in a series of dynamic stressing experiments. From the dynamic pressure measurements obtained in these experiments a record is made of the time delay, τ_i , between the peak incident pressure (‘1’ in figure 2.5) and the first pressure pulse arising from cavitation bubble collapse (‘3’ in figure 2.5) an expanded view of this can be seen in figure 2.6. What is actually recorded here is the process of a cavitation bubble, growing from pre-existing

nuclei, under tension. The bubble grows and then subsequently collapses and rebounds, emitting a pressure wave into the liquid as it does so. Each subsequent growth and collapse is shown in the pressure cycles seen in figure 2.5. Hence the interval τ_i , which encompasses the attainment of maximum cavity radius and its subsequent decrease to a minimum value, is reduced by increasing P_s (τ_i therefore provides a convenient measure of cavitation activity). In order to understand this important point fully it is necessary to briefly consider some pertinent aspects of cavitation bubble dynamics.

2.4 Bubble dynamics

Several accounts of this topic are available and the following section closely follows the review by Plesset and Prosperetti (1977). In terms of the dynamics of vapour bubbles, we consider separately those bubbles formed in subcooled and superheated liquids, respectively. In the former case, the low vapor density means that latent heat flow does not affect the bubble's motion, which is inertially controlled: in this case the liquid is described as cavitating. The opposite condition prevails in the case of boiling phenomena.

Rayleigh (1917) studied the collapse of an empty cavity in a large mass of incompressible liquid. Neglecting surface tension and viscosity, he showed that the bubble boundary $R(t)$ obeyed the relation

$$R\dot{R} + \frac{3}{2}(R)^2 = \frac{p(R) - p_\infty}{\rho} \quad [2.1]$$

where ρ is the liquid density, p_∞ is the pressure in the liquid at a large distance from the bubble, and $p(R)$ is the pressure in the liquid at the bubble boundary. Assuming incompressibility, the liquid velocity at a distance r from the bubble centre is given by,

$$u(r,t) = \frac{R^2}{r^2} \dot{R} \quad [2.2]$$

The pressure in the liquid is found from the general Bernoulli equation to be

$$p(r,t) = p_\infty + \frac{R}{r} [p(R) - p_\infty] + \frac{1}{2} \rho \frac{R}{r} \dot{R}^2 \left[1 - \left(\frac{R}{r} \right)^3 \right] \quad [2.3]$$

where the pressure p_∞ is constant. Equation [2.1] may be extended to include the effects of surface tension σ and viscosity, μ . For a spherical bubble, viscosity affects only the boundary condition so that it becomes,

$$p(R) = p_i - \frac{2\sigma}{R} - \frac{4\mu}{R} \dot{R} \quad [2.4]$$

where p_i is the pressure in the bubble. Plesset (1949) extended Equation [2.1] by allowing p_∞ to be a function of time. Thus the generalized Rayleigh equation may be written as

$$R\ddot{R} + \frac{3}{2}(R)^2 = \frac{1}{\rho} \left\{ p_i - p_\infty - \frac{2\sigma}{R} - \frac{4\mu}{R} \dot{R} \right\} \quad [2.5]$$

where the pressure in the gas at the bubble wall, p_i (and p_{inf}) may be a function of time.

We consider first the dynamics of gas bubbles, whose content is a permanent, noncondensable gas. Minnaert (1933) reported the first study of the small-amplitude (linearized) oscillations of a permanent gas bubble in a liquid. His work involved the

forced radial oscillations of a bubble which may arise when it is immersed in an alternating pressure field whose wavelength is large compared with the bubble radius. The pressure field is introduced in the Rayleigh equation as

$$p_{\infty}(t) = P_{\infty}(i + \varepsilon \cos \omega t) \quad [2.6]$$

where P_{∞} is the average ambient pressure, ω is the sound frequency, and ε is the dimensionless amplitude of the pressure variation. The oscillations take place about the equilibrium radius R_0 given by

$$R_0 = \frac{2\sigma}{p_i - p_{\infty}} \quad [2.7]$$

so that one may write

$$R = R_0[1 + x(t)] \quad [2.8]$$

The natural frequency of the bubble, ω_0 , is given by

$$\omega_0^2 = 3\kappa \frac{p_{i,eq}}{\rho R_0^2} - \frac{2\sigma}{\rho R_0^3} \quad [2.9]$$

in which κ is the polytropic exponent where

$$p_i = p_{i,eq} \left(\frac{R_0}{R}\right)^{3\kappa} \quad [2.10]$$

and energy dissipation arises only from liquid viscosity and compressibility. The results of an analysis involving the complete set of linearized conservation equations of mass, momentum and energy, may be summarised as follows (see Plesset and Hsieh 1960; Prosperetti 1976). There are essentially three length scales involved, namely, the bubble radius R_0 , the wavelength of sound in the gas λ_g , and the thermal penetration depth in the gas, L_{th} . If R_0/λ_g is small, the pressure within the bubble is spatially uniform, leading to isothermal behaviour. Adiabatic behaviour corresponds to the case where $R_0 \gg L_{th}$. In the first case, the oscillations are too slow to maintain

an appreciable temperature gradient in the bubble, whereas in the latter they are so fast that most of the gas contained in the bubble is practically thermally insulated from the liquid. For sufficiently high frequencies such that λ_g is of the order of R_0 , pressure non-uniformities develop in the bubble and a polytropic pressure-volume relationship loses its thermodynamic meaning. Except for very small bubbles for which viscosity is very important, the low-frequency damping is dominated by thermal effects, whilst the high-frequency damping is due to acoustic effects.

2.4.1 Nonlinear oscillations

In an oscillating pressure field, equation [2.5] takes the following form:

$$R\ddot{R} + \frac{3}{2}(\dot{R})^2 = \frac{1}{\rho} \left(p_{i,eq} \frac{R_0}{R} \right)^{3x} - p_\infty (1 - \eta \cos \omega t) - \frac{2\sigma}{R} - 4\mu \frac{1}{R} \dot{R} \quad [2.11]$$

where, polytropic behaviour is assumed. For large bubbles, such as those produced by underwater explosions, the most significant damping mechanism is acoustic energy radiation and therefore equation [2.1] cannot be used (Hoyt 1977). Noltingk and Neppiras (1950) demonstrated that very rapid growth followed by a violent collapse to very small values of the radius could occur within a single period of the driving force. Lauterborn (1976) has studied the behaviour of an air bubble of radius $R_0 = 10^{-3}$ cm in water under a static pressure $P_{inf} = 1$ Bar and has reported the resonances that accompany the increasing pressure amplitude and the complicated effects of the initial conditions on the ensuing oscillatory motion, including subharmonic components. But it is not possible to express in a simple way the relation between the initial conditions and the value of the amplitudes in the steady-state oscillations, particularly as a small

change in the initial conditions can cause markedly different transients and steady-state motions.

Other studies of equation [2.1] have been reported, including the case of free oscillations with and without viscous effects (Prosperetti 1975). Flynn (1975*a,b*) reported a formulation of the general problem of cavitation dynamics, including an analysis of the gas behaviour and large-amplitude free oscillations. Fujikawa and Akamatsu (1980) studied the effects of liquid compressibility, non-equilibrium vapour condensation, intracavity heat conduction and the temperature discontinuity at the phase interface.

2.4.2 Mass-diffusion effects

The presence or absence of gas bubbles in a liquid and their behaviour are in part determined by mass-diffusion across the bubble-liquid interface. Henry's law relates the partial pressure of a gas acting on a liquid surface, p_g , and the saturation gas concentration in the liquid denoted by c_s :

$$c_s = ap_g \quad [2.12]$$

Here a is a constant characteristic of the particular gas-liquid combination and is primarily a function of temperature. Equation [2.2] is valid also at a nonplane interface. The pressure p_g is determined from the dynamical Rayleigh equation but we first consider a situation in which the ambient pressure is fixed and equal to P_{inf} , then, unless the gas concentration c at the bubble surface satisfies equation [2.2] the bubble will not be in equilibrium, and it will either grow or shrink according to whether $c > c_s$ or $c < c_s$.

In an oscillating pressure field a bubble may grow even in an under-saturated solution. If the oscillation amplitude is large enough so that the gas-liquid solution at the bubble surface becomes under-saturated during the compression half-cycle and supersaturated during the expansion half-cycle then a mass exchange of alternating direction takes place between the bubble and the liquid. The average flux over one oscillation is zero in the case of a plane interface but for a spherical bubble the surface area is on average greater during the mass inflow than during outflow, resulting in a net increase in the mass of gas within the bubble. This rectified mass diffusion (Blake 1949), is augmented by decreasing thickness of the diffusion layer adjacent to the bubble surface during the expansion half-cycle and its increase during the compression half-cycle.

When the liquid is not saturated, the bubble eventually disappears if the mass flux caused by rectified mass diffusion does not balance the loss of mass required by Henry's law. The amplitude at which the two fluxes are equal gives the threshold for bubble growth by rectified diffusion.

2.4.3 Cavitation bubbles and vapour bubbles

For a predominantly vapourous bubble, which grows rapidly to many times its initial size, mass-diffusion effects are negligible and the gas content only plays an important role in the final stages of an ensuing collapse. As noted above, we may distinguish between cavitation bubbles and those formed in boiling phenomena. In the latter, thermal (not inertial) effects dominate bubble growth. The former is referred to as

cavitation bubbles and the latter as ‘boiling’ or ‘vapour’ bubbles. For a cavitation bubble, the internal pressure remains practically constant until the final stages of collapse but a much greater vapour pressure effect is obtained in the case of a boiling bubble. Hereafter focus is turned to the dynamics of a cavitation bubble, for which Equation [2.5] gives

$$\dot{R}^2 = \left(\frac{R_0}{R}\right) \dot{R}_0^2 + \frac{2}{3} \frac{p_r - p_\infty}{\rho} \left[1 - \left(\frac{R_0}{R}\right)^3 - \frac{2\sigma}{\rho R} \left[1 - \left(\frac{R_0}{R}\right)^2 \right] \right] \quad [2.13]$$

i.e. neglecting viscous effects and taking the ambient pressure to be independent of time and with constant internal pressure. The subscript zero denotes the initial conditions for growth. If $p_v > p_\infty$ it is seen that for $R \gg R_0$ the velocity is approximately equal to its asymptotic value

$$\dot{R} = \left(\frac{2}{3} \frac{p_r - p_\infty}{\rho} \right)^{\frac{1}{2}} \quad [2.14]$$

If $p_v > p_\infty$, but an initial impulse is imparted to the bubble wall, equation [2.3] predicts that the bubble would reach a maximum radius that, neglecting surface tension, is given by

$$R = \left[1 + \frac{3}{2} \rho \dot{R}^2 (p_\infty - p_v)^{-1} \right] R_0 \quad [2.15]$$

Under the same assumptions one can obtain an expression similar to [2.3], valid for the collapse of the bubble starting from some initial radius R_i . If the initial velocity is taken to vanish, one has

$$\dot{R}^2 = \frac{2}{3} \frac{p_\infty - p_v}{\rho} \left[\left(\frac{R_0}{R} \right)^3 - 1 \right] + \frac{2\sigma}{\rho R} \left[\left(\frac{R_i}{R} \right)^2 - 1 \right] \quad [2.16]$$

In the absence of surface-tension effects, Equation [2.6] gives the time required for complete collapse:

$$t_0 = \frac{\Gamma\left(\frac{5}{6}\right)}{\Gamma\left(\frac{1}{3}\right)} \left[\frac{3\pi\rho}{2(p_\infty - p_v)} \right]^{\frac{1}{2}} R_i \cong 0.915 \left(\frac{\rho}{p_\infty - p_v} \right)^{\frac{1}{2}} R_i \quad [2.17]$$

which is Rayleigh's result. Experimental confirmation of the collapse time predicted by equation [2.7] (*ca.* 300 μ sec for a 0.378 cm bubble in water) has been reported by Lauterborn (1972a).

An important feature of the collapse stage is that, due to instability, analyses which assume spherical symmetry are inaccurate. Equation [2.6] predicts a velocity which approaches infinity as $R^{-3/2}$ as $R \rightarrow 0$. This non physical behaviour is principally due to the neglect of liquid compressibility which is significant for a bubble-wall velocity comparable with the speed of sound in the liquid. A modification of the Rayleigh equation which takes into account liquid compressibility was obtained by Gilmore (1952). The result is that $R \propto R^{-1/2}$ as $R \rightarrow 0$, in contrast to the incompressible approximation.

Hickling and Plesset (1964) analysed the effects of liquid compressibility numerically. A significant feature of their analysis, which continued past the bubble's rebound, was the formation of a shock wave in the liquid. The peak pressure had an approximate $1/r$ dependence during the rebound, with cavity pressures of tens of kilobars. Due to the expansion wave produced during collapse, the Kirkwood-Bethe approximation gives good results up to relatively large Mach numbers but for bubble growth at very large velocities the same accuracy could not be expected, due to the propagation of a shock wave into the liquid. Prosperetti and Lezzi (1986) discuss modifications to the Rayleigh-Plesset equation which are accurate up to Mach numbers of *ca* 0.3. Another shortcoming of equation [2.6] is the neglect of the variation of p_v due to the fact that condensation of the vapour cannot keep up with the bubble-wall motion when its velocity becomes of the order of the speed of sound in the vapour.

Hsieh (1970) obtained approximate analytic expressions for the maximum cavity radius in a viscous liquid subject to a transient pressure pulse. Flynn (1982) has reported numerical investigations into the behaviour of small bubbles in a liquid such as water when exposed to microsecond duration pulses of ultrasound. He considers the differences in maximum collapse pressures associated with stable and transient cavities. Whereas the collapse of a stable cavity would result in the generation of a pressure of *ca* 100 bars (at minimum radius), the maximum pressure in a collapsed transient cavity p_m may be many orders of magnitude higher. A significant conclusion is that, for small values of the initial radius R_n , there may exist a well-defined pressure amplitude P_t at which a nucleus will grow explosively into a transient cavity. This

critical pressure is called the pressure threshold for transient cavitation at which a small change in the pressure amplitude P_A causes a very large change in p_m .

Thresholds for transient cavitation have been reported by Flynn (1975a) who partitioned the acceleration dU/dt of the cavity interface into an inertial and a pressure acceleration function, IF and PF , respectively. The former is governed by the term $-3U^2/2R$ in the equation of motion of the cavity and the latter is the sum of all pressure terms in the same equation. As a cavity contracts from its maximum radius R_m , the function PF at first becomes negative, reaches a minimum and then becomes positive, ultimately arresting the inward motion of the interface. IF is always negative and its magnitude increases as the collapse speed increases and the cavity radius decreases. In the expansion of a cavity of initial radius R_n , there exists a critical value of the maximum radius R_m such that, for R_m less than this critical value, the entire cavity motion is controlled by PF and the cavity is called a stable cavity. When P_A causes R_m to exceed this critical value, the motion is controlled during most of its contraction by IF and the cavity is called a transient cavity. At this critical value of P_A , the plot of IF as a function of R_m intersects a similar plot of PF at the minimum of PF . The pressure threshold P_t is then that value of P_A for which IF intersects PF at its minimum.

Flynn (1982) notes that thresholds are significant in the prediction of transient cavitation because, if a threshold exists, transient cavitation can be produced by pressures much less than might otherwise be required. The example is given of a nucleus with a radius of $0.5 \mu\text{m}$ which does not have a threshold at a frequency f_A of 10 MHz but does have one at 1 MHz. At 1 MHz, such a nucleus grows explosively

under a microsecond pulse of sinusoidal waves with a Gaussian envelope creating pressure amplitude of 2.2 Bar: the resulting collapse produces a maximum pressure p_m of 4 kBar (the pulse used in these calculations has a negative pressure peak of magnitude P_A , followed by a positive peak of the same magnitude). At 10 MHz, the growth and collapse of a 0.5 μm nucleus would result in a maximum pressure of 4 kBar only when P_A is increased to 12 Bar. When a well-defined threshold for transient cavitation exists, it is possible that microsecond pulses of ultrasound will produce transient cavities at pressure amplitudes much less than would be anticipated from estimates based on the pressure applied on the cavity. Acoustic cavitation produced by such pulses has been reported in experiments by Crum and Fowlkes (1986).

It is interesting to note some of the general statements made by Flynn (1982) concerning the nature of cavitation produced by a microsecond pulse of ultrasound – particularly in relation to the pressures and temperatures resulting from bubble collapse. At $f_A = 1$ MHz and $P_A = 6$ Bar, a nucleus with $R_n = 1$ μm will expand to a maximum radius of $7.4 R_n$: the collapse is estimated to produce a maximum pressure of 28 kBar and a maximum temperature of 10^4 °K. Typically the maximum temperature lasts for less than a nanosecond. In a frequency range 1 – 10 MHz, only nuclei with $R_n < 2\text{--}3$ μm will grow explosively into transient cavities and the maximum size of nuclei for which there is a well-defined threshold decreases as f_A increases. At a given frequency and pressure amplitude the maximum pressure increases as R_n decreases. Furthermore, at a given initial radius R_n and pressure amplitude, p_m increases as f_A is decreased.

2.4.4 Spherical bubbles in non-Newtonian fluids

Fruman (1999) has reported the results of integrating the generalized Rayleigh-Plesset equation [2.5] incorporating the following integral term to represent the viscous stress,

$$3 \int_R^{\infty} \left(\frac{\tau_{rr}}{r} \right) dr = -4 \left(2\sqrt{3}^{-n-1} \frac{m}{n} \left| \frac{\dot{R}}{R} \right|^{n-1} \frac{\dot{R}}{R} \right) = \eta(R, \dot{R}, m, n) \frac{\dot{R}}{R} \quad [2.18]$$

where m and n are the power law parameters and $\eta(R, \dot{R}, m, n)$ is the apparent viscosity. The results of a rapid pressure variation were compared in a Newtonian fluid and three different power-law fluids. Despite considerable differences in η , the temporal evolution of the bubble's radius was found to be practically indistinguishable from the Newtonian situation. Fogler and Goddard (1970) reported large elastic effects on the temporal evolution of spherical bubbles in viscoelastic fluids but later works conclude that viscoelasticity has a very limited retardation effect on bubble growth and collapse in dilute polymer solutions e.g. see Ting (1977). These later findings are supported by Ryskin (1990), who concludes that bubble growth is unaffected by the polymer, but that the final stage of collapse is.

Kim (1994) has reported numerical studies of spherical bubbles in Maxwell fluids in which the Reynolds number Re and Deborah number De were defined as $Re = R_0(\rho p_0)^{1/2} / \eta$ and $De = \lambda / T$, and p_0 is the uniform pressure in the fluid, R_0 is the initial bubble radius, T is the Rayleigh time scale and λ and η are the fluid's relaxation time and viscosity, respectively. While highly oscillatory behaviour of the bubble radius was reported for moderate Re and De over several growth-collapse

rebound cycles, asymptotic behaviour was found for large $ReDe$, and fluid elasticity was found to accelerate the early stages of collapse while retarding its later stages. Kim (1994) argues that this is due to the dominance of inertia in the early stages of collapse, the viscoelastic stresses not having had sufficient time to grow sufficiently, and notes that, even for small De , the viscoelastic stress is significant when the rate of deformation is large.

The behavior of spark generated bubbles in an unbounded fluid, including water, polyethylene oxide (PEO) and Guar Gum solutions have been widely reported (e.g. Chahine 1979). Even at polymer concentrations which invoke marked viscoelastic effects, the bubbles remained spherical during growth and collapse, the duration of the latter phase being equal to the Rayleigh time computed using the maximum radius of the bubble. The time and amplitude of the first and second rebounds were also unaffected. Similar findings have been reported for laser-induced bubbles in solutions of CMC and PAM in which, even at very large polymer concentration, the bubble behavior is little affected by rheological properties other than the infinite-shear viscosity (Brujan *et al.* 1996).

Pearson and Middleman (1977) have described how bubble collapse provides a means to study the elongational flow of polymer solutions and low viscosity melts. The collapse of a single spherical gas bubble within a large body of fluid creates a uniaxial elongational flow in the surrounding fluid, and collapse under constant bubble pressure produces nearly constant strain rate kinematics.

The B-P experiment involves the transmission of a pulse of tension by the liquid to the face of the piston; and that cavitation may result from this pulse. It follows that in the case of experiments in which cavitation activity is detected, the magnitude of the tension transmitted by the liquid is sufficient to result in the development of a transient net negative pressure in the presence of a background static pressure (P_s). Thus an estimate of the magnitude of tension capable of being transmitted by the liquid can be obtained from knowledge of P_s .

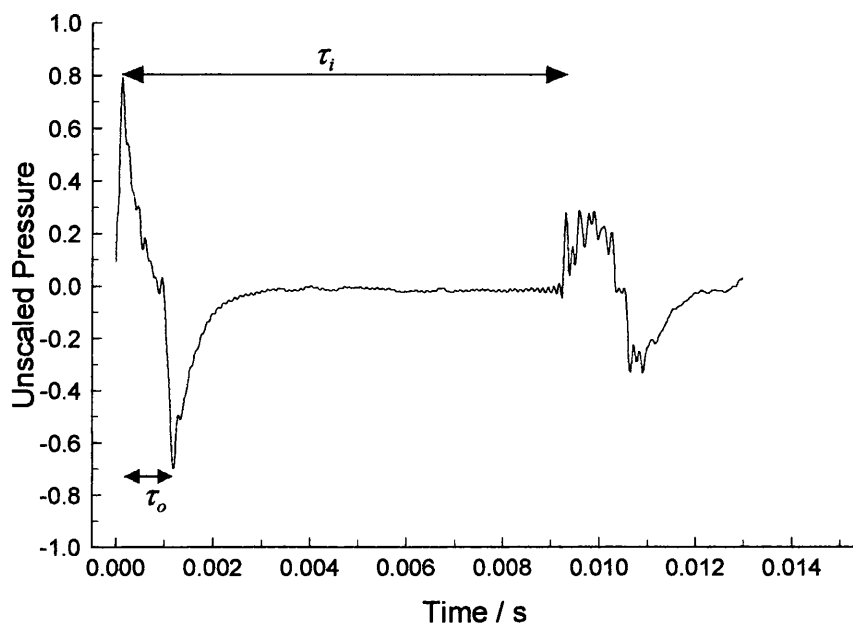


Figure 2.6 Expanded pressure record obtained from a 603B transducer showing the time intervals τ_i and τ_o

The results of such experiments on a mutigrade oil are shown in figure 2.7, in which τ_i is plotted as a function of P_s (absolute, in p.s.i.) and from which F_c is estimated in the following way. The time delay τ_o , between pulses corresponding to '1' and '2' in figure 2.5 and is shown in expanded form in figure 2.6, represents the time required for the upward travelling pressure wave to return, as tension, to the lower transducer's location: it also represents the smallest time interval for which a cavity growth-collapse cycle could occur given that a bubble would have to grow and collapse

infinitely quickly in order that $\tau_i = \tau_o$. Thus F_c is estimated by extrapolation of the data in figure 2.6 to that pressure P_s at which $\tau_i = \tau_o$; this condition represents the complete suppression of cavitation.

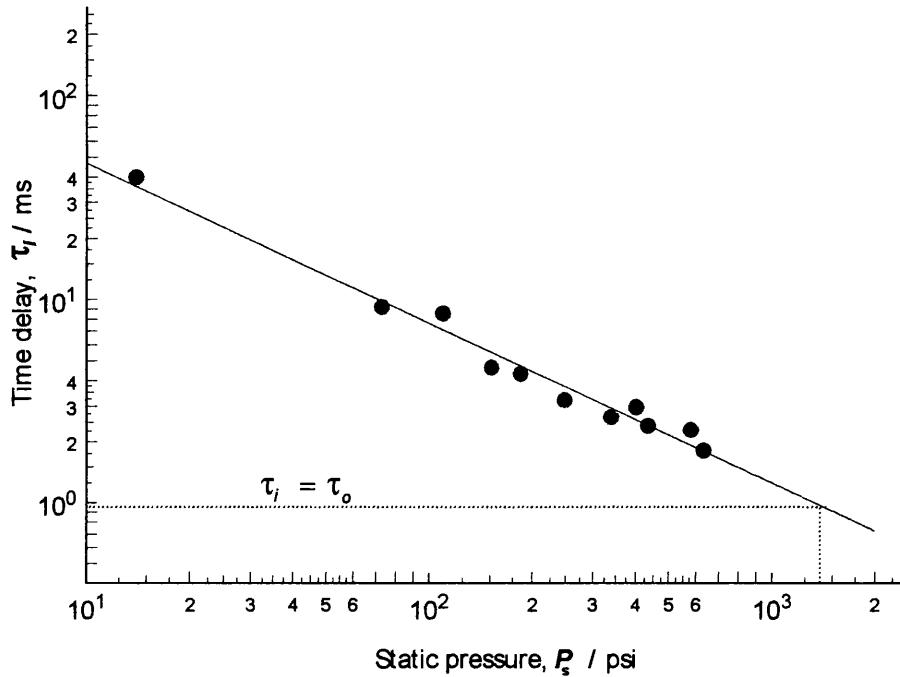


Figure 2.7 The time interval τ_i as a function of applied static pressure, P_s (in p.s.i.) for a petrol-engine oil. Also shown is the time interval τ_o used to estimate F_c .

The following Chapter now reports how this form of the B-P dynamic stressing apparatus has been used herein to investigate the tensile properties of water, as a precursor to using the technique to investigate the properties of a range of non-Newtonian fluids (dilute aqueous polymer solutions over a range of molecular weights and polymer concentrations).

CHAPTER 3

Tensile Properties of Water

Chapter 3

Tensile Properties of Water

3.1 Introduction

It will be recalled from the work reviewed in Chapter 1 that the concept of a well-defined threshold stress for cavitation inception has been extensively studied from a theoretical perspective. The theoretical estimates of the tensile strength of water are in the region of 500 – 1300 Bar (Temperley, 1947; Fisher, 1948) when undergoing homogeneous nucleation, where there is little dependence of F_c on stressing rate (Fisher, 1948). The majority of experimental techniques involve heterogeneous nucleation in which case a dependence of F_c on stressing rate may be expected (Trevena, 1982). Recent reviews of the experimental methods to determine F_c have found two broad groups of experimental results (Herbert and Caupin, 2005; Williams and Williams, 2004). The first group consists of the results of various ‘quartz inclusion’ studies (Zheng et al, 1991) which present values of F_c in the range 800 Bar to 1300 Bar. Such studies, which involve extremely small sample volumes, are thought to involve homogeneous nucleation conditions which give rise to values of F_c close to the theoretical limit. However, these studies rely on long extrapolations into the negative pressure regime. A second group of results involves experiments in which heterogeneous nucleation is responsible for the recorded cavitation events. It is this second group which is the focus of the work reported in the present paper. It consists of the results of experiments involving various techniques which produce values of F_c in the range 50 Bar to 250 Bar (Henderson and Speedy, 1987; Briggs, 1950; Galloway, 1954; Greenspan and Tschiegg, 1967; Jones et al 1981).

There is also a third group of results (Williams and Williams, 2004), containing anomalously low values of F_c , representing the outcomes of dynamic stressing experiments in which a pulse of tension is generated within a liquid by the reflection of a compressional wave at a suitable boundary. In the 'shock tube' work of Richards *et al* (1980), this reflection took place at a flexible membrane while in the 'bullet-piston' (B-P) technique this reflection occurs at the free surface of the liquid. Early B-P work suggested that degassed, distilled water was incapable of sustaining a tension greater than 10 Bar (Davies *et al*, 1956). In subsequent B-P work, Couzens and Trevena (1969) found a value of 8.5 Bar for ordinary tap water and 15 Bar for degassed, purified water, while Couzens and Trevena (1974) and Sedgewick and Trevena (1976) reported values of 10 Bar for purified water. These anomalously low values however can be explained by the pressure transducers and data sampling methods employed (Williams and Williams, 2000).

No satisfactory explanation has been given for the extremely broad range of values represented by the second group of results described above. A principal difficulty in reconciling the results of such studies is clearly the diverse range of experimental techniques employed. Each of these techniques has different characteristics in terms of the corresponding rates of tensile stress development it invokes within a test liquid. It is arguable therefore that what has been lacking is a single technique in which the rate of tensile stress development $\dot{\Omega}_r$ may be varied in a systematic manner in order to investigate its effect on the determination of F_c .

This chapter reports how a modified form of the B-P technique has been used as the basis for such an investigation.

3.2 Dynamic testing of purified water

In most cavitation experiments the basis for all other work is taken from the value obtained for water. The water undergoes filtration and deionisation to remove any impurities in the sample. These impurities if left within the sample can act as nucleation sites and enhance cavitational activity. The next section shows the results obtained for purified water including the pressure tension cycles that were obtained. The modified B-P experiment (as described in chapter 2) was used to carry out a series of experiments at different static pressures with a constant applied stressing rate i.e. the pulse caused by the bullet impact on the piston was always kept constant (results for different stressing rates can be seen in section 3.3). It is worth noting at this point that the stressing rate of the experiment under the modified B-P technique could be closely monitored and changed if necessary. Figures 3.1-3.4 show the pulse-tension cycles that occurred when applying static pressures of 0, 100, 200, 250 psi respectively (these values are the noted gauge pressures, however for actual pressure an additional 14.7 psi was added for the presence of atmospheric pressure). It is clear that the gap between the initial pulse-tension cycle and that of the secondary pulse-tension cycle is reduced as the pressure increases. The timescale on the x-axis is the same for the values for 100, 200 and 250 psi but has been increased for 0 psi.

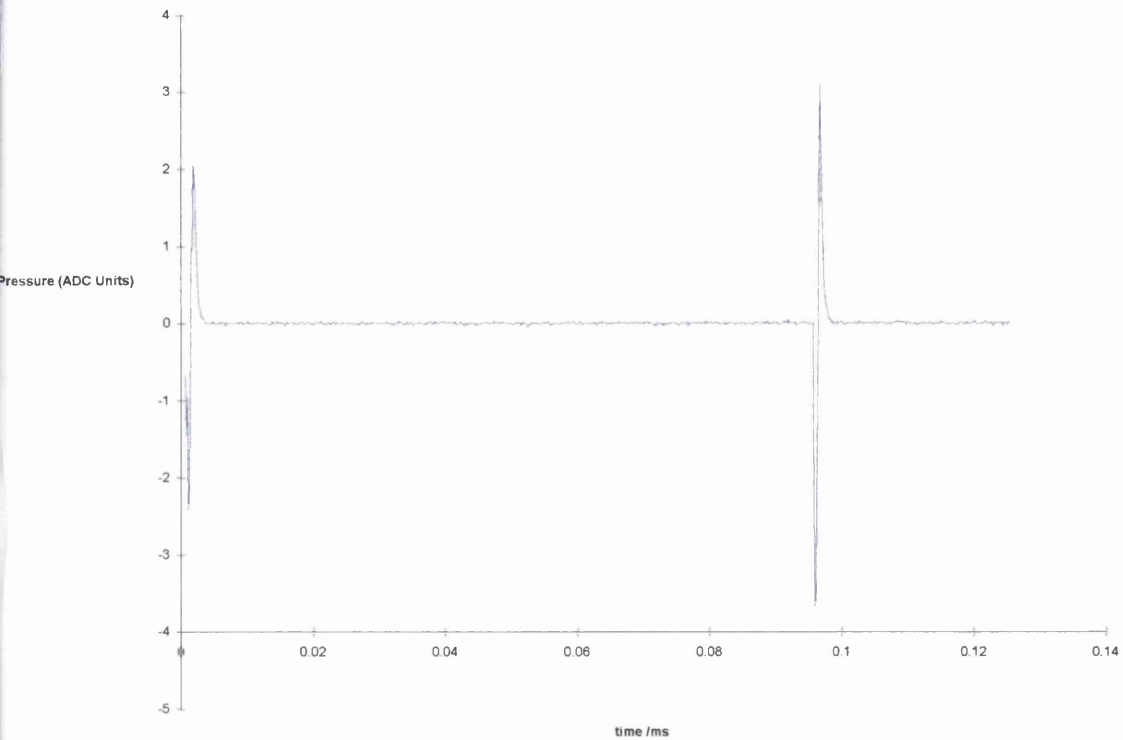


Figure 3.1 Pressure-tension record for purified water at 0 psi

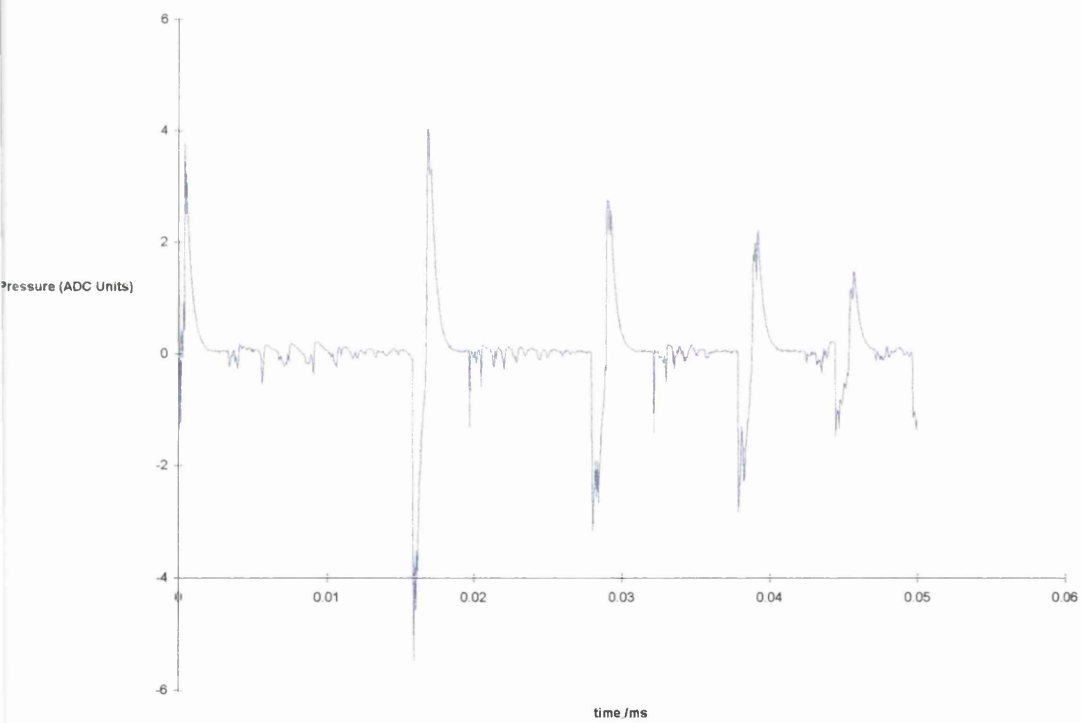


Figure 3.2 Pressure-tension record for purified water at 100 psi

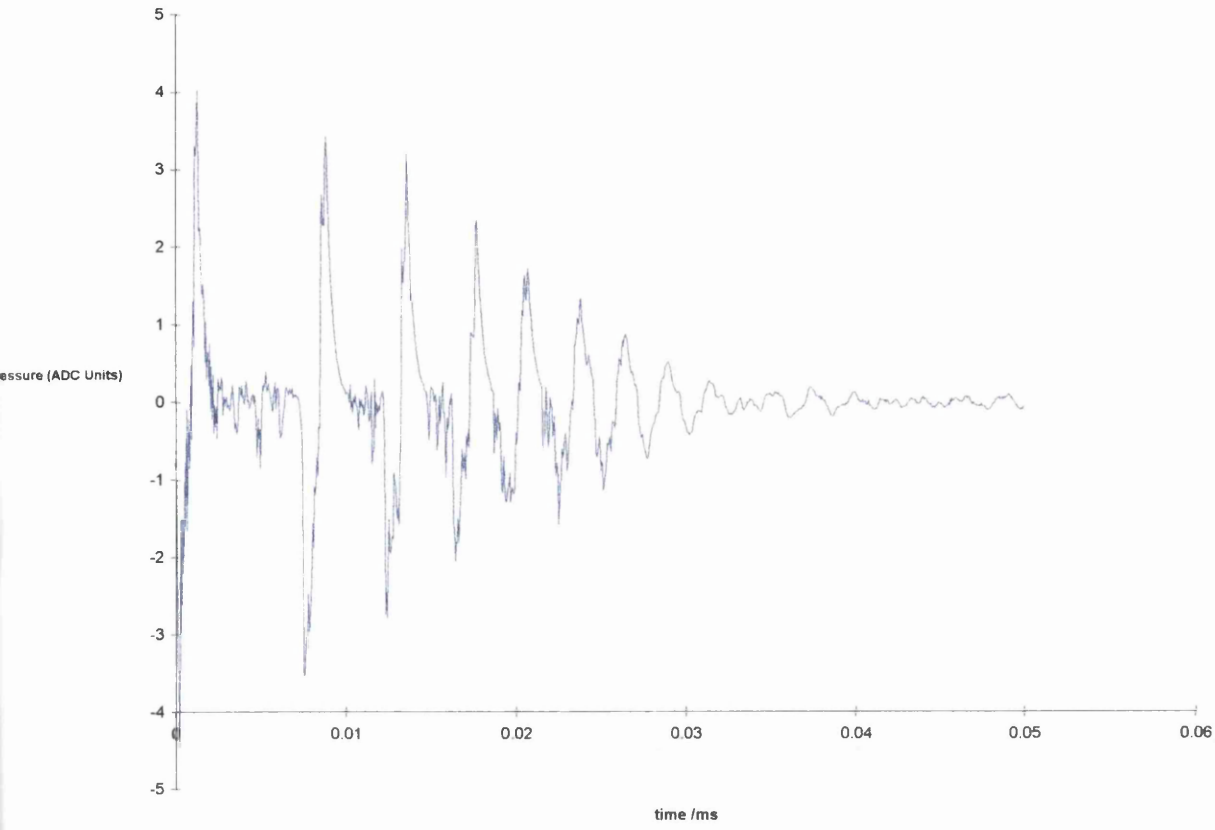


Figure 3.3 Pressure-tension record for purified water at 200 psi

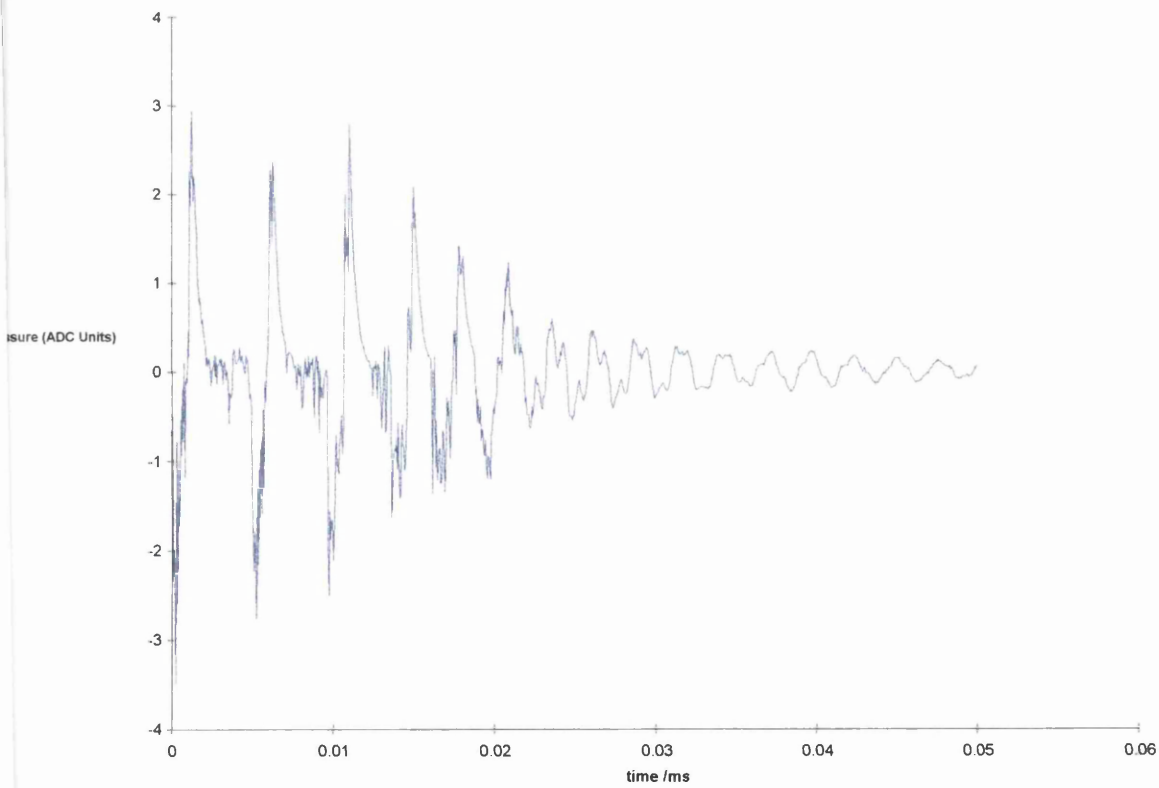


Figure 3.4 Pressure-tension record for purified water at 250 psi

All the results were repeated five times with reproducible results occurring on all pressures. The time gaps between first and second pulse cycles have been recorded in table 3.1

Static pressure applied (Psi)	14.7	34.7	54.7	84.7	114.7	164.7	214.7	264.7	314.7
Time gap (ms) (average value)	79.6	34.4	22.3	17.3	12.7	8.93	7.4	5.2	4.85

Table 3.1 Pressure applied and time gaps achieved for purified water

From the data in table 3.1 we are able to plot a log-log graph of the static pressure and time gap as presented at figure 3.5. A line of best fit is also presented here and it can be seen that there is good agreement to the results and the fitted line. From this data, as mentioned in chapter 2, we can extrapolate back to determine the tensile strength of the solution. The result obtained for water was 104 Bar, which corresponds well with previous bullet-piston work (Williams et al 1997).

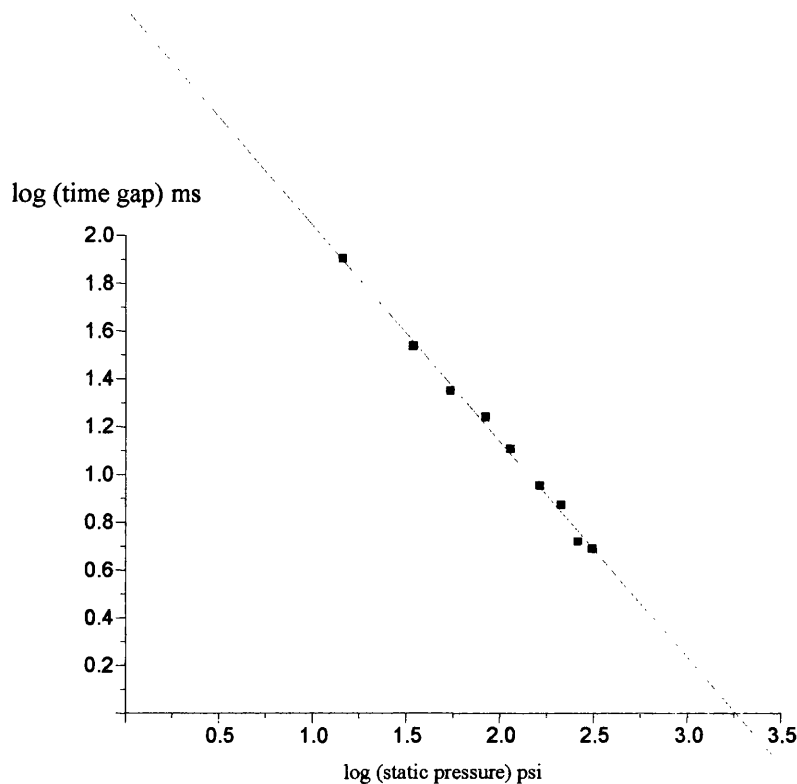


Figure 3.5 A representation of the results obtained for purified water from the bullet-piston experiment giving rise to a tensile strength of 105 Bar.

3.2.1 The effect of stressing rate on tensile strength measurements of purified water

The effect of stressing rate has long been established with Trevena (1982) showing that increasing the stressing rate would increase the tensile strength of a solution. However, until now there has not been a single experiment that has been able to systematically test a solution with a range of stressing rates whilst keeping all other parameters constant. By varying the gap distance between the piston base and the top of the stun gun we can vary the pressure applied from the captive bolt as it strikes the base of the column. Within the work presented here the gap size was varied from 3.75 to 4.2 cm which resulted in stressing rates in the order of 0.6 to 0.17 Bar/ μ s.

This rate of stressing can also be altered by varying the strength of bullet that is used in the stun-gun. Although this method has not been tested within this research it would be a viable alternative to change the stressing rate. All parameters except the rate of stressing were kept fixed.

It is interesting to look at the pressure-tension cycles for the different levels of stressing, figures 3.6-3.8 show the cycles for different gap sizes at atmospheric pressure. Where the y-axis represents unscaled pressure recorded directly from the transducer,

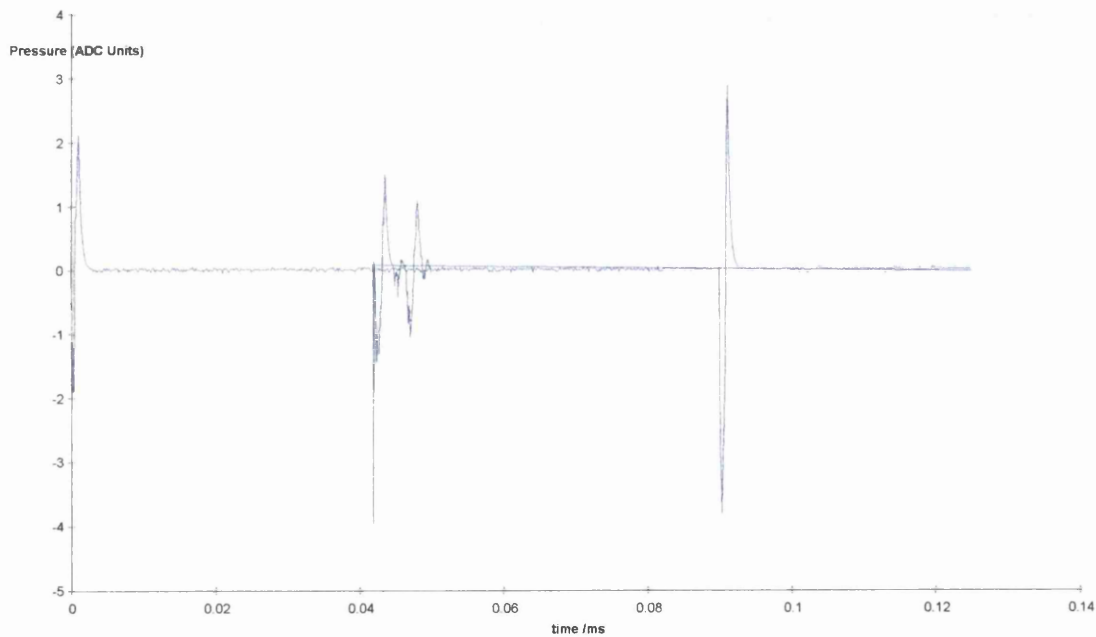


Figure 3.6 Pressure-tension record for purified water at 0 psi at gap size 3.6 cm

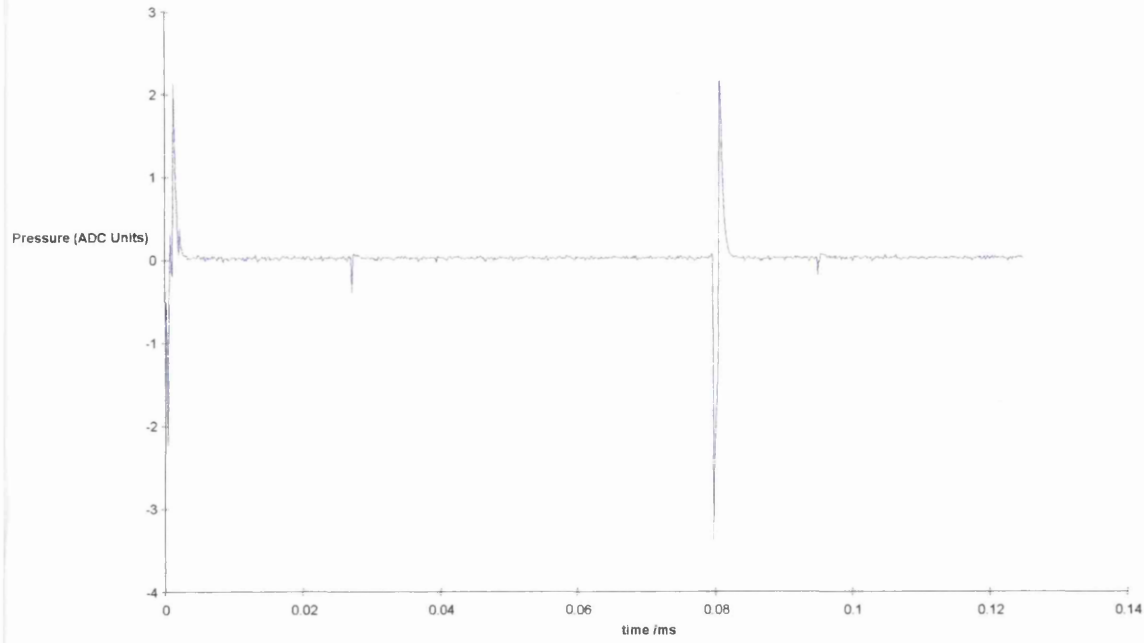


Figure 3.7 Pressure-tension record for purified water at 0 psi at gap size 3.7 cm

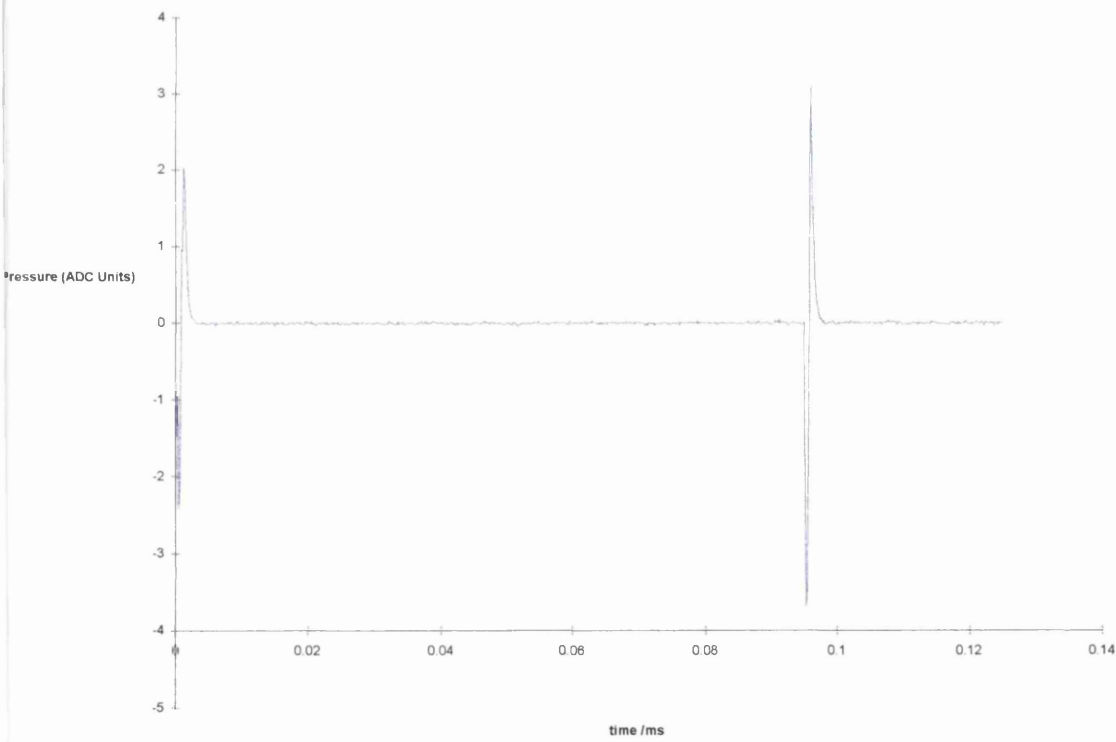


Figure 3.8 Pressure-tension record for purified water at 0 psi at gap size 3.8 cm

It is clearly evident that the peak tension achieved is significantly higher for the smaller gap size, as would be expected with a greater force being driven into the piston base. Similarly we can show the difference in pressure cycles at each different applied static pressure which show agreement with the above figures. However to be able to give a quantitative measurement for the rate of stressing we have to look at the maximum rate of change of pressure. An obvious problem with this is that of the pressure transducers not being able to accurately record the maximum amplitude of the cycles, as mentioned in chapter 2, however the time gaps achieved are recorded with great accuracy. To determine the rate of stressing we have to work back from the obtained values for the tensile strength of each solution. The peak amplitude on the first cycle corresponds to the tension achieved prior to cavitation, also this value is the effective tensile strength of the fluid which we have found. By using the time gap involved in achieving the breaking tension we can then determine the rate of stressing. A table of the time gaps associated with each stressing rate can be seen in table 3.2.

Pressure	Time gap (ms) at each stressing rate		
	0.3 Bar/ μ s	0.4 Bar/ μ s	0.6 Bar/ μ s
14.7	79.6	85.2	90.1
34.7	34.4	38.9	40.9
54.7	22.3	24.1	25.1
84.7	17.3	18	19
114.7	12.7	14.1	15.2
164.7	8.9	9.9	10.9
214.7	7.4	8.4	9.1
264.7	5.2	6	7
314.7	4.85	5.2	6.1

Table 3.2 Time associated between first and second pressure pulses under different stressing rates and applied static pressures.

The plots associated with determining the tensile strength from the time associated with initial bubble growth can be seen in figure 3.9. The log-log plot of static pressure versus initial time gap shows that as the stressing rate is increased, the line of best fit increases its gradient resulting in determining a higher tensile strength.

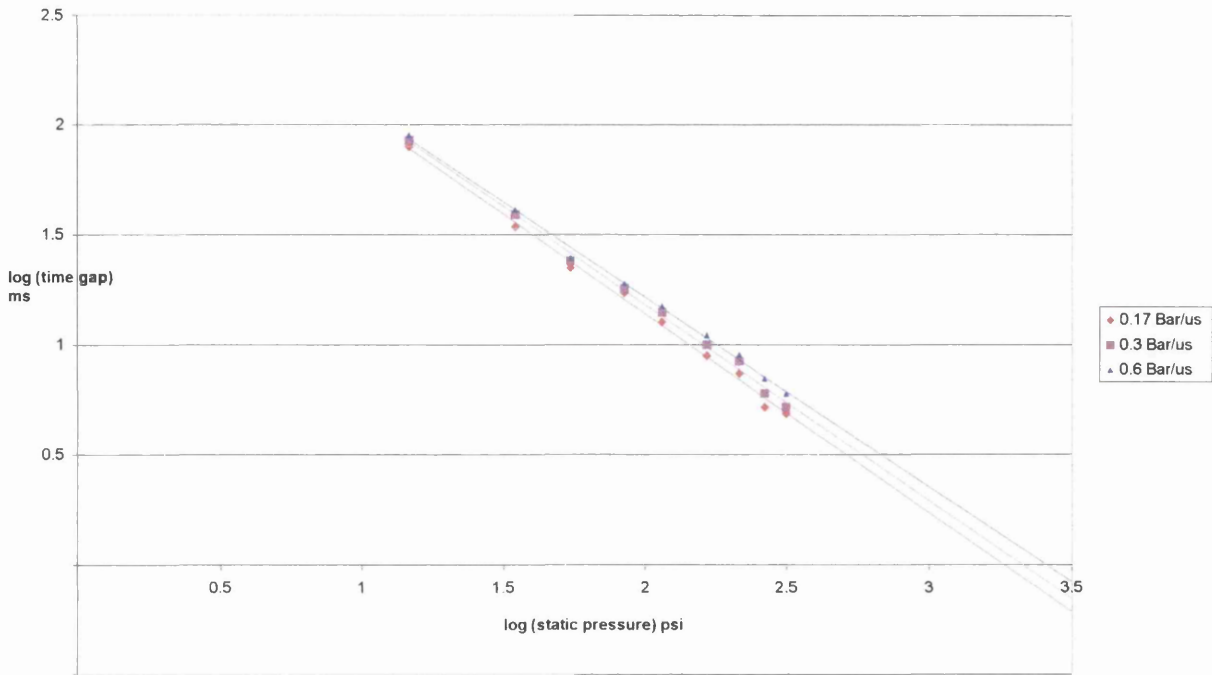


Figure 3.9 The time interval as a function of applied static pressure (psi) for purified water at three different rates of stressing

It is worthwhile noting that even though the initial values appear similar, the gradient of the fitting line is altered dramatically by the variation in values at higher static pressures in the area above the liquid column.

The resulting difference in the tensile strength by varying the stressing rate can be seen in the table 3.3 below.

Gap Size (cm)	Tensile Strength (Bar)	Stressing Rate (Bar/ μ s)
3.75	240	0.6
3.9	168	0.4
4.0	110	0.3
4.2	60	0.17

Table 3.3 The effect of stressing rate on the tensile strength of water

These results can also be seen graphically (figure 3.10) which seem to indicate a linear increase of tensile strength with increasing stressing rate. The B-P unfortunately has limitations as to the operating conditions in which it can deliver, namely running the experiment safely. This means the range of stressing rate could only be undertaken from 0.17 to 0.6 Bar/ μ s. A smaller gap between piston and captive bolt would increase the likely event of breaking the apparatus whilst a larger gap failed to generate a pressure pulse.

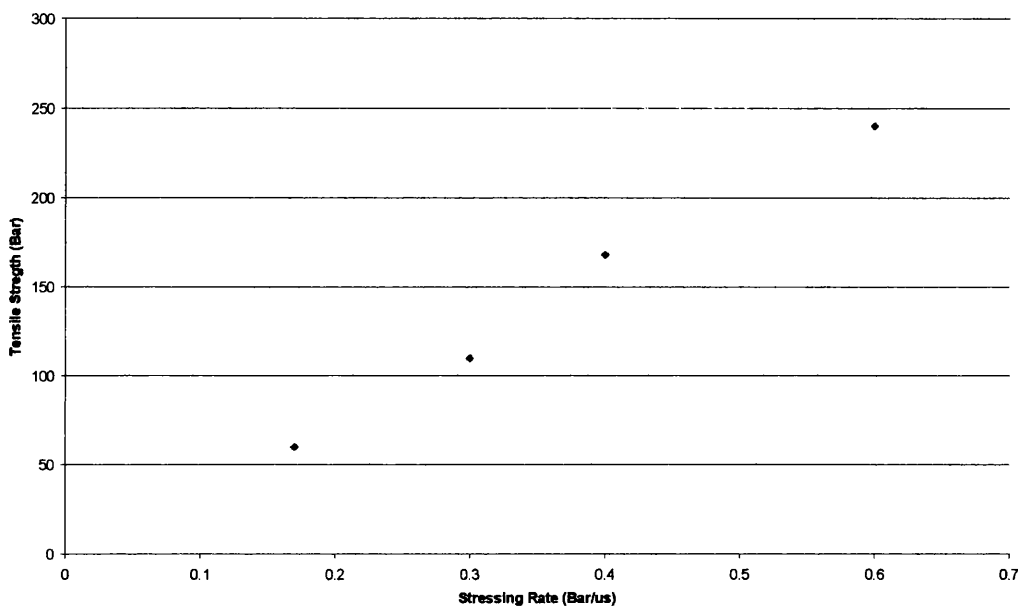


Figure 3.10 The effect of stressing rate on the tensile strength of water

It is evident that with increasing rates of stressing the tensile strength of the sample is increased, in agreement with Trevena's work. It is important to note that in a similarly built experiment the rates of stressing could be quite different due to the effect of the gun and the absorbency of pressure on the supports. Even with a small variation in stressing rate the effect on the effective tensile strength can be quite large.

It is therefore important to investigate if the rate of stressing can alter the trends between different fluid samples.

Since there is a linear relationship between the tensile strength and stressing rate delivered to a fluid sample (figure 3.10), we can characterise the fluid sample by a tensile parameter in the form

$$X = F_c / (dF_c / dt)$$

By taking the linear gradient of the line of best fit from the data shown in figure 3.10 we obtain a value of $X=425$ for purified water. Within a set industrial application a given rate of stress development would be applicable, enabling estimation of the tensile strength of a fluid at that stress rate, as long as we could test this at any other given stress rate. With the values that we have obtained for purified water this equation estimates the tensile strength within a 15% accuracy.

3.3 Discussion

These measurements on degassed, purified water at 25°C for different rates of stressing ($0.187 \text{ bar/ms} \leq \dot{\Omega}_r \leq 0.77 \text{ Bar/ms}$) reveal a marked dependence of F_c on $\dot{\Omega}_r$, with F_c being significantly larger at the higher stressing rates, some 224 Bar ($\dot{\Omega}_r = 0.77 \text{ Bar/ms}$) compared to 59 Bar at the lowest stressing rate ($\dot{\Omega}_r \approx 0.187 \text{ Bar/ms}$). $F_c(\dot{\Omega}_r)$ also shows a linear relationship over the stressing rates considered. At the highest stressing rate employed herein ($\dot{\Omega}_r = 0.77 \text{ Bar/ms}$) the value of F_c obtained (224 Bar) is comparable to values obtained by Henderson and Speedy (1987), Greenspan and Tschiegg (1967), Galloway (1954) and Briggs (1950), where

$160 \text{ Bar} \leq F_c \leq 250 \text{ Bar}$, and is almost identical to the value determined by Herbert and Caupin (2005) where $F_c \approx 225 \text{ Bar}$ at 25°C . Also shown in figure 3.11 is the value of F_c for purified water resulting from another pulse-reflection technique, (Williams *et al*, 1997). This value of F_c (300 Bar at $1 \text{ Bar}/\mu\text{s}$) follows the trend of $F_c(\dot{\Omega}_p)$ established in the present work.

D / cm	F_c / Bar	$\dot{W}_F / \text{Bar ms}^{-1}$
4.2	59 ± 2.5	0.18675 ± 0.0146
4	110 ± 3	0.369 ± 0.0153
3.9	168 ± 4	0.5875 ± 0.044
3.7	224 ± 5	0.77 ± 0.043

Table 3.4 Values of F_c and $\dot{\Omega}_p$ for various gap widths D .

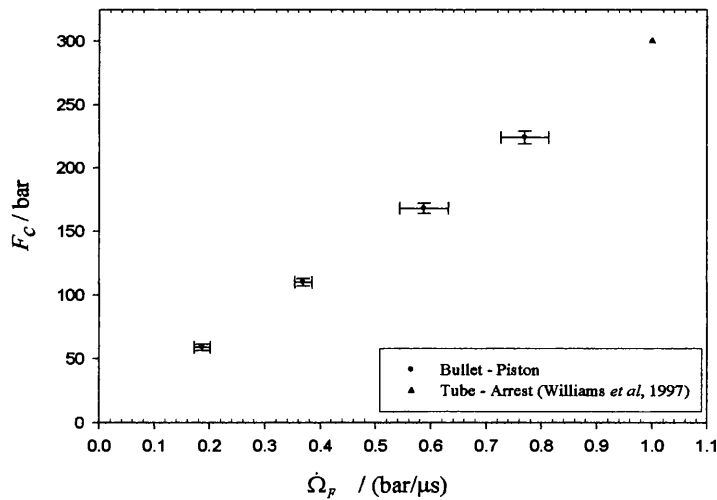


Figure 3.11 F_c as a function of $\dot{\Omega}_p$ for degassed, purified water at 25°C . Also shown is the result from the tube-arrest dynamic stressing technique (Williams *et al*, 1997).

3.4 Conclusions

The present results reveal that under a range of rates of tensile stress development, samples of degassed, purified water present markedly different values of effective tensile strength which range from *ca.* 60 Bar to *ca.* 250 Bar. These values span the range reported in the second group of experimental results described in section 3.1, which involve various stressing techniques, each of which may be assumed to produce a different characteristic rate of tensile stress development. It is significant therefore that in the present work, results have been produced from a single technique, consisting of experiments conducted within the same apparatus in which the rate of stressing is deliberately varied. The results of such a study have not previously been reported. They clearly establish the importance of stressing rate in considerations of the effective tensile strength of liquids under conditions where heterogeneous nucleation prevails and emphasise that any attempt to reconcile the results of previous cavitation studies should take this factor into account.

The latter point is emphasised by reference to the various results obtained for the tensile strength of other liquids. In work on glycerol, Bull (1956) found a tensile strength of 60 Bar while Carlson and Henry (1973) reported 600 Bar. It is interesting to note that the rate of stressing was some 10^4 times lower in Bull's work than in Carlson and Henry's. Similar findings have been reported for mercury, in which Briggs (1953) was unable to generate static tensions greater than 425 Bar but Carlson (1975) found that tensile failure occurred at a tension of 19,000 Bar, at a stressing rate of *ca.* 10^6 Bar/ms: at a lower rate (1 bar/ms), Williams *et al.* (1998) found a limit for F_c of *ca.* 3,000 Bar. It is noteworthy that the characteristic times of the pulses used

herein correspond to those involved in some medical applications of low frequency ultrasound (Rosenschein and Rassin 1998); and the tensile strength of water reported here considerably exceeds the values of tension thought to be generated *in vivo* by some ultrasound devices.

It should be noted that the findings for the values of purified water over a range of stressing rates raises a few points in regard to the previous experimental work, on the original B-P technique, as the rate of stressing was not constant during this work. The very make-up of the B-P experiment meant that different bullet strengths and varied gaps were used in the experiment, required to increase the pressure in the system, to find one fixed value for the tensile strength of purified water. It is therefore hypothesised that the anomalously low values for water were actually found due to different stresses being applied during the experiment. Simulating the data that might have been made using the original B-P technique can be made using data gained during the research for this thesis. Data obtained from high stressing rate experiments and also from low stressing rate tests produces a graph similar to figure 3.12. This was generated by selecting time gaps produced at a low stressing rates for low pressures and at high stressing rates for high pressures. The blue line of best fit is significantly steeper than that previously generated and results in tensile strength in the order of 35 Bar. This, even though not as low as reported in the work by Sedgewick and Trevena, may explain further the low values that had been found.

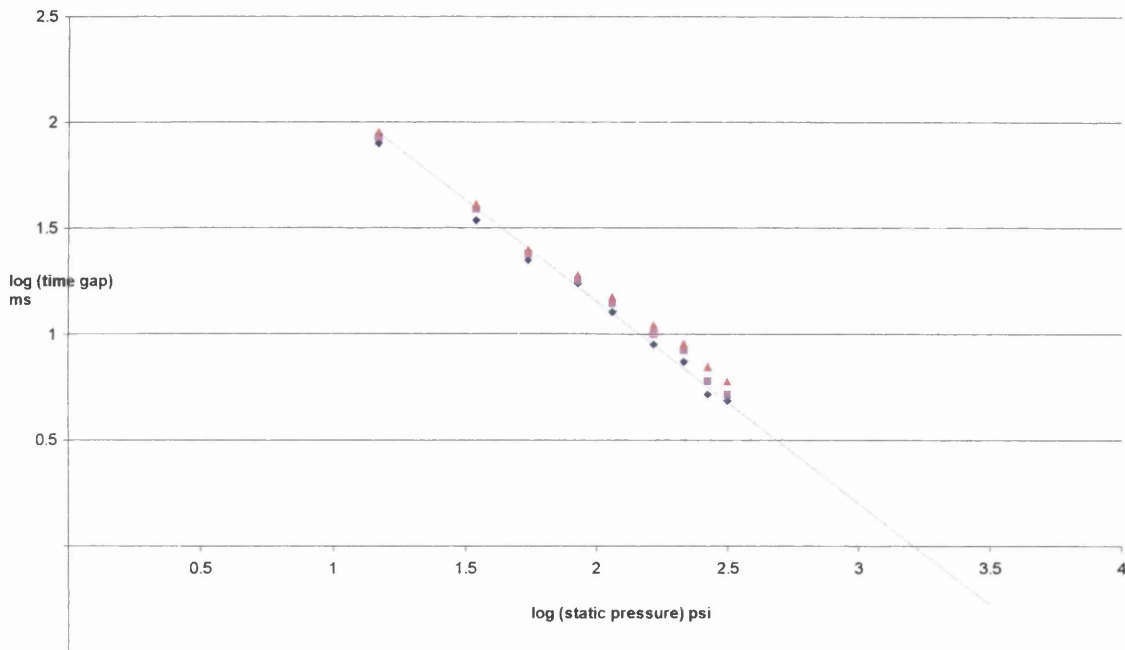


Figure 3.12 Time gap between pressure peaks as a function of static pressure. (Results for all stressing rates shown.)

The results presented here show that it would be possible, on testing the same liquid, in this case water, to obtain variation in the tensile strength by altering the stressing rate. The original B-P technique requires experiments undertaken at different stressing rates to obtain one value of the tensile strength. These new results show clearly how the anomalously low values obtained may have arisen and establish that the B-P can yield new information on the tensile properties of water when used and analysed appropriately. The following chapter now reports on the basic B-P variable stressing-rate technique to investigate the tensile properties of aqueous polymer solutions.

CHAPTER 4

Tensile Properties of Polymeric Solutions

Chapter 4

Tensile Properties of Polymer Solutions

4.1 Introduction

It is well established that in many circumstances, the addition of high molecular weight polymer in low concentration (less than 100 ppm) to a Newtonian solvent has little effect on the mechanical properties of the resulting dilute polymer solution. For example, the effect on shear viscosity is virtually insignificant with a small increase in its absolute value and very little shear thinning. At the same time, there are some situations where the addition of very small concentrations of polymer can lead to very significant changes in mechanical response; 'drag reduction' in turbulent flow being an obvious example. This field has been well worked for several decades and is mentioned here only as an example of an 'extravagant effect' for a 'small input' (Chen and Walters 1996). There are other examples of this which are of significant potential practical relevance. We refer particularly to the effect of polymer additives on cavitation and extensional viscosity.

As noted previously in this thesis, the occurrence of negative pressures in many flows of engineering relevance result in the cavitation of liquids and the related phenomenon of liquid-jet formation. The interaction of these liquid-jets with the shockwaves formed about oscillating cavitation bubbles leads, in many instances, to damage to solid surfaces (Trevena 1987). An important example is found in the engine bearing context, where the need to study cavitation in lubricating oils is clearly established (Dowson and Taylor 1979).

Despite theoretical and experimental studies demonstrating that the viscoelasticity conferred upon liquids containing polymer additives influence their cavitation properties, the results are often contradictory – particularly with regard to the specific effects on cavitation damage potential and cavitation threshold.

Recent studies of the effects of polymer additives on lubricant flow in dynamically-loaded journal bearings conclude that their role in reducing wear may be associated with mitigating effects of viscoelasticity on cavitation, but the precise nature of such effects remains unclear. Indeed, no mitigating effects have been found in some studies of cavitation-induced pressures in viscoelastic liquids, in which the presence of relaxation mechanisms with characteristic times in the range 10^{-3} s to 10^{-4} s lead to transient pressures some 30 times larger than in Newtonian liquids of comparable shear viscosity (Trevena 1987). Although these findings are supported by evidence that small amounts of polymer can lead to enhanced cavitation damage, they are complicated by consideration of the time-scales of the various relaxation and retardation mechanisms associated with different polymers (McComb and Ayyash 1980) and confused by contradictory results, even for the same polymer (Shima *et al.* 1986). This crucial issue of the timescale of the stressing events in cavitation threshold determination work is the purpose of the work considered in this chapter because similar uncertainty pertains to the related question of the role of polymer additives in determining the cavitation threshold (or effective tensile strength) of liquids. This is a parameter of crucial importance in relation to the establishment of flow boundary conditions in (fluid) mechanical engineering and process design, such as in the prediction of bearing performance.

Under dynamic stressing there is evidence that the presence of polymer can lower cavitation threshold, such as in the stressing of water containing polyacrylamide additives by the bullet-piston reflection method (Trevena 1987). This work demonstrated a reduction of liquid effective tensile strength, the reduction increasing with increasing polymer concentration. However, when this system was investigated using an ab initio technique, the cavitation threshold was found to be increased by the same polymer additive, and when subjected to static stressing (in a modified Berthelot tube) the presence of polymer made no discernible difference to the effective tensile strength of the liquid.

In view of the scientific and engineering importance of the questions posed by these findings, and the commercial and environmental benefits linked to their solution, there is clearly a pressing need for a systematic study of the specific effects of polymer additives on the cavitation and related rheological properties of liquids under dynamic stressing. As previously noted for many industrial applications such as ink jet printing and engine oil manufacturing, the importance of tensile strength of a fluid is high, since this knowledge can help reduce damage on the process, i.e. ink jet nozzle or engine bearing. In the manufacture of inks polymers are often added to increase shear viscosity, however these polymers can also affect the extensional viscosity and the tensile strength of these solutions. This chapter represents the first reported results for the tensile strength of a range of concentrations and molecular weight for a polymeric system with a clear definition of the parameters.

The tensile strength of a range of molecular weight polyethylene glycol in solution was undertaken by dynamic stressing using the bullet-piston technique as described in chapter 2.

4.2 Polyethylene glycol solutions

The shear viscosity measurements were made on the Advanced Rheometric Expansion System (ARES) rheometer (Rheometrics) and the zero shear value was obtained. In industry, polyethylene glycol is used to increase the shear viscosity.

Table 4.1 shows the shear viscosity measurements for the samples.

		Concentration (% polymer by weight)					
		0.5	1	2	4	8	16
Molecular weight	600	7.7	8.3	8.7	9	9.3	9.9
	1500	7.9	8.5	8.9	9.1	9.5	10.7
	6000	8.1	8.7	9.1	9.7	11	15
	10000	8.6	9	9.4	10.7	13.2	20
	20000	8.7	9.1	9.8	11.4	15.2	25

Table 4.1 Shear viscosity measurements (η (Pa.s))

It can be seen that the increased concentration and molecular weight increase the shear viscosity of the sample.

4.2.1 Tensile strength results

As with the experiments for deionised water (chapter 3) the values for the time gap between primary and secondary cycles over a range of applied static pressures were obtained. The samples were tested over a range of concentrations and molecular weights. The lowest molecular weight tested was 600. Figures 4.1 – 4.12 show the pressure tension results obtained for these solutions at 0, 100, 200 and 250 psi for concentrations 1, 5 and 10%. Records for pressures at 20, 50, 150 and 300 psi have been omitted for brevity. The pressure tension cycles for 6000 and 10000 Mw at the same concentrations are shown for comparative reasons in section 4.6.

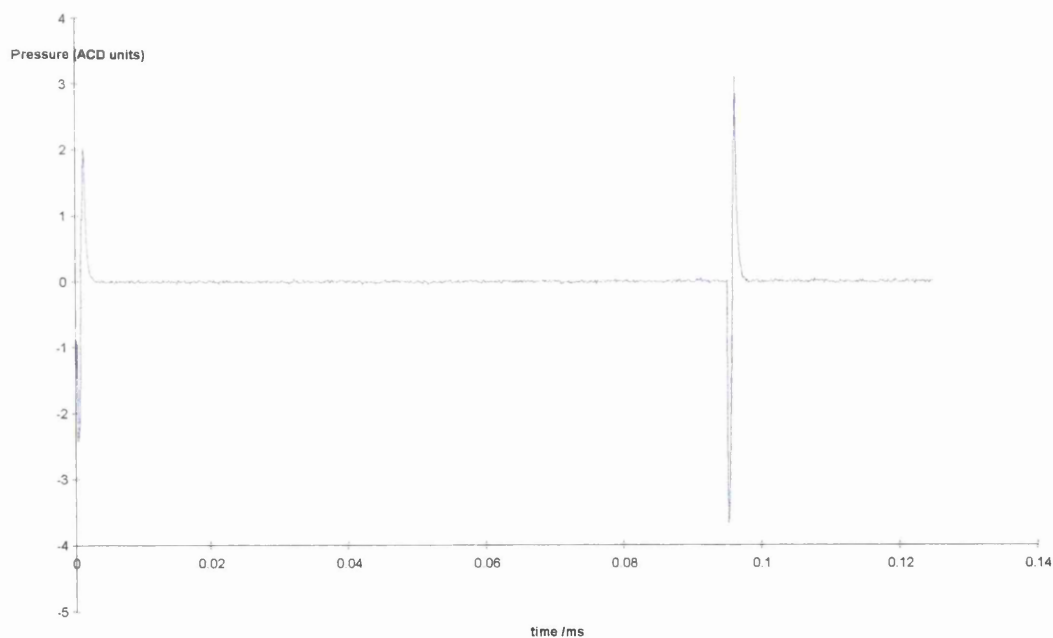


Figure 4.1 Pressure-tension cycle for a 0 psi static pulse for 1% 600 Mw solution.

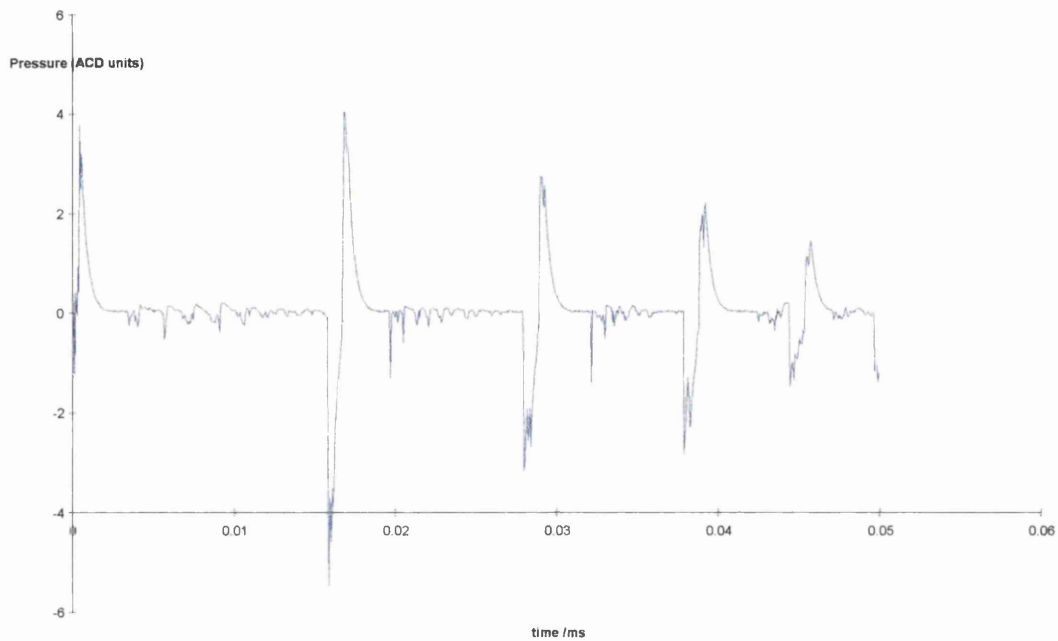


Figure 4.2 Pressure-tension cycle for a 100 psi static pulse for 1% 600 Mw solution.

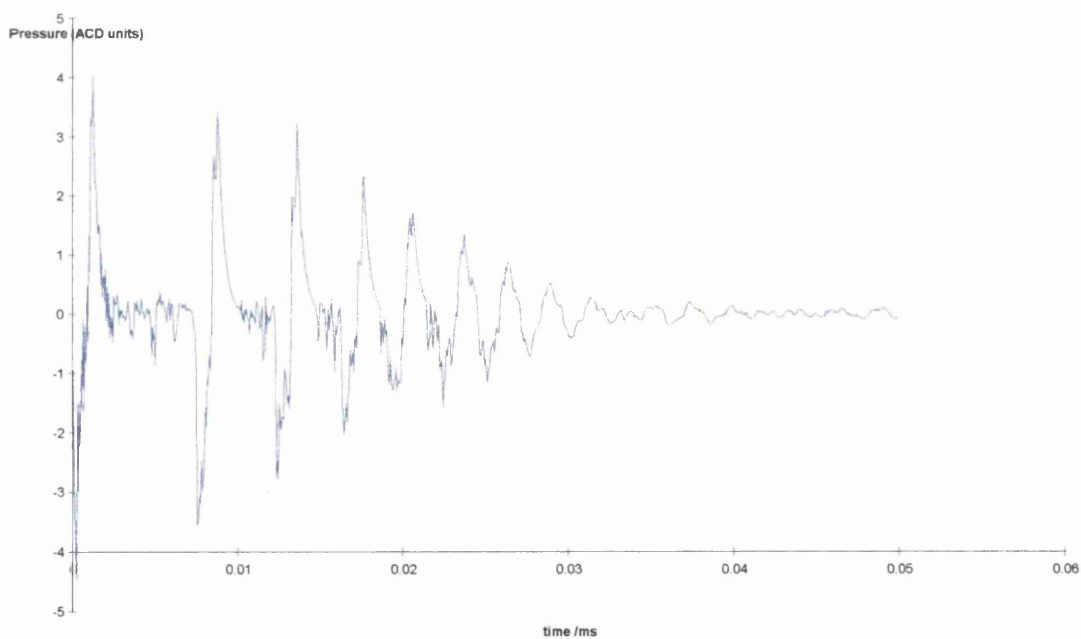


Figure 4.3 Pressure-tension cycle for a 200 psi static pulse for 1% 600 Mw solution.

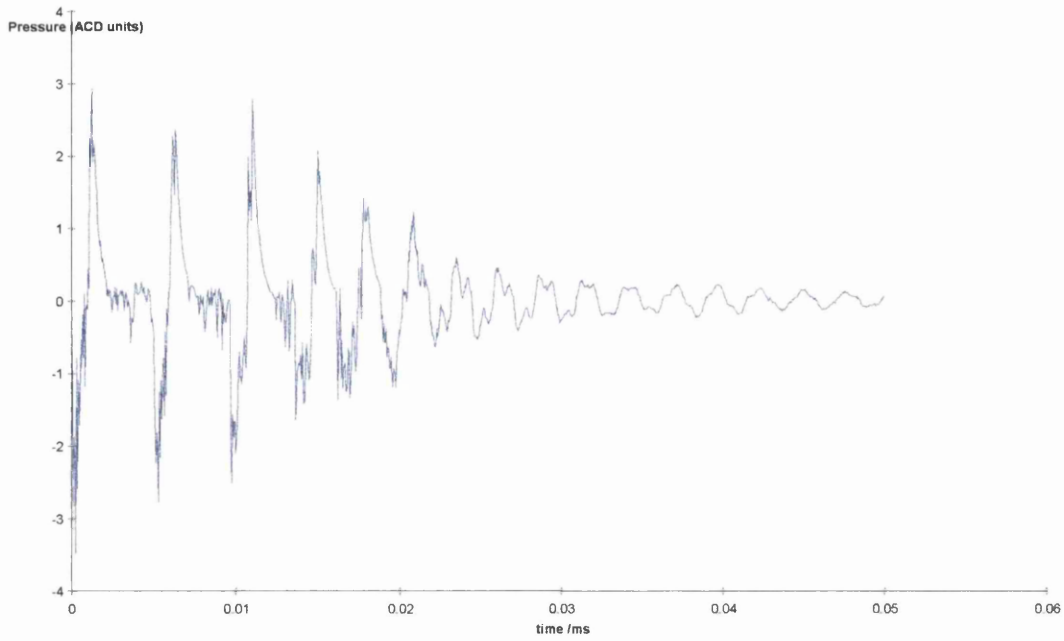


Figure 4.4 Pressure-tension cycle for a 250 psi static pulse for 1% 600 Mw solution.

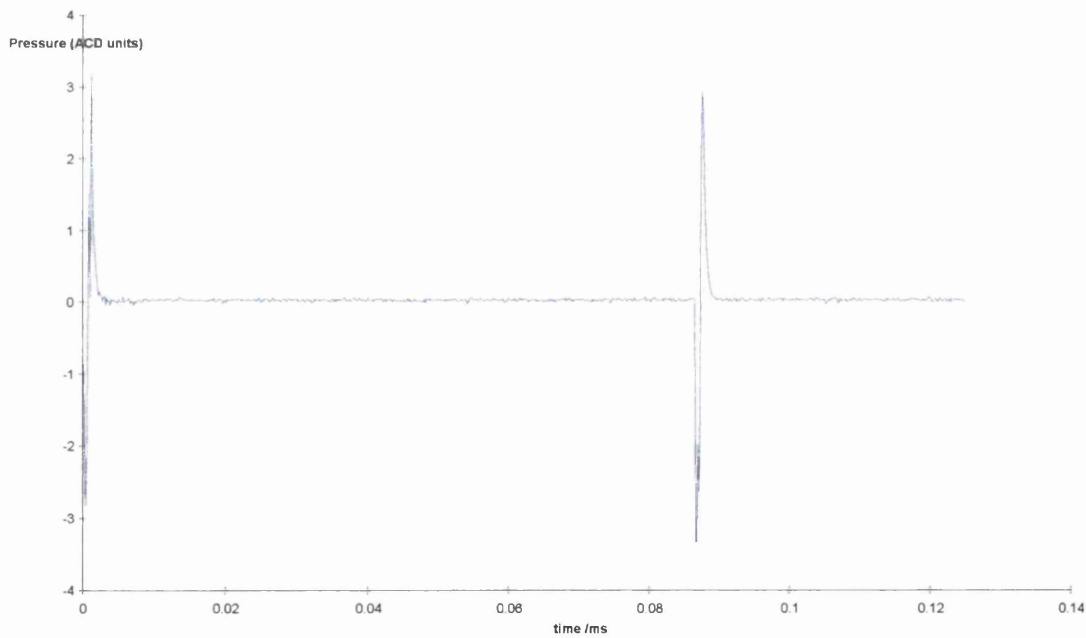


Figure 4.5 Pressure-tension cycle for a 0 psi static pulse for 5% 600 Mw solution.

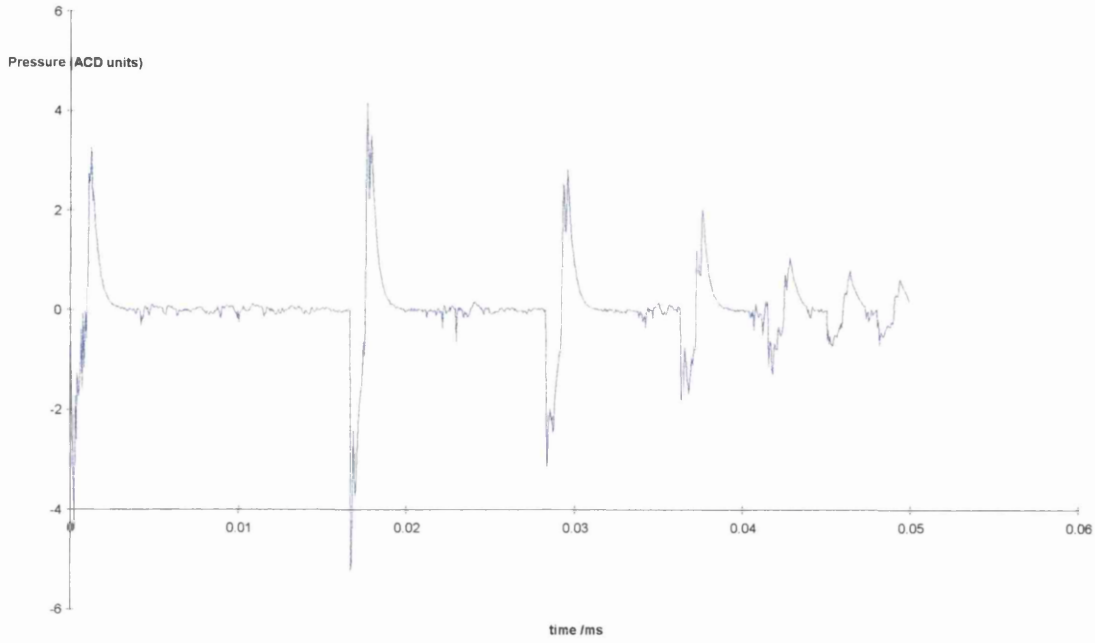


Figure 4.6 Pressure-tension cycle for a 100 psi static pulse for 5% 600 Mw solution.

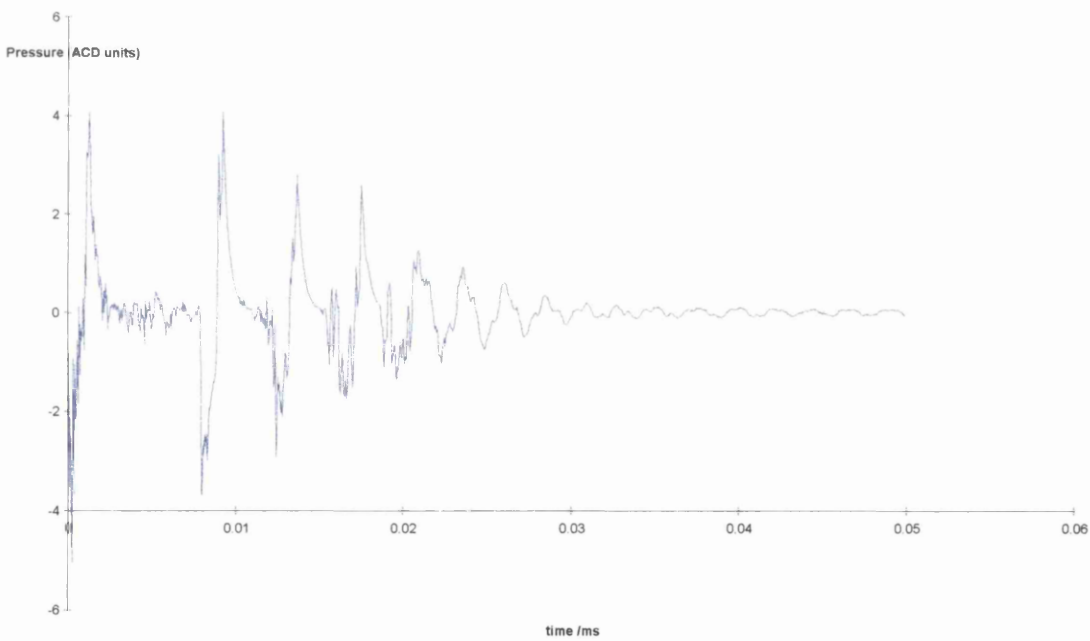


Figure 4.7 Pressure-tension cycle for a 200 psi static pulse for 5% 600 Mw solution.

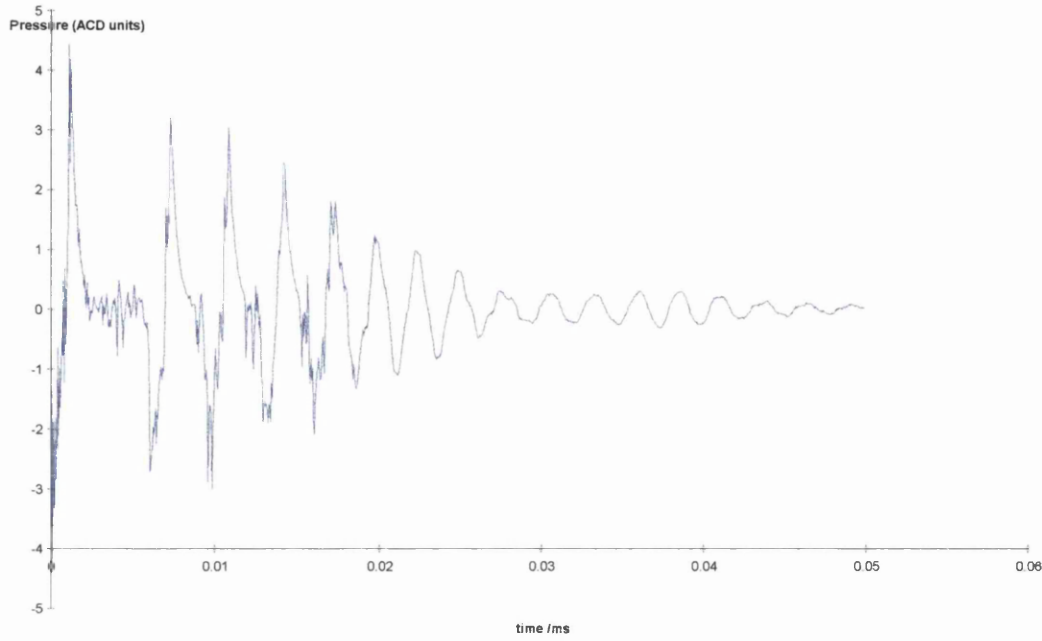


Figure 4.8 Pressure-tension cycle for a 250 psi static pulse for 5% 600 Mw solution.

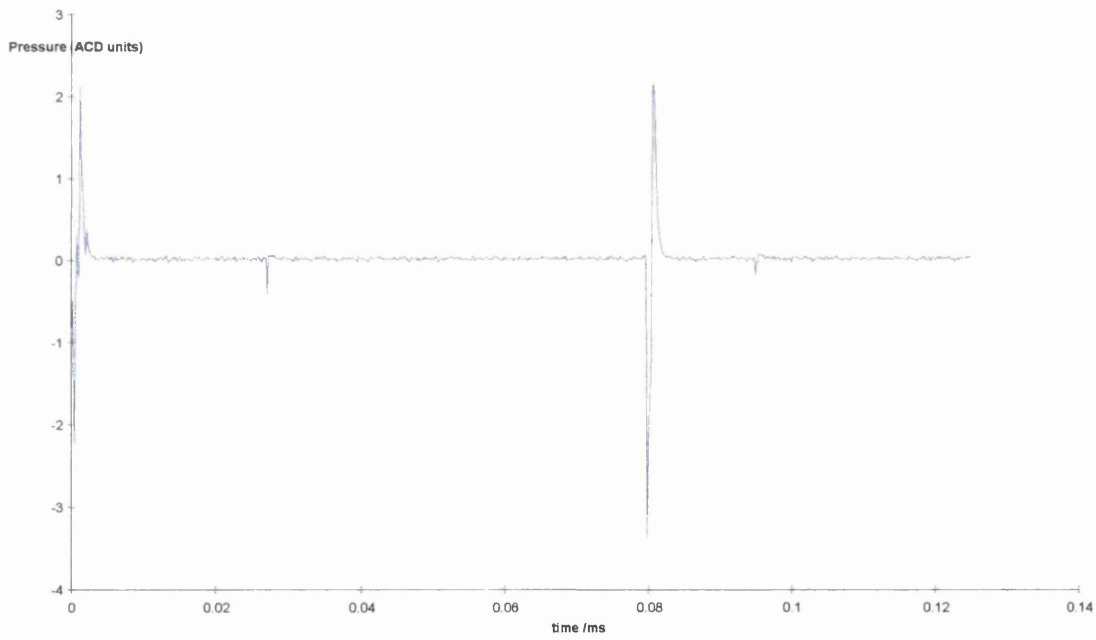


Figure 4.9 Pressure-tension cycle for a 0 psi static pulse for 10% 600 Mw solution.

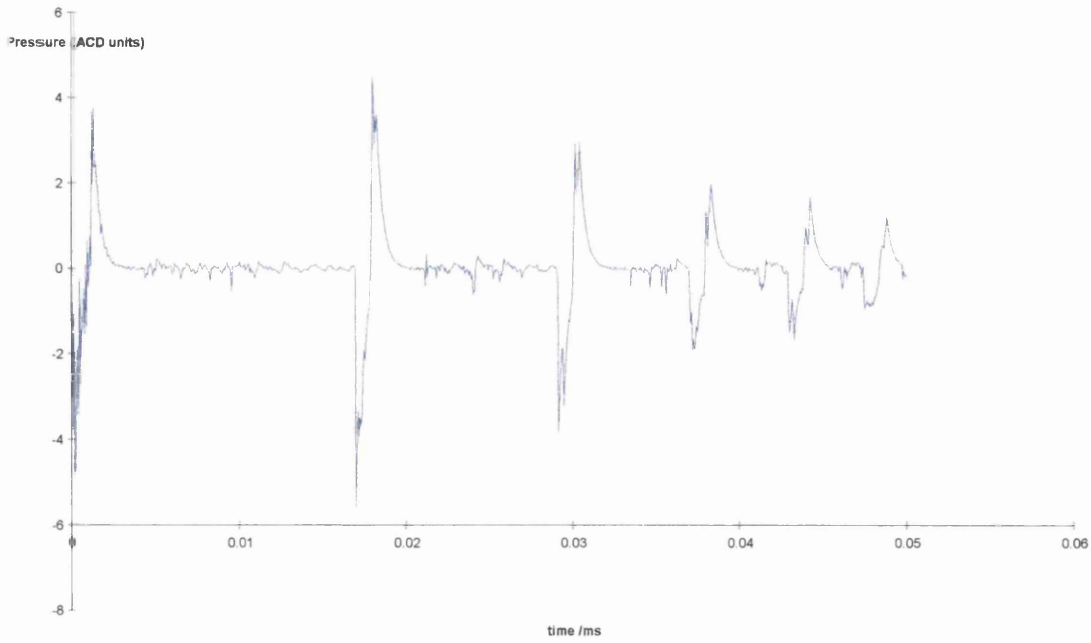


Figure 4.10 Pressure-tension cycle for a 100 psi static pulse for 10% 600 Mw solution.

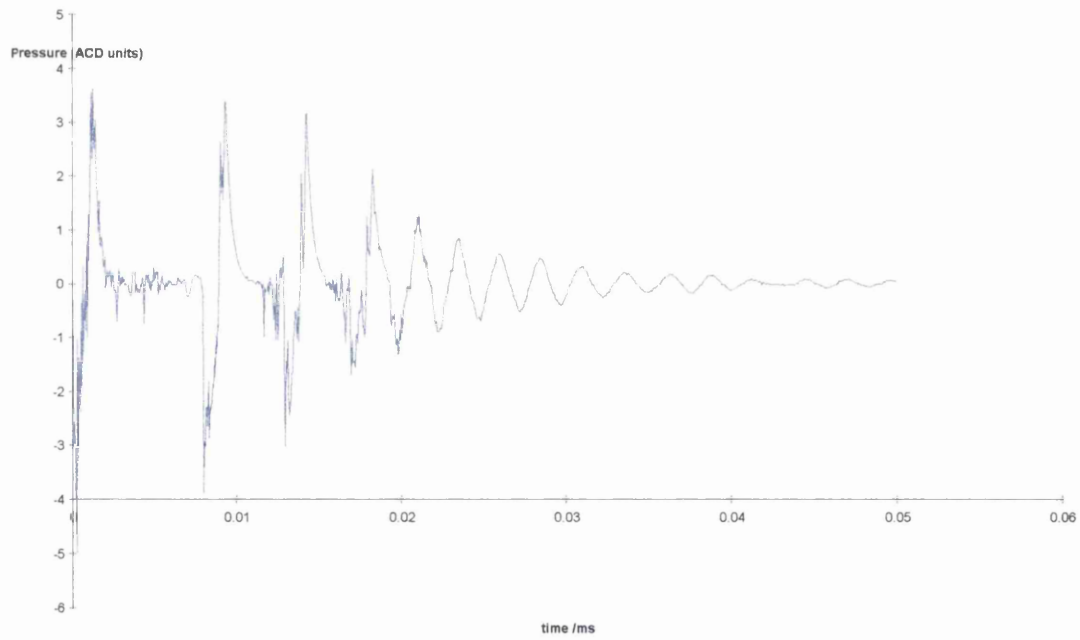


Figure 4.11 Pressure-tension cycle for a 200 psi static pulse for 10% 600 Mw solution.

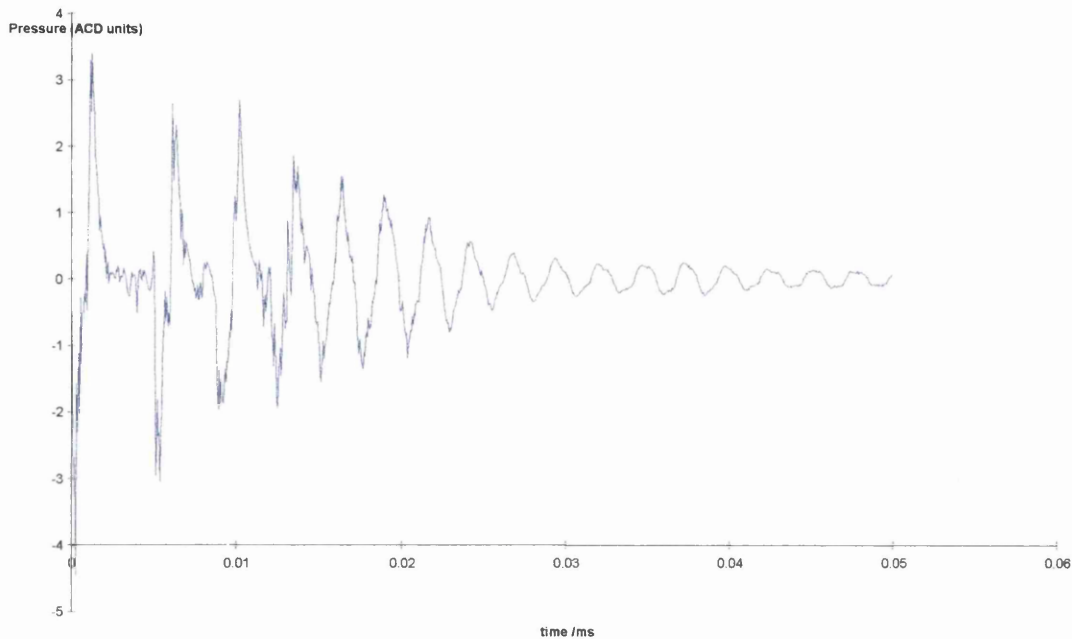


Figure 4.12 Pressure-tension cycle for a 250 psi static pulse for 10% 600 Mw solution.

From the pressure tension cycles we can obtain the time taken for initial bubble growth collapse by taking the time between the primary and secondary pressure peaks. An interesting effect can be seen that at high static pressure the negative peaks are much broader than at low static pressures. This, although not researched here, would likely be due to a memory effect of the fluid. By taking a log-log plot of the applied static pressure above the liquid column and the time between primary and secondary pressure pulses the effective tensile strength may be determined by extrapolating back to a zero time gap between pulses. Figures 4.13 – 4.15 show the results for 1500 Mw PEG at 1, 5 and 12.5 % concentration. The subsequent figures 4.16 – 4.19 show the comparative graphs for each molecular weight.

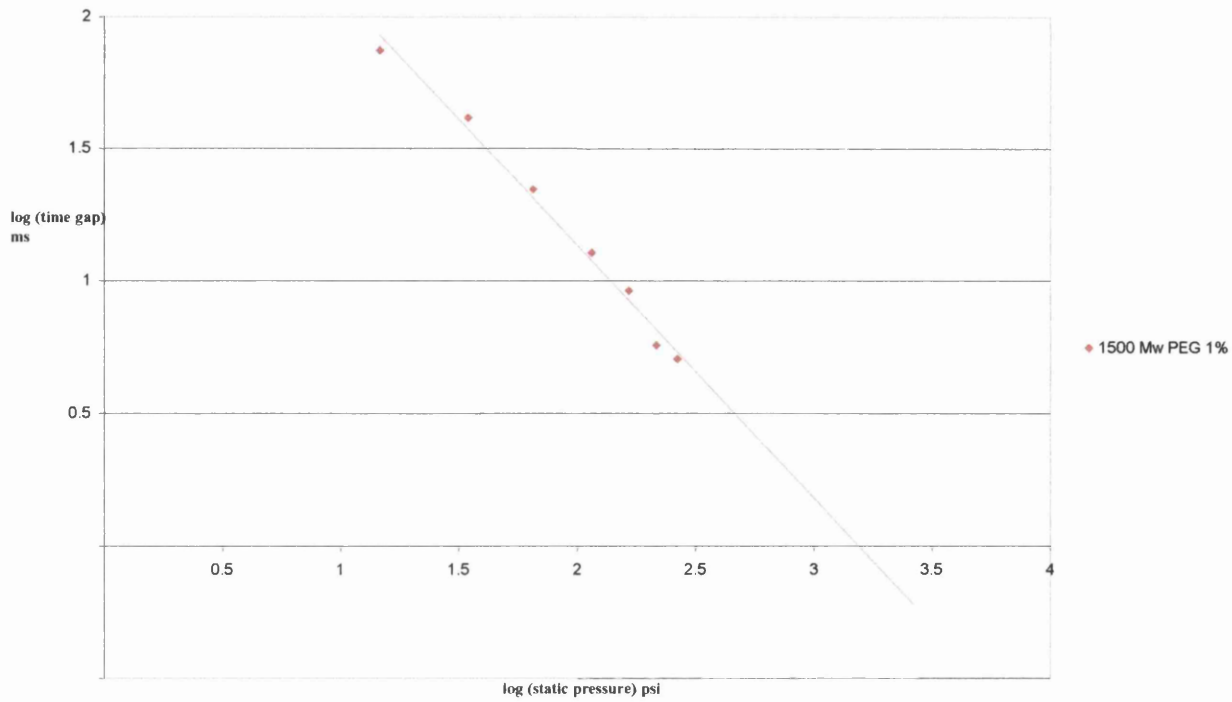


Figure 4.13 Log-log plot of time between pressure peaks as a function of applied static pressure for 1500 Mw at 1% concentration

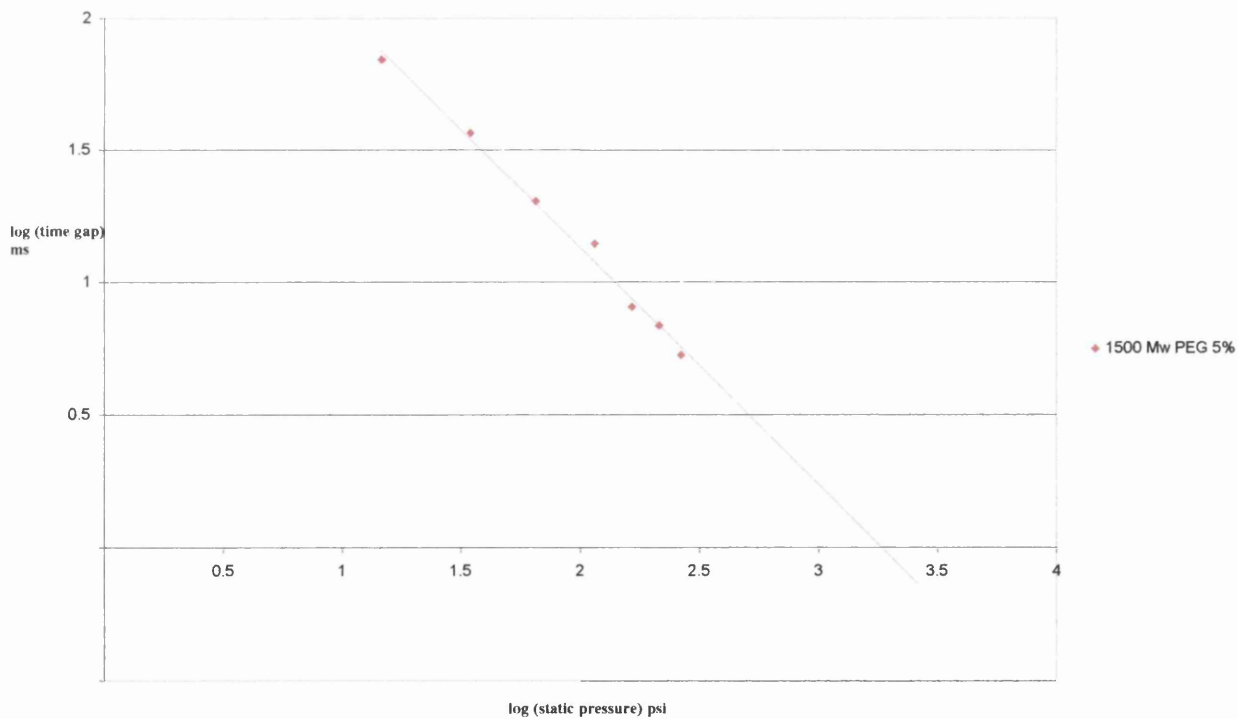


Figure 4.14 Log-log plot of time between pressure peaks as a function of applied static pressure for 1500 Mw at 5% concentration

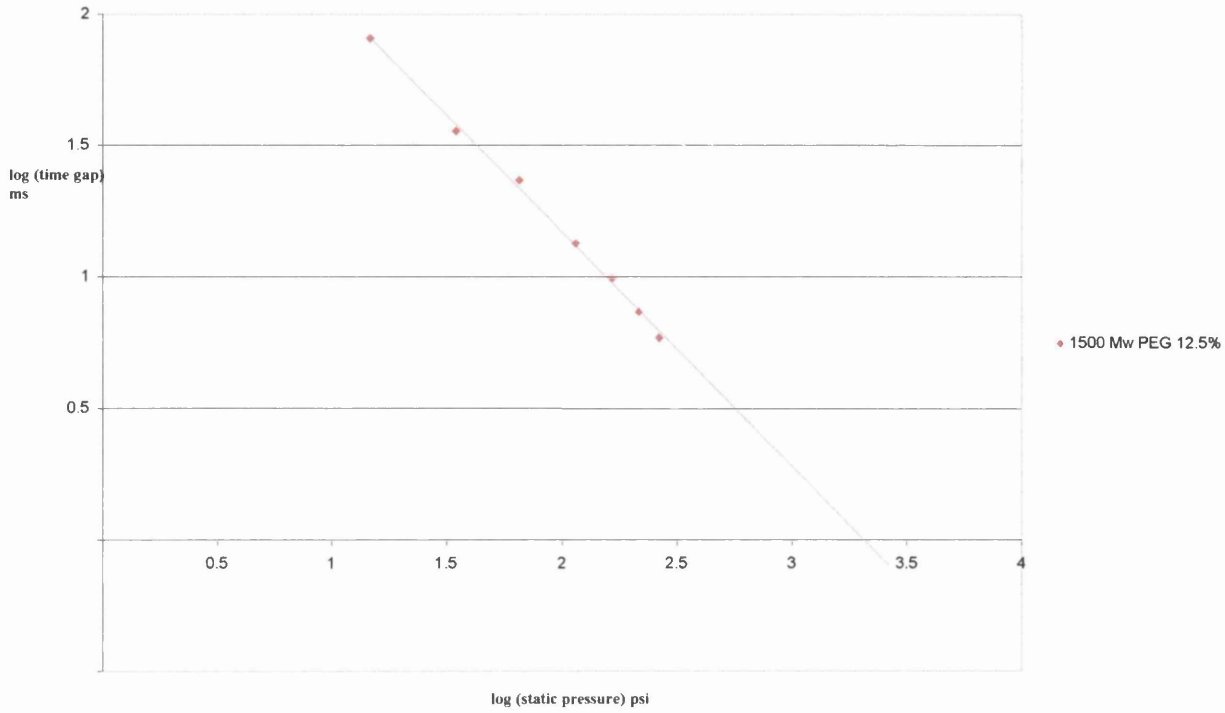


Figure 4.15 Log-log plot of time between pressure peaks as a function of applied static pressure for 1500 Mw at 12.5% concentration

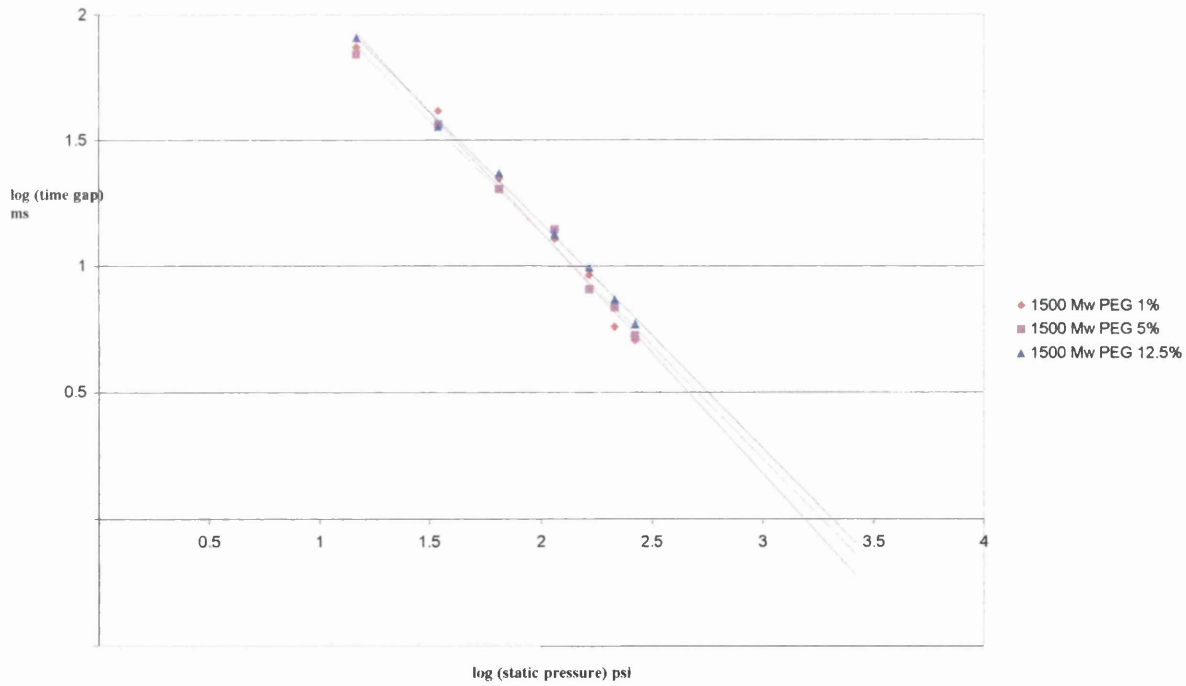


Figure 4.16 Log-log plot of time between pressure peaks as a function of applied static pressure for 1500 Mw at 1%, 5% and 12.5% concentration.

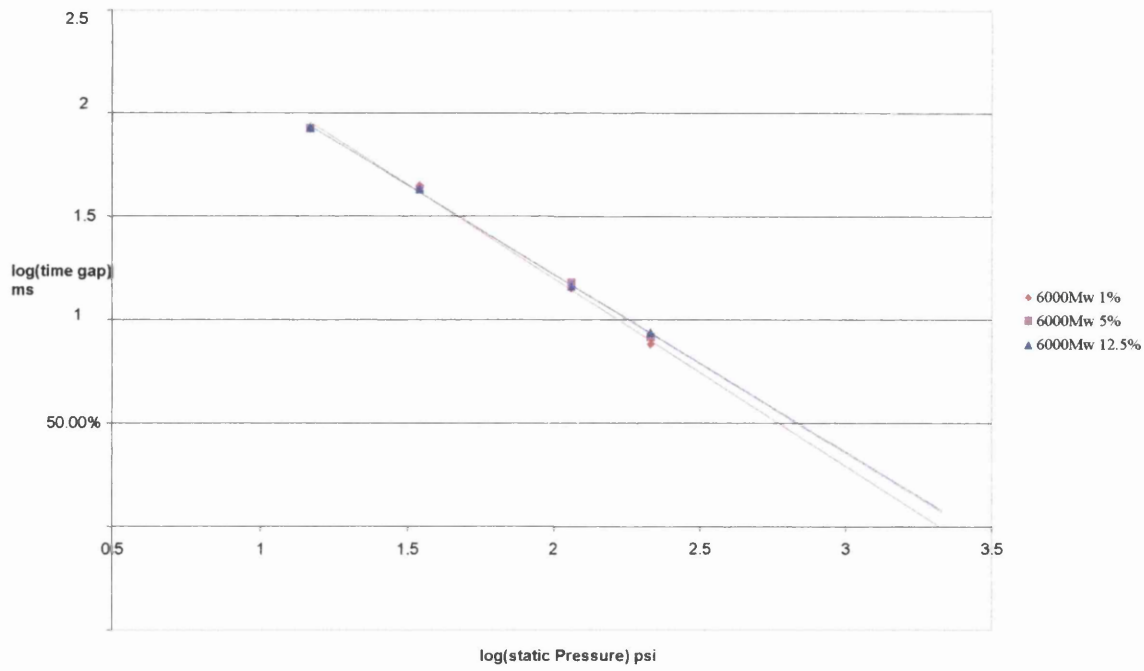


Figure 4.17 Log-log plot of time between pressure peaks as a function of applied static pressure for 6000 Mw at 1%, 5% and 12.5% concentration.

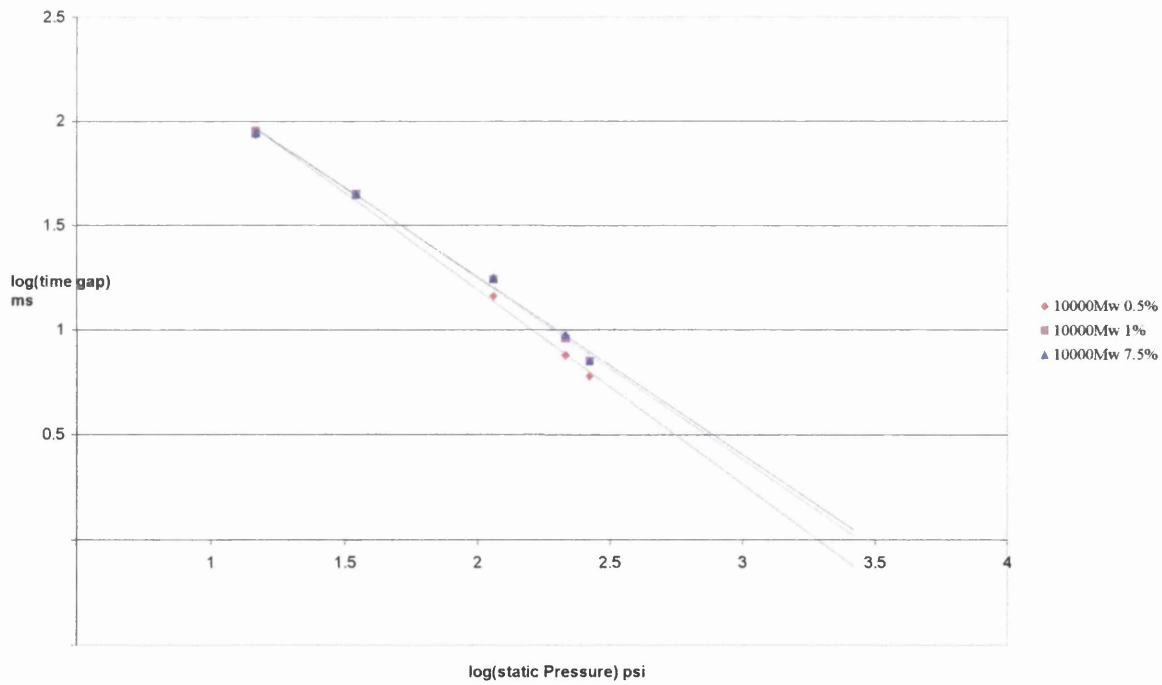


Figure 4.18 Log-log plot of time between pressure peaks as a function of applied static pressure for 10000 Mw at 1%, 5% and 12.5% concentration.

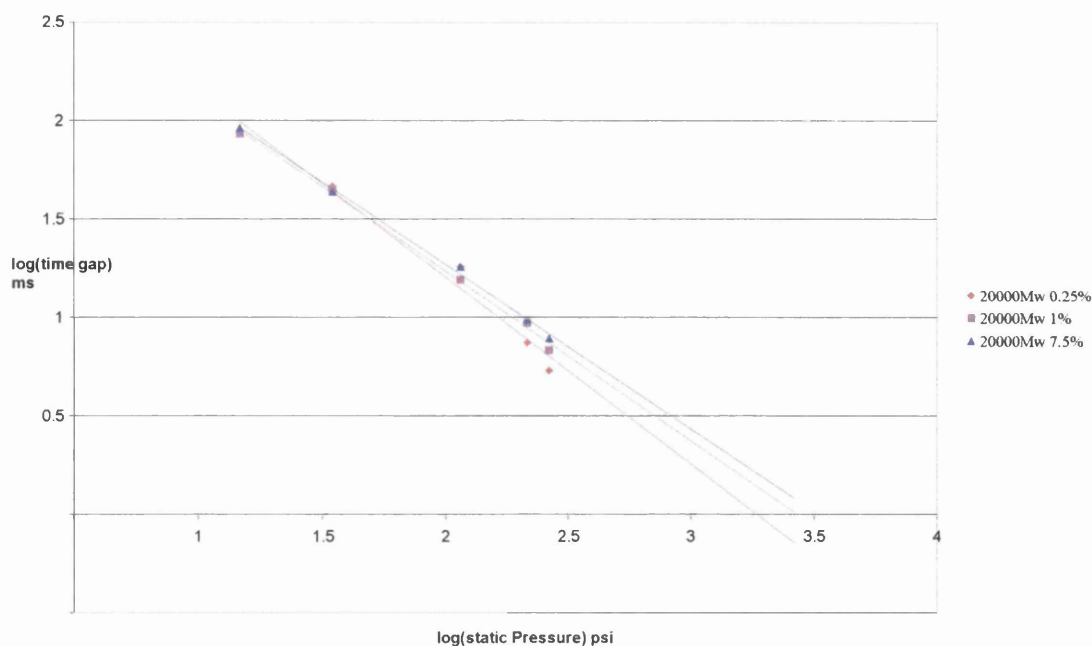


Figure 4.19 Log-log plot of time between pressure peaks as a function of applied static pressure for 20000 Mw at 1%, 5% and 12.5% concentration.

Results for the tensile strength for the different PEG solutions can be seen in table 4.2.

A graph of these results can be seen in figure 4.20.

		Concentration (% polymer by weight)								
		0.25	0.5	1	2.5	5	7.5	10	12.5	15
Molecular weight	600	-	-	102	106	112	115	118	120	120
	1500	-	-	105	115.	126.	139.	140.	140.	141
	6000	-	-	132	149	164	169	171	171	-
	10000	-	131	156	188	200	200	201	-	-
	20000	126.	162.	185.	221.	223.	223.	-	-	-

Table 4.2 The tensile strength, F_c , of solutions of PEG over a range of molecular weights and concentrations.

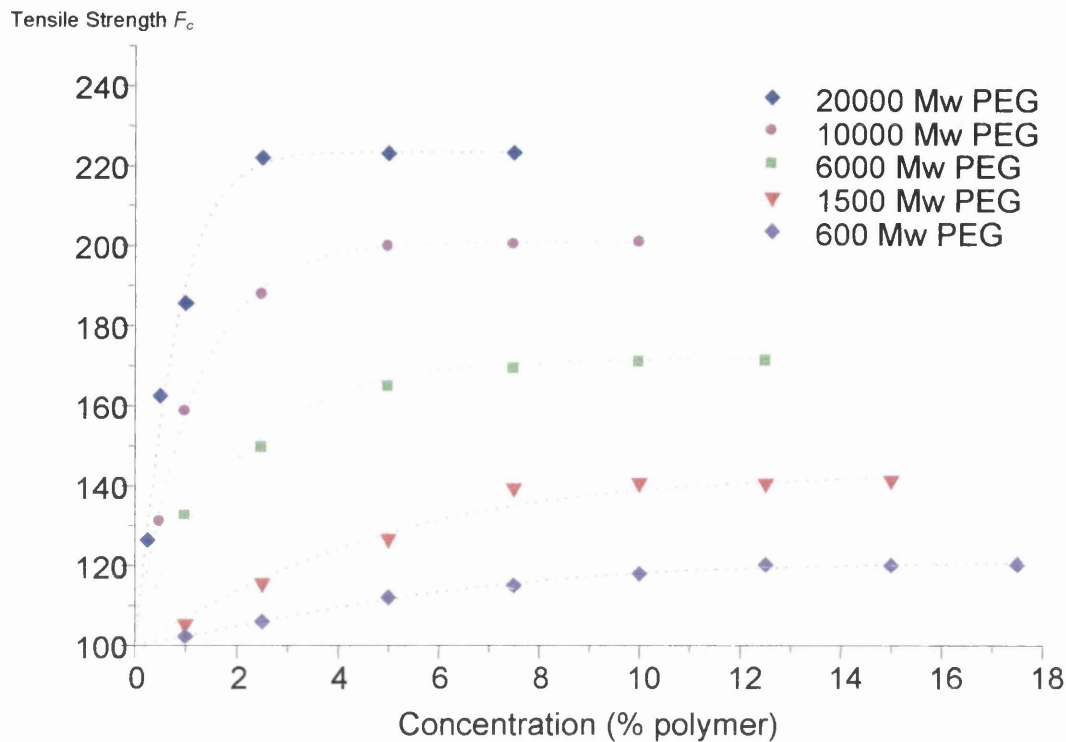


Figure 4.20 The tensile strength of PEG solutions as a function of polymer concentration and molecular weight.

This indicates that at each molecular weight the addition of polymer causes the tensile strength of the fluid to rise but it is also evident that there seems to be a restriction on the growth of the tensile strength of the fluid, and on all the molecular weights a plateau point is reached. An important point on these graphs is that if the lines associated with each molecular weight were extended as the graph shows, they would intersect the y axis at approximately 100 Bar which agrees with (reasonable accuracy) the result obtained for deionised water of 105 ± 5 Bar.

Figure 4.20 has two main noteworthy characteristics; Firstly the steep increase in tensile strength with additional polymer concentration and secondly there is a limiting

tensile strength associated with each molecular weight which also corresponds to a critical concentration, at which point the addition of extra polymer fails to increase the tensile strength. The point of the onset of the plateau is referred to herein as the plateau tensile strength.

Molecular weight	Plateau tensile strength	Concentration at $F_{C_{Plat}}$
600	120	11.5
1500	140	9
6000	170	6
10000	200	4
20000	222	2.5

Table 4.3 Plateau tensile strength against concentration

If a log-log plot of the Molecular weight versus the plateau tensile strength ($F_{C_{(PLAT)}}$) is taken, a linear relation is obtained as seen in figure 4.21.

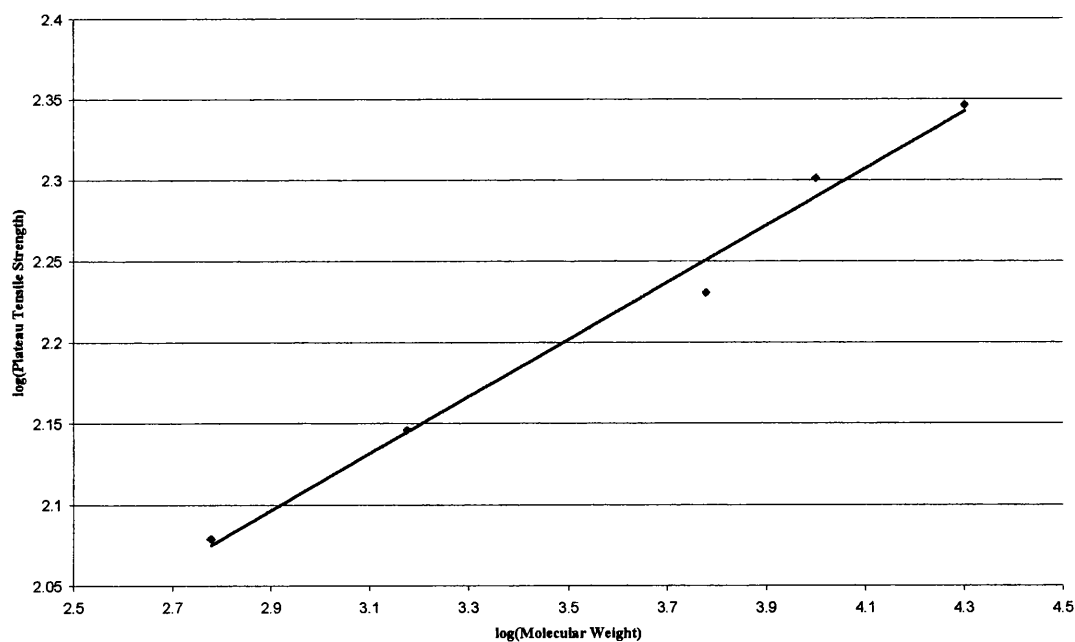


Figure 4.21 Log-log graph of molecular weight and plateau tensile strength

The line of best fit on the above graph (figure 4.21) is given as $y = 0.1755x + 1.5878$

rearranging for $F_{c(PLAT)}$ we obtain

$$F_{c(PLAT)} = 38.7 Mw^{0.1755}$$

Hence with other molecular weight polyethylene glycol solutions we can predict the plateau value for the tensile strength.

Similarly it is interesting to look at the concentration at which the maximum tensile strength is first achieved, hence giving an estimate for the least amount of polymer needed to achieve the largest achievable increase in tensile strength. Figure 4.22 shows a graph of concentration verses molecular weight on a semi-log scale.

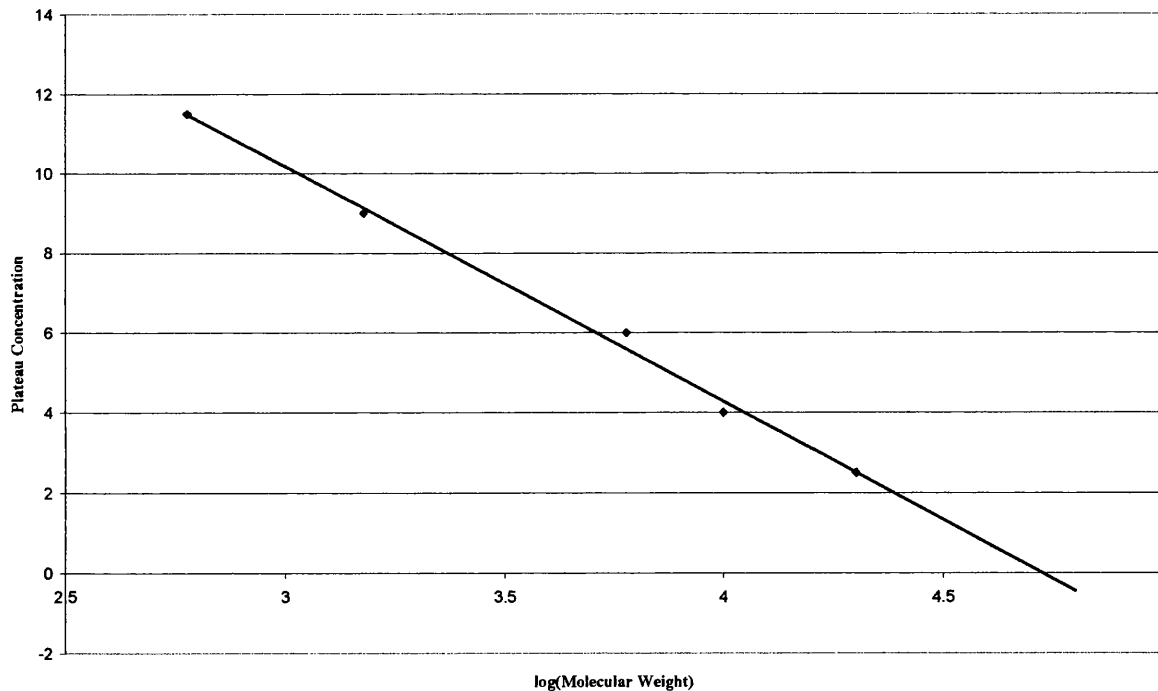


Figure 4.22 Graph of plateau concentration as a function of molecular weight

4.3 Effect of stressing rate on polymer solutions

In section 3.3.1 the effect of stressing rate on purified water reveals that increasing the stressing rate also increases the tensile strength. It has been shown that the effect of concentration and molecular weight creates a distinctive trend, observed also for purified water, namely, an increase in stressing rate has a linear increase with tensile strength. However, it is important to verify that the trend is repeatable at different stressing rates.

We have taken as an example the 6000 Mw solutions and repeated them at different stressing rates (0.17-0.6 Bar/ μ s). It is the author's understanding that this is the first reported work on the effect of stressing rate on a range of polymer solutions.

		Concentration (% polymer by weight)				
		0	1	2.5	7.5	12.5
Stressing rate (Bar/ μ s)	0.6	240	286	330	373	379
	0.4	168	194	226	255	258
	0.3	110	132	149	169	171
	0.17	60	71	82.5	94	95

Table 4.4 The effective tensile strength F_c at a range of concentrations of 6000 Mw PEG solution over a range of stressing rates.

To obtain the tensile strength data in table 4.4, a systematic range of testing was undertaken at various static pressures. A range of gap sizes was then used to alter the pressure applied at the base of the piston and hence alter the rate of stressing developed on the fluid. The results can be seen graphically in figure 4.23.

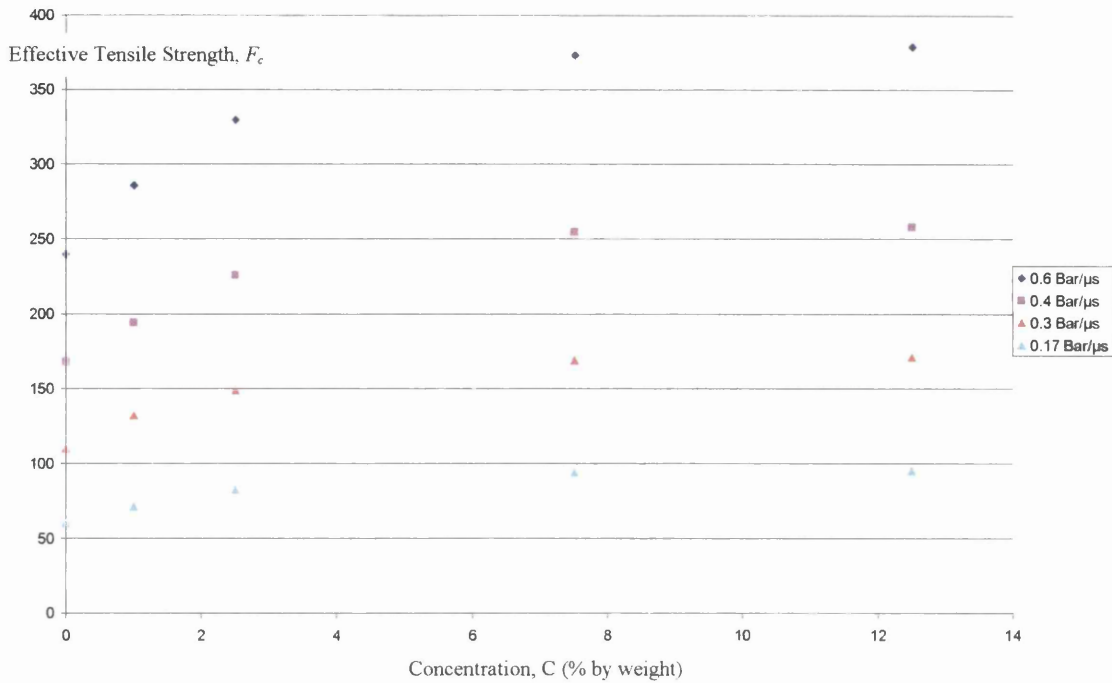


Figure 4.23 The effective tensile strength F_c as a function of concentration for 6000 Mw PEG solutions over a range of stressing rates.

Figure 4.23 and table 4.4 show that with increased stressing rate the tensile strength of the solution also increases. It is important to note that the trend associated with each fluid applies across the range of stressing rates (albeit at a high stress regime).

In chapter 3, on purified water (section 3.2.1), a linear relationship between the tensile strength and stressing rate can be observed. Figure 4.24 shows that this relationship also applies to the polymeric solutions tested. By taking the gradient of these lines the tensile parameter can be obtained on each of these solutions to determine its tensile strength for a given rate of stressing. From the small amount of data that we presently have, these estimations at the high stress development regime have given predictions within 15%.

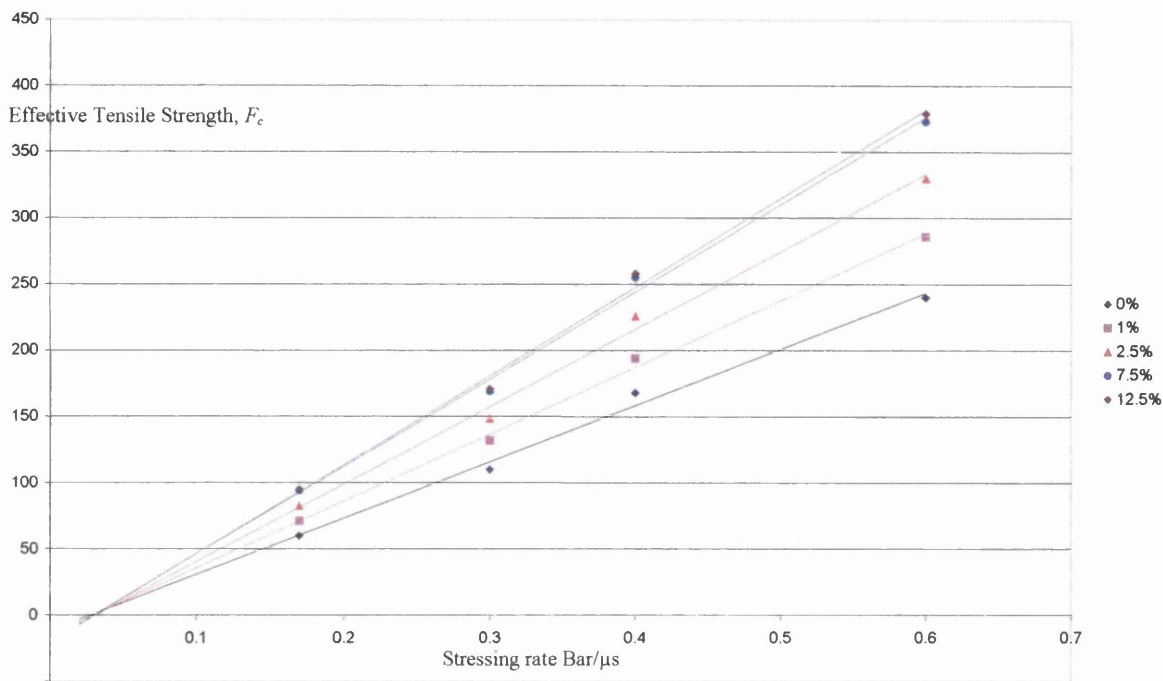


Figure 4.24 The effective tensile strength, F_c , over a range of concentrations of 6000 Mw PEG at various rates of stressing

The effect of stressing rate on the tensile strength of polymer solutions has only been examined for PEG samples at 6000 Mw and further research to confirm the trends observed would need to be undertaken at various other molecular weights.

4.4 PAA results

Similar experiments were conducted on a high molecular weight polyacralamide solution in purified water using a 9×10^6 Mw polymer grade at concentrations from 0.1-0.8, to try to establish if the effects seen for PEG are individual to that polymer or low molecular weight solutions. The same experimental technique as performed with the PEG solutions was carried out with the PAA. The pressure tension cycles have been omitted from this thesis as they show the same trends as previously reported for PEG solutions (Section 4.2.1).

The tensile strength data can be seen in table 4.5 and a graph of these can be seen in figure 4.25. It is apparent that there is a steep increase in the tensile strength of the fluid when initially increasing the polymer concentration, as previously seen with the PEG solutions.

Concentration (% by weight)	0	0.1	0.2	0.3	0.4	0.5	0.6	0.7	0.8
Tensile strength F_c	104	160.57	191.2	208.1	212	212.5	216.4	217.2	218.9

Table 4.5 Tensile strength of PAA at a range of concentrations

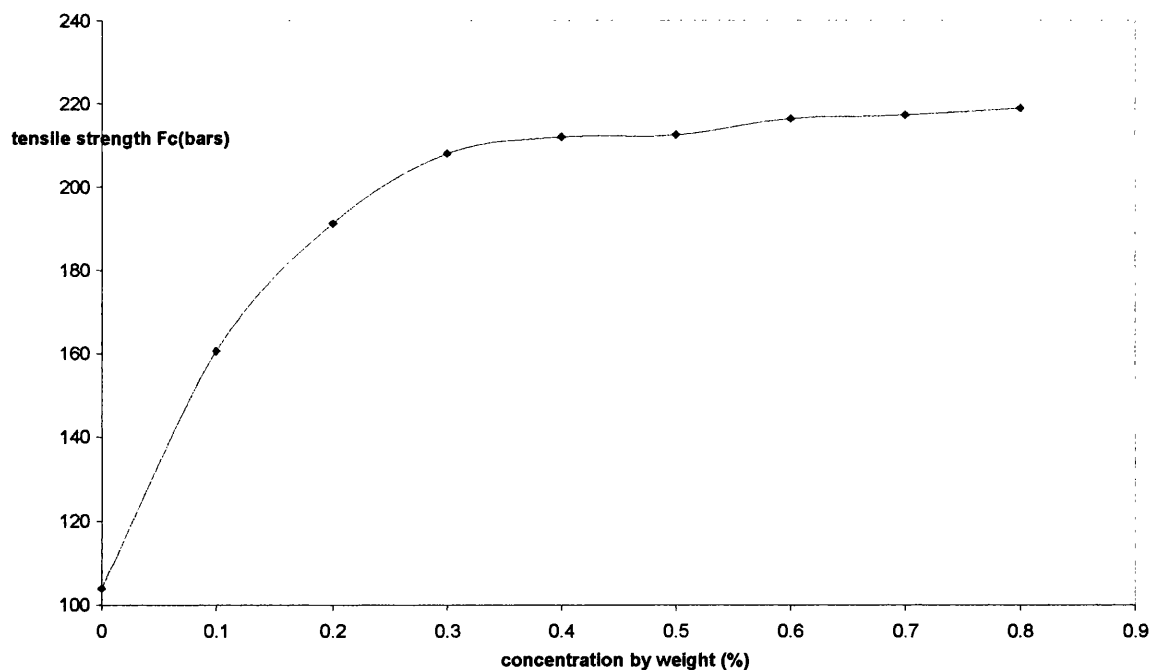


Figure 4.25 Tensile strength as a function of concentration for PAA solutions

These preliminary studies into the effect of PAA on the tensile strength of solutions seem to suggest a similar occurrence, of the onset of a tensile strength plateau with increasing concentration, to what has been seen in PEG. This is an area where more time and research is required to further establish this result across a broader range of molecular weights and polymers.

4.5 Results and discussion

The work reported in this chapter is the first to address the issue of the influence of polymer additives on liquid tensile strength by an appropriate experimental technique i.e. one in which the timescale of the dynamic stressing event and the rate of stressing (rate of tensile stress development) may be systematically controlled. In all previous studies the latter feature has been essentially an *ad hoc* parameter with no adequate means of controlling it or of varying it significantly.

The present results cover systematic testing of the tensile strength of polymeric liquids over a range of concentrations and molecular weight. For the first time in such experiments it is shown unequivocally that with increasing molecular weight there is an increased effective tensile strength of the solution. However, the results also reveal that increasing polymer concentration results in a clearly defined stress saturation level – with an apparent plateau in terms of effective tensile strength.

The present work addresses an important and longstanding anomaly in the cavitation literature concerning the role of (high molecular weight) polymeric additives in determining the cavitation thresholds of dilute aqueous polymer solutions. It is

important to recall that previously, under pulsed dynamic stressing, other researchers had claimed that the presence of polymer could result in a decrease of the (effective) cavitation threshold, such as in the stressing of water containing polyacrylamide additives by the bullet-piston reflection method (Trevena 1987). Their work claims to demonstrate a reduction of liquid effective tensile strength, the reduction increasing with increasing polymer concentration. However, when this same polymer system was investigated using an *ab initio* technique, the cavitation threshold was found to be increased by the same polymer additive, and when subjected to static stressing (in a modified Berthelot tube) the presence of polymer made no discernible difference to the effective tensile strength of the liquid. The results of the present work make explicit the crucial role of timescale in the recording of effective cavitation threshold strength (i.e. tensile stress) parameters. It highlights that in future work (as indeed in all rheological testing) it is essential to consider the stress timescale of the particular flow process being considered in order to design the appropriate means of estimating cavitation resistance. The present results highlight that significant errors could arise in cavitation stress estimates, as the test liquid may be subjected to stressing in experiments involving inappropriate timescales. Moreover the choice of appropriate timescale of the stressing event for cavitation threshold determination must also, clearly, take into consideration the characteristics of the polymer additive – both in terms of the polymer's molecular weight and its concentration in solution. Neither of these issues has previously been considered in a systematic manner in the cavitation research literature – hence the discrepancy between various estimates of the level of cavitation resistance of such solutions and their dependence on concentration and polymer characteristics.

CHAPTER 5

Extensional Rheology

Chapter 5

Extensional Rheology

5.1 Introduction

Distinctive trends in the effect of polymer weight and concentration on the tensile strength of a sample have been clearly observed in the previous two chapters. These results obtained using the bullet-piston technique use high stressing rates in the order of 0.1-0.7 Bar/ μ s. These rates are of importance in the motor industry because they are of the same order as that found in the lubrication of journal bearings. However in other industrial applications such as printing applications, the stressing rates are far lower. This means the values obtained in the bullet-piston technique are not quantitative in relation to the ink printing industry. It is therefore necessary to use a technique which can calculate the tensile strength at these lower stressing rates. It would therefore be appropriate to use an extensional rheometer, which operates at these lower stressing rates, to determine the tensile strength of a polymeric sample.

5.2 Capillary breakup extensional rheometer (CaBER)

The CaBER is a device designed to measure the extensional viscosity and longest relaxation times of polymer solutions. A picture of the CaBER can be seen in figure 5.1. The operational procedure of the CaBER requires a small amount (<0.5 ml) of sample liquid to be placed between two horizontal vertically aligned plates.

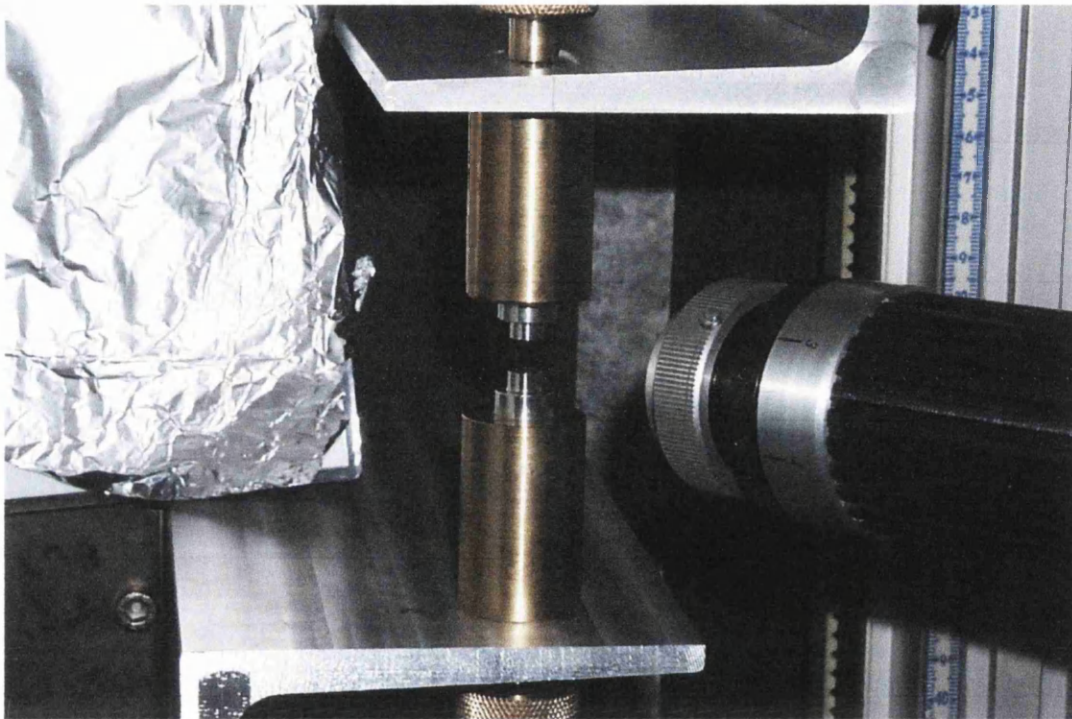


Figure 5.1 The CaBER

The top plate is rapidly separated from the bottom plate at a set speed to a set distance. After cessation of stretching, the fluid at the mid-point of the formed filament undergoes an extensional strain rate defined by the extensional properties of the fluid. This sequence of events is filmed on a high speed camera system, a Kodak EKTAPRO 4540mx Imager. With analysis of the images the extensional properties of the fluid may be determined. The CaBER experiment has been used by many different

workers to investigate the extensional properties of polymeric systems, including Rodd et al. (2005), Anna and McKinley (2000) and Wunderlich et al. (2000).

Once the plates have stopped, a filament is observed between the two reservoirs. The capillary thinning geometry of the filament is used to determine the strain rate and stress on the fluid. In analysing the filament a slender filament approximation is used, taking the assumptions that the filament is thin and the axial velocity does not vary radially. With these assumptions the local extension rate can be given by (Anna 2000):

$$\dot{\epsilon} = \frac{2}{R} \frac{dR}{dt}$$

where $\dot{\epsilon}$ is the extension rate, R is the radius and t is the time. Assuming the filament is perfectly cylindrical there is no shear component.

The calculation of the stress can be expressed in differential form, presented in Szabo et al (1997) as,

$$\tau_E = \frac{2\sigma}{R} \frac{\partial (R^2 \tau_E)}{\partial z} = \frac{\sigma}{R^2} \frac{\partial R(1 + RR'')}{\partial z} + \rho \frac{\partial v}{\partial t} + \rho v \frac{\partial v}{\partial z} + \rho g + F$$

where τ_E is the extensional stress, σ is the surface tension, v is the axial velocity, ρ is the density and g is the acceleration due to gravity. F is included for any other terms which may be deemed important such as any contributions to shear stress. However within the capillary thinning experiment many assumptions can be made; forces arising from gravity, inertia and curvature as well as any shear forces are neglected.

This results in a simplification for the extensional stress as,

$$\tau_E = \frac{2\sigma}{D_{mid}}$$

5.3 Operation

The upper and lower plates of the CaBER are aligned both vertically and horizontally before the experiment takes place. A small amount (<0.5 ml) of the sample is placed using a syringe between the plates, with a separation of 3 mm. This forms a liquid bridge as can be seen in image 1 of figure 5.2. The upper plate is then moved a set distance at constant speed before stopping, figure 5.2 shows a typical procedure of the plates being separated. In many similar experiments the method of separation is important for measurement purposes. Many other techniques separate the plates in an exponential manner to impose constant stress rates across the fluid sample. However this takes much longer and allows more fluid to drain from the liquid bridge before cessation. This causes problems with the lack of fluid left to film the filament breakup over a long time period. The separation process takes approximately 0.2 seconds, which leaves enough fluid to extensively film the breakup procedure. It can be seen from figure 5.2 that as the upper plate is moved upwards the liquid bridge is pulled apart until the formation of a filament. This filament is normally centred in the horizontal direction and slightly higher than centre in the vertical plane due to the effect of gravity on the surrounding liquid.

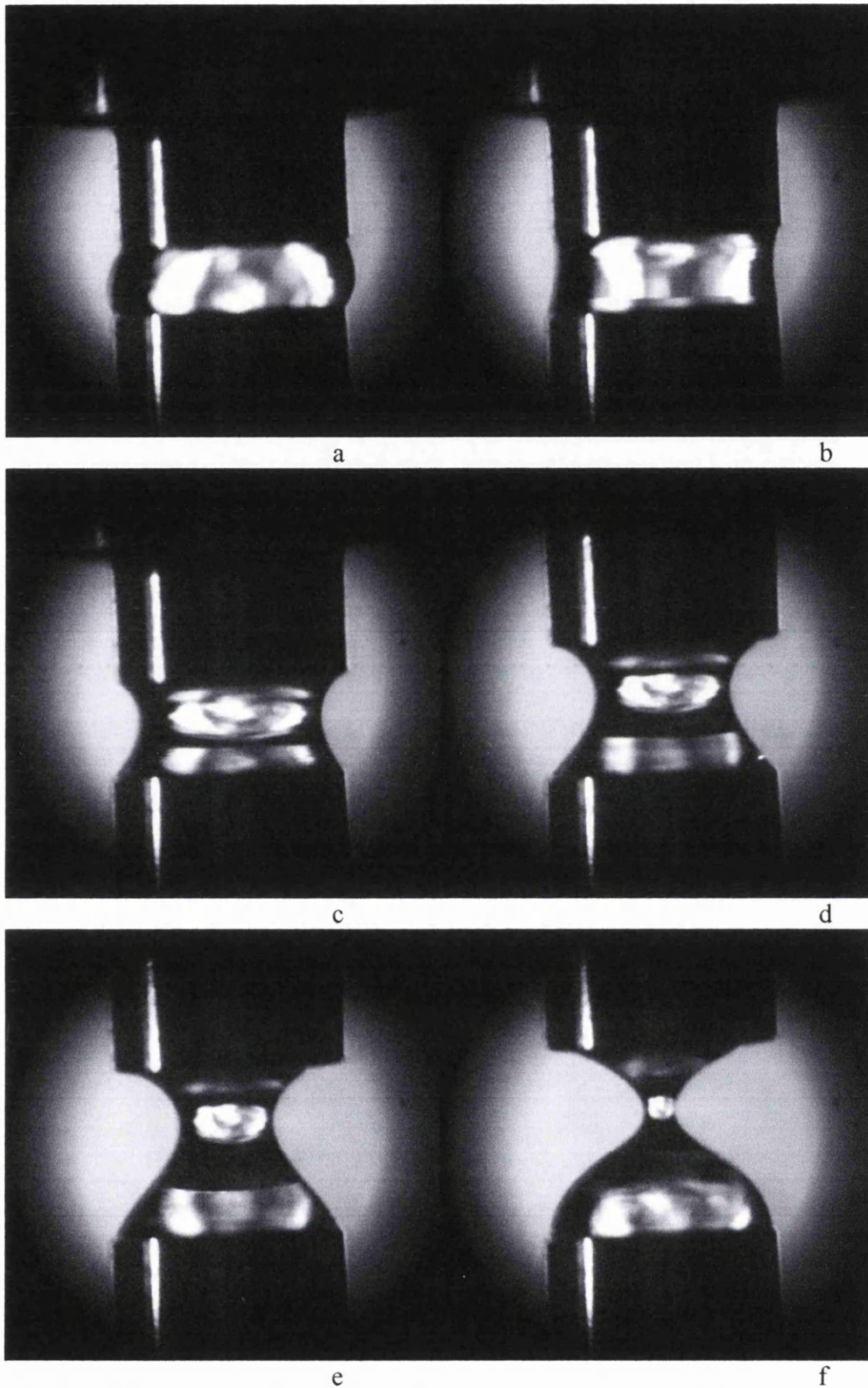


Figure 5.2 Typical set of images during separation of plates a-f (time gap between frames is 0.035 seconds with a complete separation in 0.2 seconds) . (PEG 600 Mw 0.5% concentration).

After the upper plate has stopped, the filament breaks under the forces acting on it; gravity and surface tension being major factors. The sequence of images showing the breakup of the filament, figure 5.3, shows how the low molecular weight polyethylene glycol solution (600 Mw at 0.5% concentration) has a very uniform symmetrical split. Measurements of the filament diameter are taken from each frame in relation to the time since the plates have stopped. This has been achieved both manually and by using a computer programme (ImageJ) which looks at the contrast in colour across a set line and records the width of darker parts of the image across that line (hence recording the dark parts of the filament). This corresponds well to the manual readings and hence in this work results have been obtained via the computer package to analyse three of five repeated samples, manually checking the remaining two for accuracy.

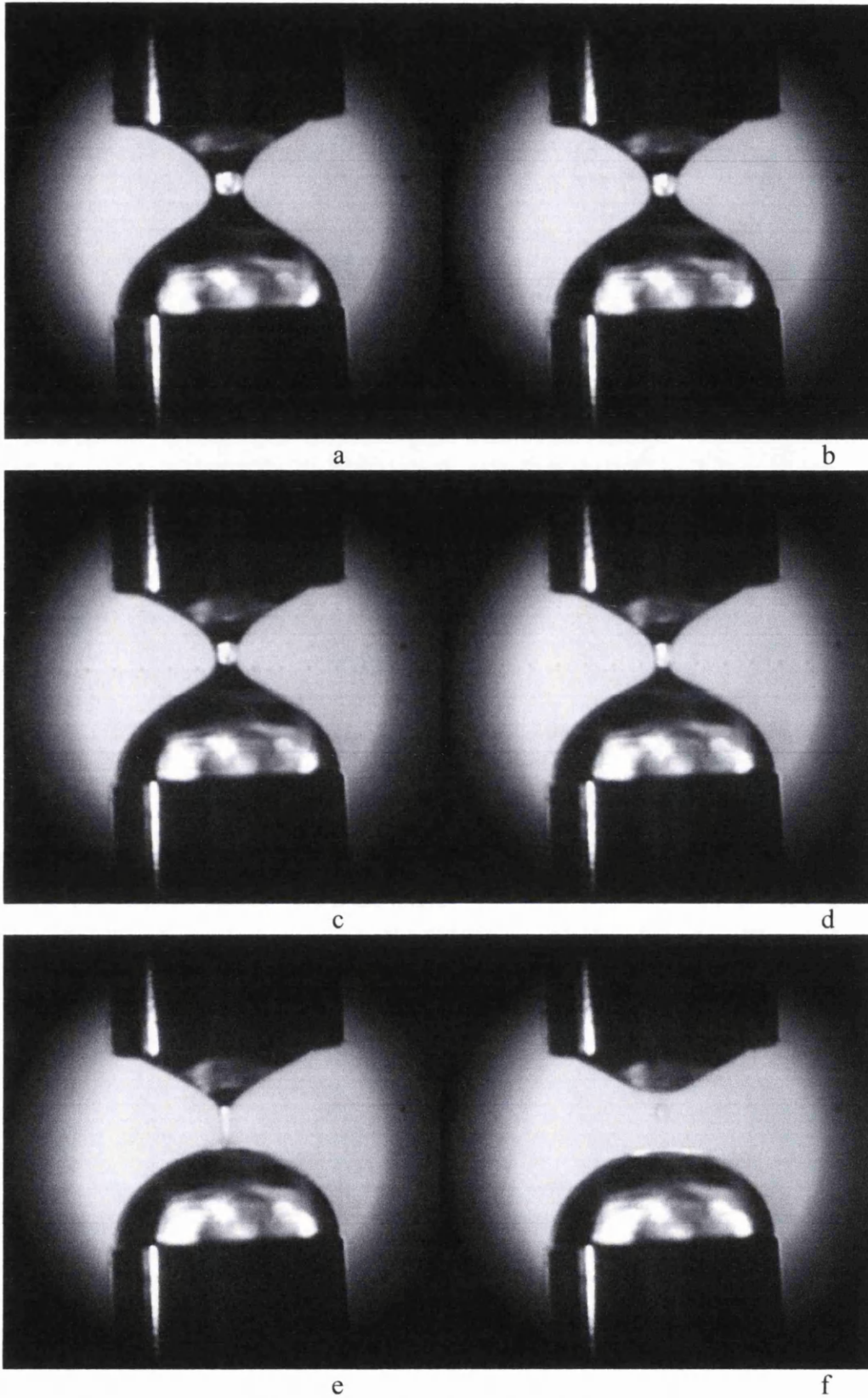


Figure 5.3 Sequence of images a-f showing the splitting of the filament after the upper plate has ceased moving. Time between each frame is $4/4500$ seconds. (PEG 600 Mw 0.5% concentration).

The graph below (figure 5.4) shows a typical filament diameter versus time for a low molecular weight polymer solution. The analysis of the images was completed both by using a custom-coded macro with ImageJ and also manually for verification purposes. The principle behind the analysis techniques is to look at the midpoint of the filament and to follow the diameter profile. The first part of the graph may include a few frames where separation is still ongoing but clearly shows a gradual decrease in filament diameter until a set point where a sharp rise in speed of decrease is noted. The filament lasts for <0.025 seconds and eventually ruptures.

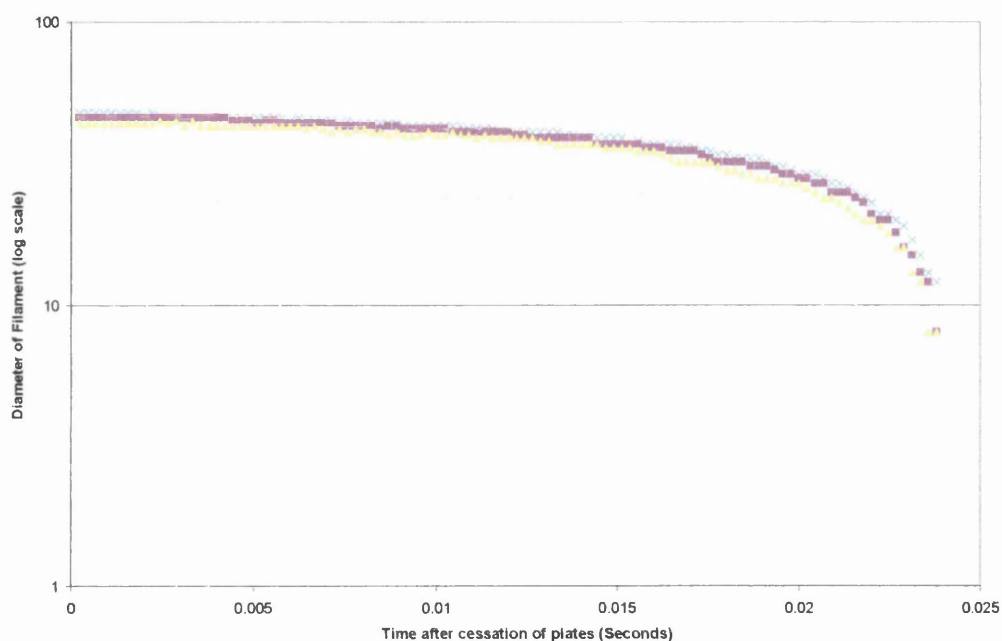


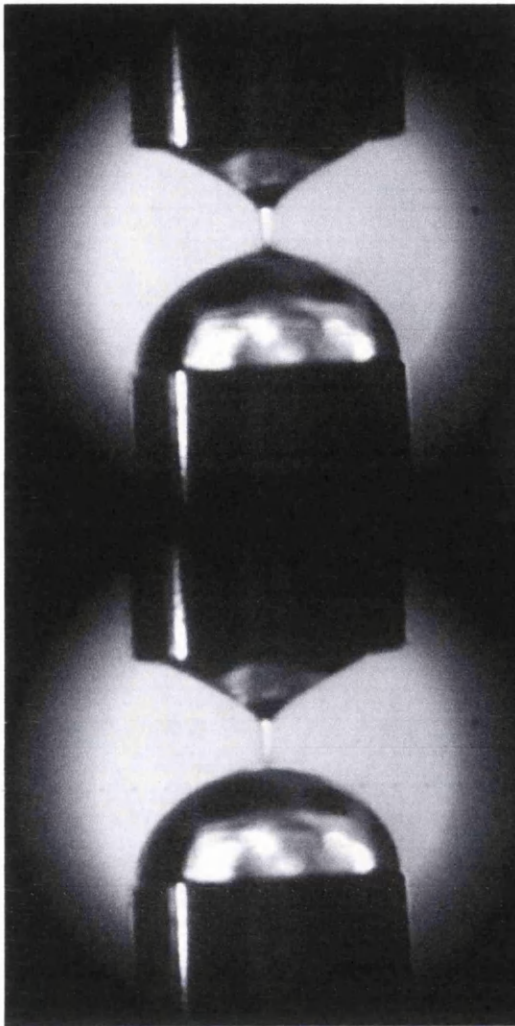
Figure 5.4 The diameter of the filament after cessation of the plates for a low molecular weight polyethylene glycol solution (600 Mw PEG 0.5% concentration) until ultimate rupture.

A sequence of images shown at the filming rate of 4500 f.p.s is shown in figure 5.5. These images clearly show that the breakup of the filament is at the base of the filament. This then 'releases' satellite particles as seen in image 'e' figure 5.5.

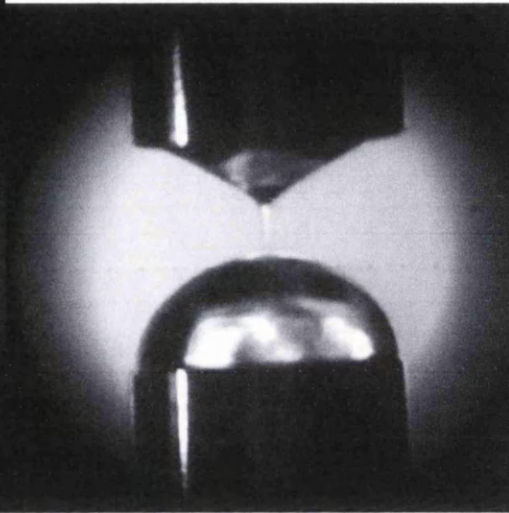
Figure 5.5

Images a-e show the filament break-up and formation of satellite drops. Each image has a time gap of 1/4500 seconds between each subsequent shot. (PEG 600 Mw 0.5% concentration)

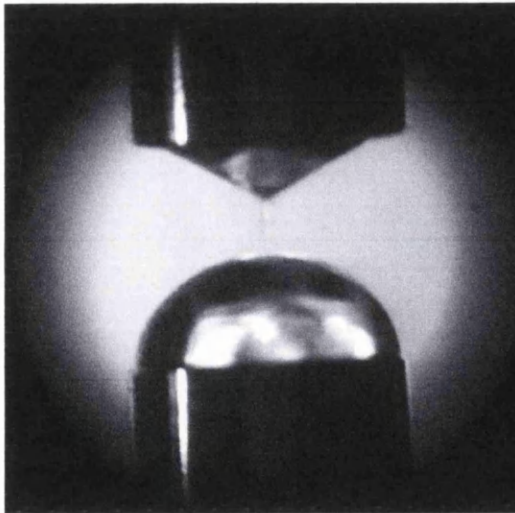
a



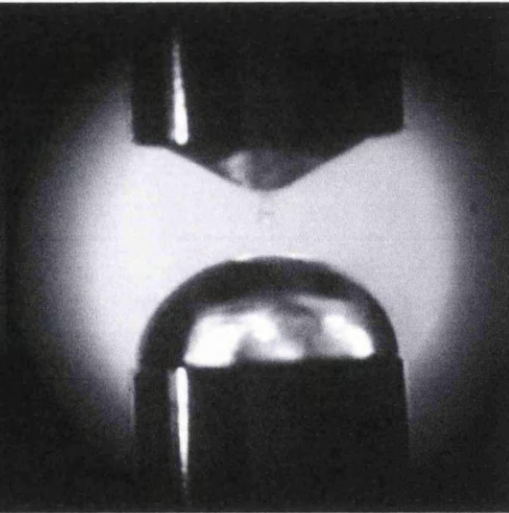
b



c



d

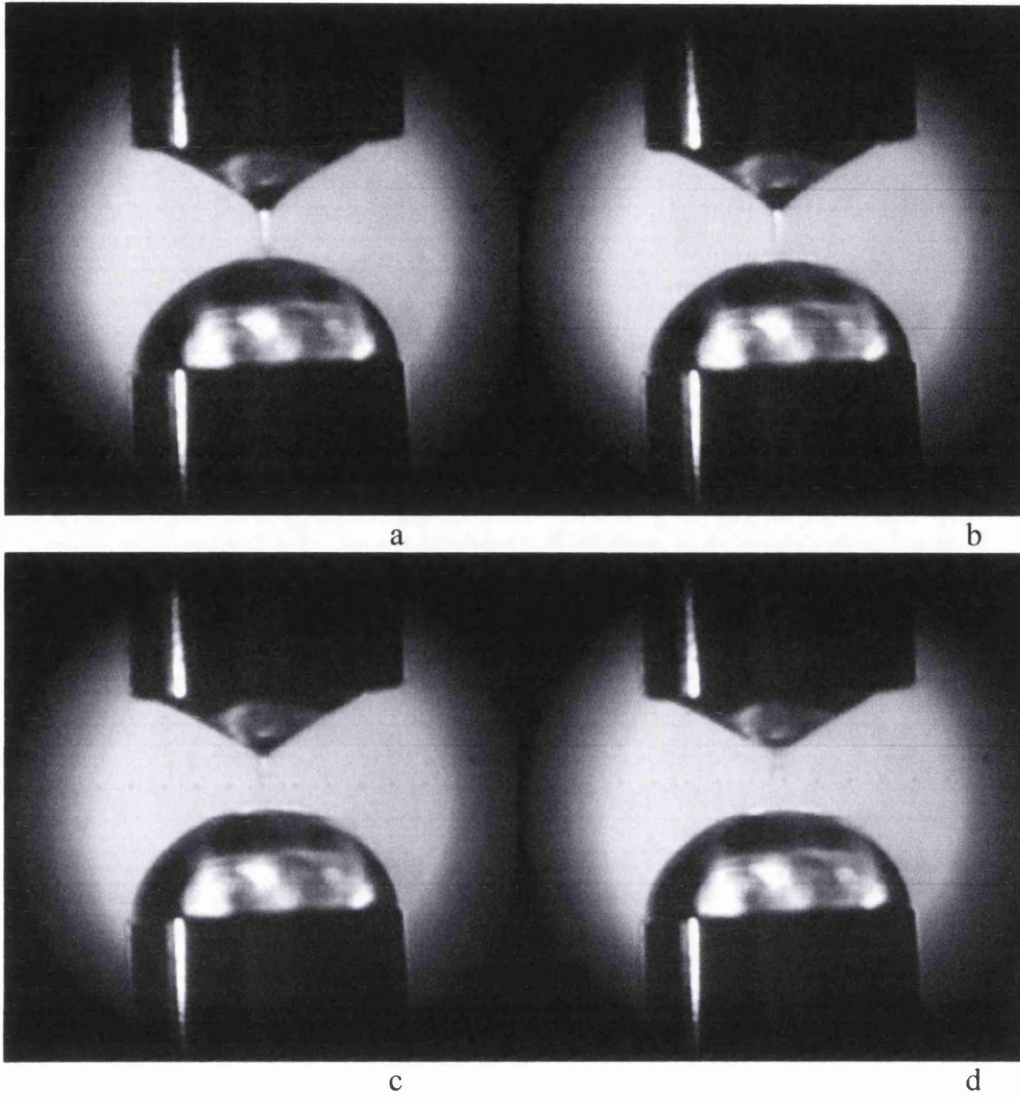


e

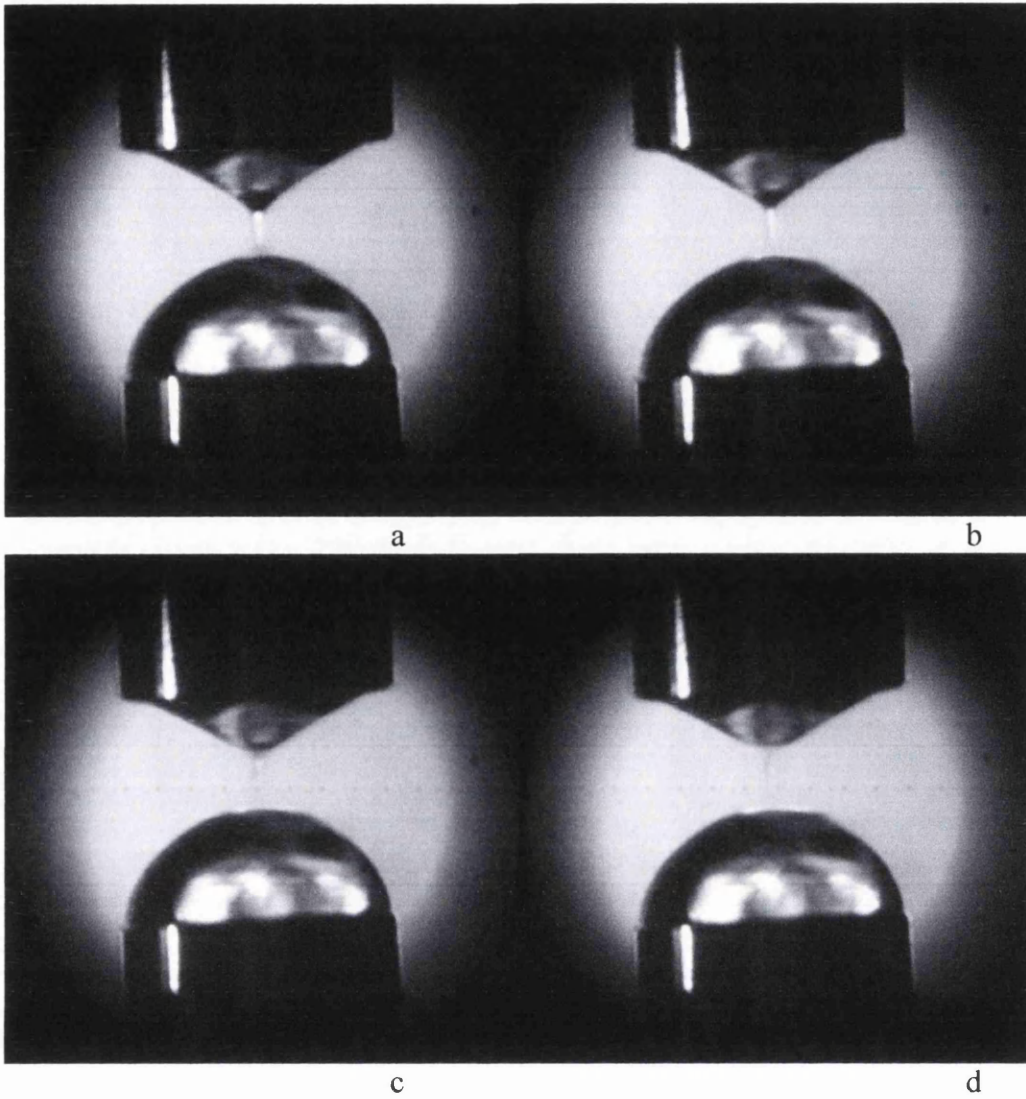
5.4 Results

To determine the tensile strength of the fluid sample as described earlier in the chapter, the mid diameter of the filament just prior to breakup is required. To obtain this value a record was taken of the splitting at high speeds and the profile of the filament was mapped. Enlarging the images taken just prior to breakup allows the pixels within the image at the middle of the filament to be determined (for this purpose the mid diameter is actually taken as the thinnest part of the filament prior to breakup and may not be exactly in the centre of the two plates). By also checking the pixels for the plate diameter we can then determine the actual filament diameter.

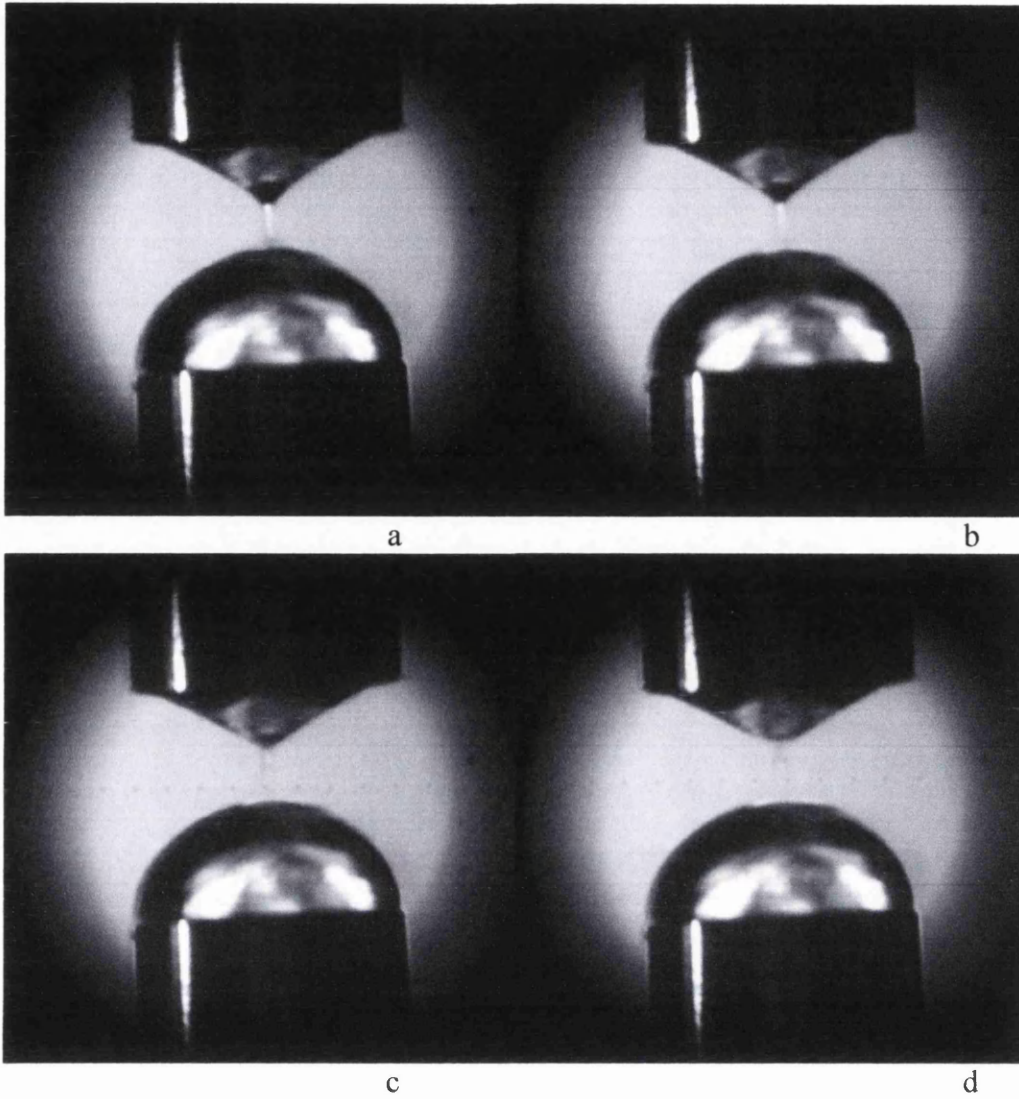
The images Sequence 1-5 just prior to breakup are shown for 0.5% concentrations over the molecular weights tested, each subsequent image is 1/4500 sec after each other. Frames just prior to breakup for all Mw and concentrations are shown in Appendix B.



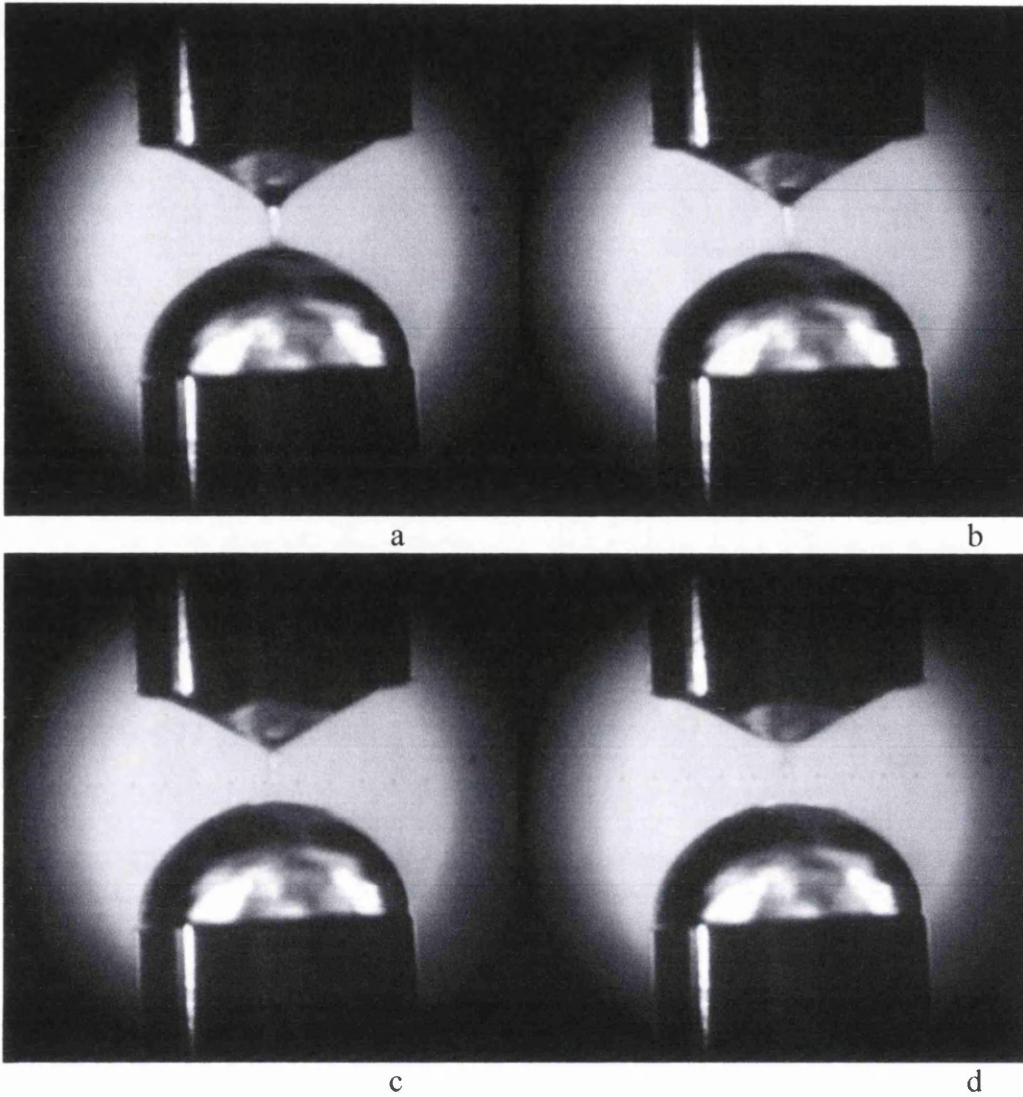
Sequence 1 Filament splitting (a-d) for 600 Mw PEG solution at 0.5% concentration



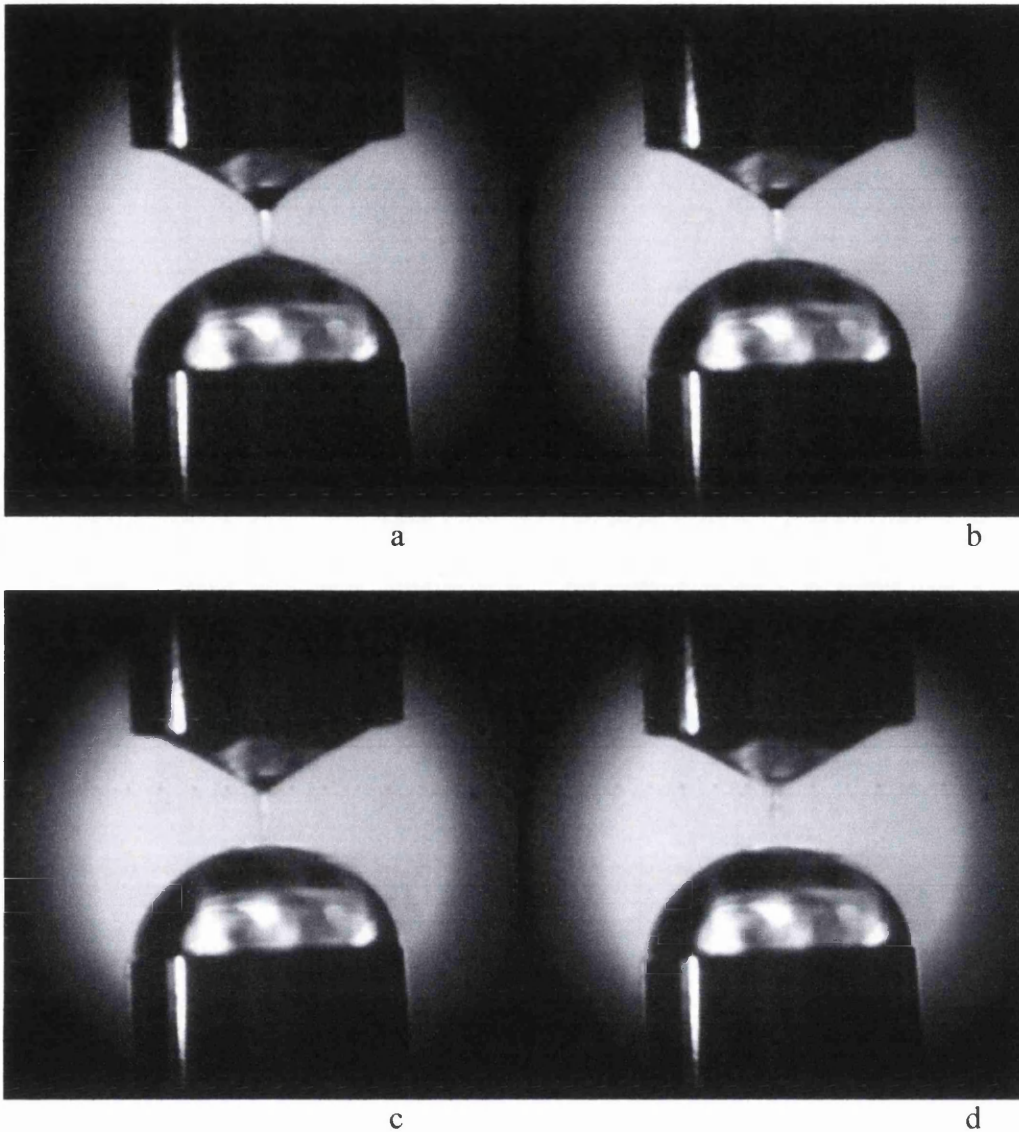
Sequence 2 Filament splitting (a-d) for 1500 Mw PEG solution at 0.5% concentration



Sequence 3 Filament splitting (a-d) for 6000 Mw PEG solution at 0.5% concentration



Sequence 4 Filament splitting (a-d) for 10000 Mw PEG solution at 0.5% concentration



Sequence 5 Filament splitting (a-d) for 20000 Mw PEG solution at 0.5% concentration

By using image analysis we can obtain the filament diameter in mm, a plot of the filament diameter versus concentration for the polymer solutions can be seen below (figure 5.6).

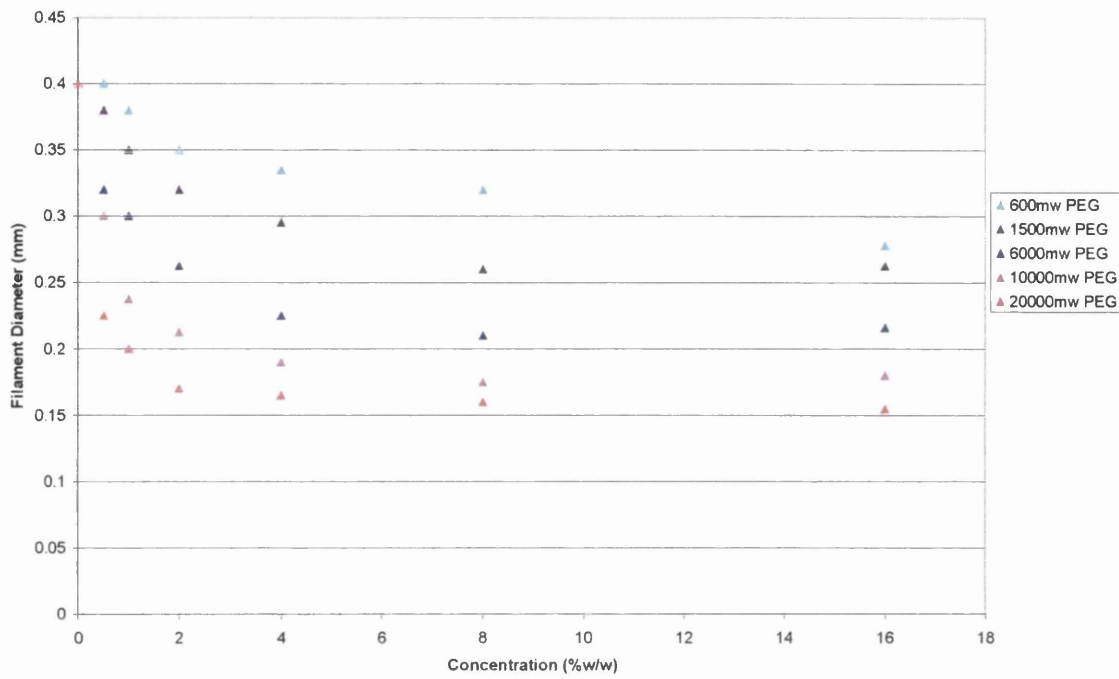


Figure 5.6 Filament diameter prior to breakup against concentration

It is noteworthy that larger diameters of the filament upon breakup, correspond to lower molecular weight polymer solutions as the polymer itself seems to strengthen the liquid sample to resist breaking-up until much smaller diameters.

An additional aspect of the filament breakup is that there is the formation of droplets during the splitting process; these are directly related to the size of the filament of breakup and hence can also be used as a ranking aid for the strength of the polymer in solution. Figure 5.7 shows diameter size versus concentration for all molecular weights.

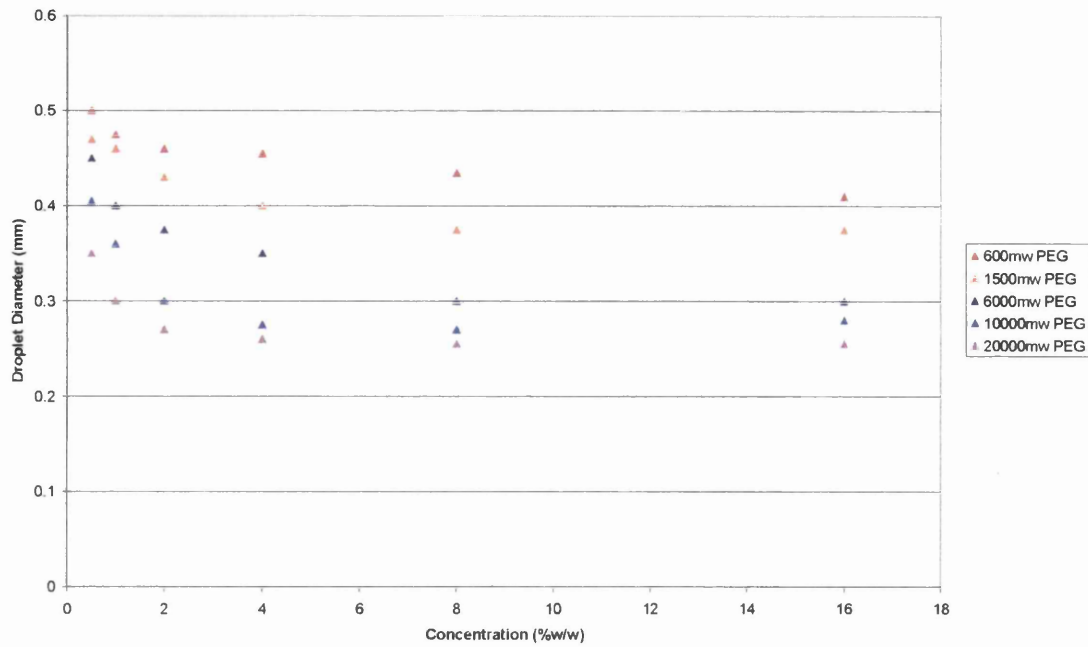


Figure 5.7 Droplet diameters against concentration.

To determine the tensile strength however we use the values obtained for mid filament just prior to breakup along with the surface tension measurements for each sample using the equation,

$$\tau_E = \frac{2\sigma}{D_{mid}}$$

The estimates we obtain for the tensile strength for this method can be seen in the table below and the subsequent graph.

Concentration (% by weight)	600 Mw	1500 Mw	6000 Mw	10000 Mw	20000 Mw
0	300	300	300	300	300
0.5	300	315.8	375	400	533.3
1	315.8	342.9	400	505.3	600
2	342.9	375	457.1	564.7	705.9
4	358.2	406.8	533.3	631.6	727.3
8	375	461.5	571.4	685.7	750
16	431.7	457.1	555.8	666.7	774.2

Table 5.1 The effective tensile strength, Pas^{-1} , for a range of polymer concentrations and molecular weights of PEG

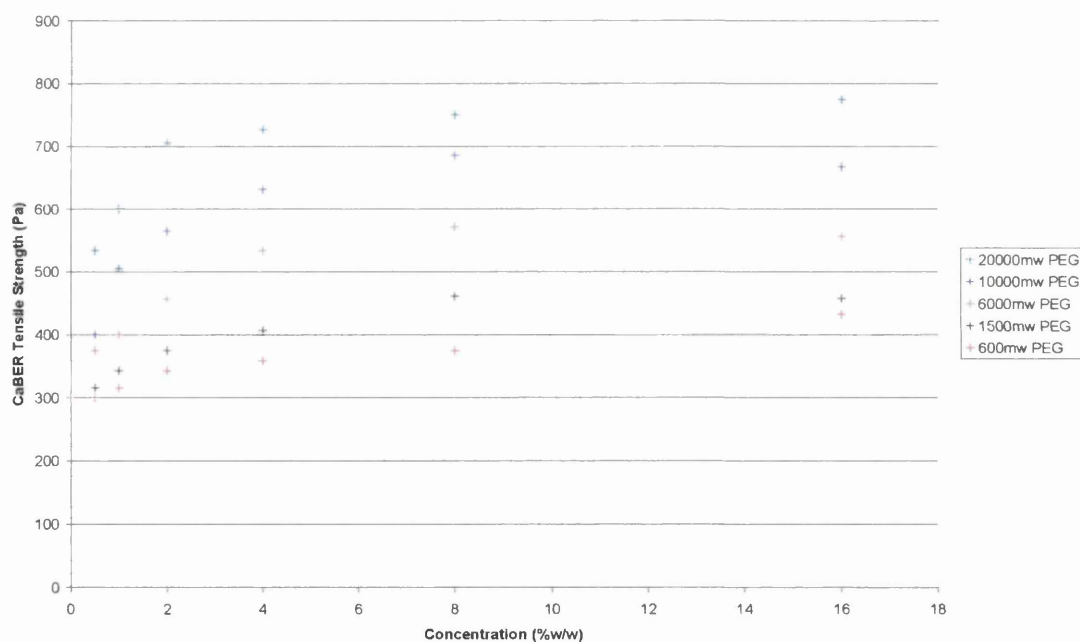


Figure 5.8 Tensile strength (from CaBER) as a function of polymer concentration for a range of PEG Mw solutions

What can be seen is that the similarity in shape and order of the graph is very close to that of the results obtained via the modified bullet-piston technique. The order of

magnitude however is significantly different with the CaBER experiment, resulting in tensile strengths of the order of approx 500 Pa whilst the B-P technique gave results in the magnitude of 150 Bar. For a graph of comparative results see figure 5.9.

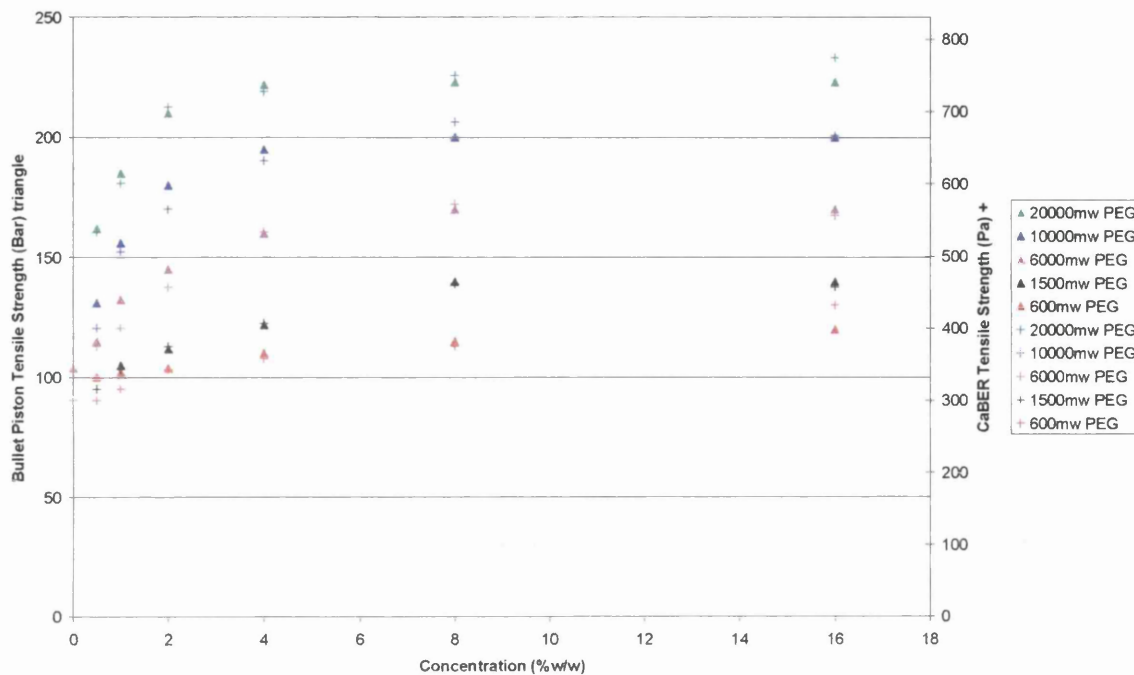


Figure 5.9 Bullet-piston and CaBER tensile strength values as a function of polymer concentration

However as was shown in chapter 3 the rate of stressing has a marked effect on the tensile strength of the fluid and with this in mind one must look at the rates of stressing applied in both experiments.

To determine the rate of stressing in the CaBER experiment the previously given equation is used,

$$\dot{\epsilon} = \frac{-2}{R} \frac{dR}{dt}$$

By looking at the rate of change of diameter at breakup the extension rates can be determined. The rates of stressing resulted were in the magnitude of 12000 – 25000 Pas^{-1} , whereas in the bullet-piston experiment these were in the range 0.3 – 0.6 Bar^{-1} .

5.5 Summary

It is clear that the pertinent rates of stress development in the cavitation experiments are orders-of-magnitude greater than those arising during the CaBER filament stretching work reported herein. However, the duration of the pulsed dynamic stressing regime is correspondingly far less: in rheological terms, in consideration of the relevant Deborah number, this means that there is far greater time available for the fluid in the filament stretching situation to relax stress by an extensional flow mechanism. The situation in terms of the cavitation experiment is more akin to the fracture of an elastic solid (where there is no corresponding relaxation of stress possible due to viscous dissipation during flow). This difference in (i) the relative rates of stressing, and (ii) the different timescales of the duration of the stressing event, leads to the large differences which are evident between the cavitation resistance of the fluids (in terms of their limiting effective tensile strength) and the corresponding values of extensional stress generated immediately prior to filament rupture. The two measures of tensile stress correspond, of course, to markedly different rheological phenomena and failure mechanisms. Despite these significant differences between a cavitation rupture event within the bulk of the liquid sample and a fluid filament breakup phenomena, it is clearly interesting and encouraging from a process engineering standpoint that both types of experiment reveal essentially the same form of dependence of the two different critical stress parameters in relation to their variation with polymer concentration and molecular weight of the polymer.

The results reported in this chapter (taken together with those in chapter 4) are in fact the first to relate cavitation failure of a fluid and its extensional breakup properties

in terms of two appropriately chosen tensile stress parameters. In addition, this work is the first to report the relationship between these stress parameters on the basis of an experimental study involving two different but complementary techniques involving a significant range of tensile stress development and a wide range of polymer concentration and molecular weight. Despite the large differences evident in the magnitudes of the tensile stress parameters estimated in the two different experiments - which arise principally due to the large differences in stressing rates/deformation rates involved in the two techniques - both show that the relevant stress limiting parameter increases with polymer concentration and molecular weight, but that such stress levels become effectively saturated (i.e. produce plateau limiting values) at essentially the same levels of concentration and molecular weight. This information has never previously been available due to a lack of a suitable cavitation technique and of the appropriate analysis of CaBER filament breakup experiments in terms of the limiting stress parameter.

The information reported here, and in chapter 4, shows for the first time that it may be possible to conduct fluid breakup measurements in extensional flow experiments in order to ascertain the likely levels of cavitation threshold stress for dilute aqueous polymer solutions. The bullet-piston experiments (chapter 4) are extremely time-consuming, difficult to perform and require relatively large volumes of fluid sample whereas the CaBER-type experiments require very small volumes of fluid sample, are quick to perform and can be achieved for relatively low cost. The results of such measurements will inform the better design (and possibly control) of numerous industrial flow processes involving relationships between cavitation breakup of fluids and their subsequent filamentation – with printing and coating flow processes

being the best known example of these. The present work is therefore most likely to find immediate applications in that field – possibly in terms of ranking the cavitation resistance of fluids involving a systematic variation of polymer additives, in a range of flow settings involving different deformation rates.

CHAPTER 6

***CONCLUSIONS AND
RECOMMENDATIONS FOR FUTURE
WORK***

Chapter 6

Conclusions and Future Directions

The work reported in this thesis is focused on determining the tensile strength of polymeric liquids by two main experimental techniques, namely the modified bullet-piston (B-P) technique and a capillary break-up extensional rheometer (CaBER). The principal motivation for this work lies in the fact that although many important associations exist between the cavitation properties of fluids (in terms of their response and ultimate failure under imposed tensile stresses) and their extensional flow properties, these associations have never previously been investigated in a systematic way using appropriate experimental techniques. Moreover, these associations require careful consideration in relation to the behaviour of fluids in industrial processes (such as printing and coating as well as motor industries) in which cavitation and filamentation may both result from the generation and application of tension in flow settings.

The principal reason underlying the lack of a study into the relationship between cavitation properties (such as cavitation resistance or tensile strength) and extensional flow properties has been that, until now, no appropriate cavitation technique has been identified or applied in this area.

Turning first to the results for a Newtonian fluid, this thesis reports the results of experiments in which samples of degassed, purified water were subjected to dynamic stressing by pulses of tension. The pulse reflection technique employed allows the rate of development of tension in the liquid, $\dot{\Omega}_p$, to be varied systematically, in order

to investigate its influence on the resulting measurement of the liquid's 'effective' tensile strength (or 'cavitation threshold'), F_c . Results are reported for experiments involving a range of stressing rates, $\dot{\Omega}_p$, $\approx 0.19 \text{ Bar}/\mu\text{s} \leq \dot{\Omega}_p \leq 0.77 \text{ Bar}/\mu\text{s}$. These experiments, which are the first of their kind to be reported for water, show an approximately four-fold increase of F_c at the highest stressing rate, this value being 224 Bar (for $\dot{\Omega}_p = 0.77 \text{ Bar}/\mu\text{s}$) compared to 59 Bar (for $\dot{\Omega}_p = 0.187 \text{ Bar}/\mu\text{s}$). These results have provided new insight into the wide range of values of F_c which are found in the literature and provide evidence to substantiate the claim made by previous workers that the rate of dynamic stressing is an important consideration in understanding the cavitation properties of liquids. It is key therefore that in the present work, results have been produced from a single technique, consisting of experiments conducted using the same apparatus in which the rate of stressing is deliberately varied. The results from these experiments clearly establish the importance of stressing rate in considering the effective tensile strength of liquids, under conditions where heterogeneous nucleation prevails, and emphasise that any attempt to reconcile the results of previous cavitation studies should take this factor into account.

The present work has also addressed and resolved an important and longstanding anomaly in the cavitation literature concerning the role of (high molecular weight) polymeric additives in determining the cavitation thresholds of dilute aqueous polymer solutions.

It is important to recall that despite theoretical and experimental studies demonstrating that the viscoelasticity conferred upon liquids containing polymer additives influence their cavitation properties, the results have been contradictory –

particularly with regard to the specific effects on cavitation damage potential and cavitation threshold. The results reported in this thesis emanate from systematic testing over a range of concentrations and molecular weight. Due to this unique experimental approach it is shown unequivocally that with increasing molecular weight there is an increased effective tensile strength of the solution. However, the results also reveal that increasing polymer concentration results in a clearly defined stress saturation level – with an apparent plateau in terms of effective tensile strength.

The results of the present work make explicit the crucial role of timescale in the recording of effective cavitation threshold strength (i.e. tensile stress) parameters. It is also the first to relate cavitation failure of a fluid and its extensional break-up properties in terms of two appropriately chosen tensile stress parameters; and to report the relationship between these stress parameters on the basis of an experimental study involving two different but complementary techniques involving a significant range of tensile stress development and a wide range of polymer concentration and molecular weight. Despite the large differences evident in the magnitudes of the tensile stress parameters estimated in the two different experiments, both show that the relevant stress limiting parameter increases with polymer concentration and molecular weight, but that such stress levels become effectively saturated (i.e. produce plateau limiting values) at essentially the same levels of concentration and molecular weight.

This information has never previously been available due to a lack of a suitable cavitation technique and a neglect of the appropriate analysis of CaBER filament breakup experiments in terms of the limiting stress parameter. As a result of the work reported in this thesis it may now be possible to conduct fluid breakup measurements

in extensional flow experiments in order to ascertain the likely levels of cavitation threshold stress for dilute aqueous polymer solutions. The bullet-piston experiments are extremely time-consuming, difficult to perform and require relatively large volumes of fluid sample whereas the CaBER-type experiments require very small volumes of fluid sample, are quick to perform and can be achieved for relatively low cost. The results of such measurements will inform the better design (and possibly control) of numerous industrial flow processes involving relationships between cavitation break-up of fluids and their subsequent filamentation – with printing and coating flow processes being the best known example of these. The present work is therefore most likely to find immediate applications in that field – possibly in terms of ranking the cavitation resistance of fluids involving a systematic variation of polymer additives, in a range flow settings involving different (extensional) deformation rates.

It is also interesting to note that the characteristic times of the pulses used in the B-P work reported in this thesis correspond broadly to those involved in some medical applications of low frequency ultrasound; and the tensile strength of water reported here considerably exceeds the values of tension thought to be generated *in vivo* by some ultrasound devices. The present findings may have significance in the context of assessing the safety of ultrasound application in relation to its potential to induce cavitation. The outcomes of the present study also suggest that the new B-P technique might prove a useful research tool for liquids such as motor lubricants which experience a range of rates of tensile stress development in the action of components such as dynamically loaded journal bearings.

REFERENCES

References

Acosta, A. J. and Parkin, B. R. (1975) 'Cavitation Inception – A Selective Review'

Journal of Ship Research, 19 (4). pp. 193-205.

Akulichev, V.A. "Cavitation nuclei and thresholds of acoustic cavitation in ocean water." in: Blake J R and Boulton Stone J M (Eds.) *Bubble Dynamics and Interface Phenomena*. Kluwer Academic Publishers Dordrecht 1994 (ISBN 0-7923-3008-0)

Anna S. L. 'Filament stretching of model elastic fluids' Thesis Harvard University
2000

Anna, S.L., C.E. Eastman, R.L Morris 'Dynamic properties of low molecular weight polystyrenes at infinite dilution' *Macromolecules* 24 (1991)

S. L. Anna, Gareth H. McKinley, Duc A. Nguyen, Tam Sridhar, Susan J. Muller, Jin Huang and David F. James 'An inter-laboratory comparison of measurements from filament-stretching rheometers using common test fluids ' *Journal of Rheology*
Volume 45, Issue 1 (2001)

Anna, S.L. and McKinley, G.H., Filament Breakup of Model Elastic Liquids, *J. Rheol.*, (2000)

Apfel R E 1981 *Acoustic Cavitation*. Ch. 7 in 'Ultrasonics' PD Edmonds (ed.)
Academic Press New York

Apfel, R.E. "The tensile strength of liquids." *Sci. Am.* 227 (1972): 58-71.

Apfel, R.E. "The role of impurities in cavitation threshold determination." *J. Acoust. Soc. Am.* 48 (1970): 1179-1186.

Banks, W. H., Mill., C.C. "Tacky adhesion - a preliminary study." *J. Colloid Sci.* 8 (1953): 137-147.

Barnett, S.B. and Kossoff, G. (Eds.) *Safety of Diagnostic Ultrasound*. Progress in Obstetric and Gynaecological Sonography Series. Parthenon Publishing 1998 ISBN 1-85070-646-8

Batchelor, G.K. *An Introduction to Fluid Dynamics*. Cambridge University Press 1967 Cambridge.

Barrow, Matthew 'Rheometrical techniques for the measurement of the uniaxial extensional viscosity of mobile fluids' Thesis University of Wales Swansea 2000

Berker A, M.G. Bouldin, S.J. Kleis and W.E. Van Arnsdale. "Effect of polymer on flow in journal bearings." *J. Non Newt. Fluid Mech.* 56 (1995): 333-347.

Bingham E.C. accepted in the inaugural meeting of the American Society of rheology (1929)

- Blake, J. R., Gibson, D. C. "Growth and collapse of a vapour cavity near a free surface." *J. Fluid Mech.* 111 (1981): 123-140
- Blake, J. R., Taib, B. B., Doherty, G. "Transient cavities near boundaries. Part I. Rigid boundary." *J. Fluid Mech.* 170 (1986): 479-497
- Blake, J. R., Taib, B. B., Doherty, G. "Transient cavities near boundaries. Part II. Free surface." *J. Fluid Mech.* 181 (1987): 197-212.
- Blake F G. Tech. Memo. Harvard Univ. Acoust. Res. Lab. No 9 (1949)
- Boguslavskii, YY and Eknadiosyants, OK. "Physical mechanism of the acoustic atomization of a liquid." *Soviet Physics – Acoustics* 15 (1969): 14-21.
- Braithwaite & McKinley Microrheometry for Studying the Rheology and Dynamics of Polymers near Interfaces *Journal of Applied Rheology*, 9, (1999), p27-33
- Braun, M.J., Hendricks, R.C. "An experimental investigation of the vaporous/gaseous cavity characteristics of an eccentric journal bearing." *Trans. ASLE* 27 (1984): 1-14.
- Brennen C E 1995 *Cavitation and Bubble Dynamics*. Oxford University Press, Oxford.
- Briggs, L. J. "Limiting negative pressure of water." *J. Appl. Phys.* 21 (1950): 721-722.

- Briggs, L. J. "The limiting negative pressure of mercury in Pyrex glass." *J. Appl. Phys.* 24 (1953): 488-490.
- Brujan, E –A. "Bubble dynamics in a compressible shear-thinning liquid." *Fluid Dynam. Res* 23 (1998): 291-318.
- Brujan, E.A. et al. (1996) "Dynamics of Laser-Induced Cavitation Bubbles in Polymer Solutions," *Acustica acta acustica* 82:423-430
- Bull, T.H. "The tensile strengths of liquids under dynamic loading." *Phil. Mag.* 8 (1956): 153-165.
- Carvalho 'Roll Coating Flows in Rigid and Deformable Gaps'
PhD Thesis, University of Minnesota (1996)
- Carlson, G. A. "Dynamic tensile strength of mercury." *J. Appl. Phys.* 46 (1975): 4069-4070.
- Carlson, G. A. and Henry, K. W. "Technique for studying dynamic tensile failure in liquids: application to glycerol." *J. Appl. Phys.* 44 (1973): 2201-2206.
- Chahine G.L. "Interaction between an oscillating bubble and a free surface." *Trans. ASME Ser. I J. Fluids Engng.* 99 (1979): 709-716.

- Chen, YL, Kuhl, T and Israelachvili, J. "Mechanism of cavitation damage in thin liquid films: collapse damage vs. inception damage." *Wear* 153 (1992): 31-51
- Cheny, J.M. and Walters, K. "Extravagant viscoelastic effects in the Worthington jet experiment." *J. Non-Newt. Fluid Mech.* 67 (1996): 125-135.
- Christenson, K.H. and Claesson, P.M. "Cavitation and the interaction between macroscopic hydrophobic surfaces." *Science* 239 (1988): 390-392.
- Coleman, A.J., Kodama, T., Choi, M.J., Adams, T., Saunders, J.E. "The cavitation threshold of human tissue exposed to 0.2-MHz pulsed ultrasound: preliminary measurements based on a study of clinical lithotripsy". *Ultrasound Med Biol* 21 (1995): 405– 417.
- Coleman, A. J., Saunders, J. E., Crum, L. A. & Dyson, M. "Acoustic cavitation originated by an extra corporeal shockwave lithotripter." *Ultrasound Med. Biol.* 13 (1987): 69-76.
- Couzens and Trevena 'Tensile failure of liquids under dynamic stressing' *J. Phys D:Appl. Phys.* 7 2277-2287 (1974)
- Couzens and Trevena Critical tension in a liquid under dynamic conditions of stressing. *Nature* 222, 473-474. (1969)
- Coyle, C.W. Macosko and L.E. Scriven 'Film-splitting flows in forward roll coating' *Journal of Fluid Mechanics* 171 pp183-207 (1986)

Coyle 'The fluid mechanics of roll coating: Steady flows, stability and Rheology'

Thesis University of Minnesota (1984)

Crum, L. A. "Measurements of the growth of air bubbles by rectified diffusion." *J.*

Acoust. Soc. Am. 68 (1980): 203-211.

Crum, L.A., Fowlkes, J.B. "Acoustic cavitation generated by microsecond pulses of ultrasound." *Nature* 319 (1986): 52-54.

Davies R.M, Trevena D.H, Rees N.J.M. & Lewis G.M. 'The tensile strength of liquids under dynamic stressing' Proc. N.P.L. Symp. On cavitation in hydrodynamics, the National Physical Laboratory Teddington vol 5 pp1-20 1956

Dowson, D., Taylor, C.M. "Cavitation in Bearings." *Ann. Rev. Fluid Mech.* 11 (1979): 35-66.

Euler letter to Pontoppidan of May 11, 1754

Evans, A., Walder, D.N. "Significance of gas micronuclei in the aetiology of decompression sickness." *Nature* 222 (1969): 251-252.

Fisher, J. C. "The fracture of liquids." *J. Appl. Phys.* 19 (1948): 1062-1067

Flynn, H.G. "Physics of acoustic cavitation in liquids", Chap. 9 of *Physical Acoustics*, Vol.1, part B, WP Mason (ed.), Academic Press, (1964).

Flynn, H.G. "Cavitation dynamics. I. A mathematical formulation." *J. Acoust. Soc.*

Am. 57 (1975a): 1379-1396

Flynn, H.G. "Cavitation dynamics. II. Free pulsations and models for cavitation

bubbles." *J. Acoust. Soc. Am.* 58 (1975b): 1160-1170

Flynn, H.G. "Generation of transient cavities in liquids by microsecond pulses of

ultrasound." *J. Acoust. Soc. Am.* 72 (1982): 1926-1931

Fogler, H., Goddard, J.D. "Collapse of spherical cavities in viscoelastic fluid." *Phys.*

Fluids 13 (1970): 1135-1141.

Fox, F.E., Herzfeld, K.F. "Gas bubbles with organic skin as cavitation nuclei." *J.*

Acoust. Soc. Am. 26 (1954): 984-989.

Frenkel, J. 1955 *Kinetic Theory of Liquids* Dover Publications: New York.

Fruman D.H. 1999 Effects of non-Newtonian fluids on cavitation: in *Advances in the*

Flow and Rheology of non-Newtonian Fluids, Part A. Eds. Siginer DA, De Kee D and

Chhabra RP.

Fujikawa, S., Akamatsu, T. "Effects of the non-equilibrium condensation of vapour

on the pressure wave produced by the collapse of a bubble in a liquid." *J. Fluid Mech.*

97 (1980): 481-512.

Galloway, WJ. "An experimental study of acoustically induced cavitation in liquids."

J. Acou.st. Soc. Am. 26 (1954): 849-857.

Gates, E.M., Bacon, J. "A note on the determination of cavitation nuclei distributions by holography." *J Ship Res* 22 (1978): 29 –31.

Gent A. N., Hamed G. R. "Adhesion and Bonding" in *Encyclopedia of Polymer Science and Engineering*, 2nd Ed. (Wiley, New York,1985) vol 1 pp 476-518

Gibson, D.C., Blake, J.R. "The growth and collapse of bubbles near deformable surfaces." *Appl. Sci. Res.* 38 (1982): 215-224.

Gilmore FR (1952) *Calif. Inst. Technol. Eng. Div. Rep.* 26-4 Pasadena Calif.

Greenspan, M., Tschiegg, CE. "Radiation-induced acoustic cavitation; apparatus and some results." *J. Res. Natl. Bur. Stand. Sect. C* 71 (1967): 299-312.

Harvey, E.N. , in: *Decompression Sickness* ed. Fulton J.F. Saunders, Philadelphia, 1951.

Hayward, A.T.J. "The role of stabilized gas nuclei in hydrodynamic cavitation inception." *J. Phys. D: Appl. Phys.* 3 (1970): 574-579.

S J Henderson and R J Speedy 'A Berthelot-Bourdon tube method for studying water under tension' 1980 *J. Phys. E: Sci. Instrum.*

Henderson S. J. and Speedy R. J., *J. Phys. Chem.* 91, 3069 (1987).

Herbert E and Caupin F. ‘The limit of metastability of water under tension: theories and experiments’, *J. Phys.: Condens. Matter* 17 (2005)

Hickling, R, Plesset, M.. “Collapse and rebound of a spherical bubble in water.” *Phys. Fluids* 7(1964):7-14.

Hoyt, J. “Effect of polymer additives on jet cavitation.” *Trans. ASME: J. Fluids Engng.* 98 (1976): 106-112.

Hoyt, M. “Underwater Explosions.” *Ann. Rev. Fluid Mech.* 9 (1977): 187-214

Hsieh, D.Y. “Bubble growth in a viscous liquid due to a transient pulse.” *J. Basic Eng.* 92 (1970): 815-818

Hsieh, D.Y. “On the dynamics of non-spherical bubbles.” *J. Basic Eng.* 94 (1972): 655-665.

Jones W. M., Overton, G.D.N & Trevena D.H. ‘Tensile strength experiments with water using a new type of Berthelot-tube’ *J. Phys.D:Appl.Phys* 14 1283-1291 (1981)

Joseph, D.D. “Cavitation and the state of stress in a flowing liquid.” *J. Fluid Mech.* 366 (1998): 367-378.

Kedrinskii, V.K., Bergardt, A.R. and Chernobaev, N.N. 1995 "Behaviour of a Liquid under Dynamic Loading." *IUTAM Symposium on Waves in Liquid/Gas and Liquid/Vapour Two-Phase Systems*, Eds. Morioka S & van Wijngaarden L, Kluwer Academic Publishers, Dordrecht ISBN 0-7923-3424-8, 429-438

Kezios, P.S., Schowalter, W.R. "Rapid growth and collapse of single bubbles in polymer solutions undergoing shear." *Phys. Fluids* 29 (1986): 3172-3181.

Kim, C. "Collapse of spherical bubbles in Maxwell fluids." *J. Non-Newtonian Fluid Mech.* 55 (1994): 37-58.

Kuper, Trevena. D.H. "The effect of dissolved gases on the tensile strength of liquids." *Proc. Phys. Soc. (London) A* 65(1952): 46-54.

H. Lakrout, P. Sergot, C. Creton, *J. Adhesion*, **69**, 307 (1999)

Leighton T G 1994 *The Acoustic Bubble*. Academic Press, London 1994

Lauterborn, W. "Numerical investigation of nonlinear oscillations of gas bubbles in liquids." *J. Acoust Soc Am.* 59 (1976): 283-293.

Lauterborn, W. "High-speed photography of laser induced breakdown in liquids." *Appl. Phys. Lett.* 21 (1972): 27-29.

Malkin and Petrie ‘ Some conditions for rupture of polymeric liquids in extension’ J.

Rheol. 41(1) 1-25 (1997)

Maris, H., Balibar, S. “Negative pressures and cavitation in liquid helium.” *Phys.*

Today Feb. 2000, 29-34

McPhee ‘A Unified view of the film splitting process. Part I’

American Ink Maker 75 pp42-49 (1997)

McPhee ‘A Unified view of the film splitting process. Part II’

American Ink Maker 75 pp51-56 (1997)

Matta & R. P. Tytus ‘Liquid stretching using a falling cylinder’

Journal of Non-Newtonian Fluid Mechanics 35 (1990) p215-229

Maris, H., Balibar, S. “Negative pressures and cavitation in liquid helium.” *Phys.*

Today Feb. 2000, 29-34

McComb and Ayyash ‘Anomalous damping of the pulsation noise pulsation noise

from small air bubbles in water’ The Journal of the Acoustical Society of America,

Volume 67, Issue 4, April 1980, pp.1382-1383

McKinley G.H., Anna S.L, Tripathi A. & Yao M “Extensional rheometry of polymeric fluids and the uniaxial elongation of viscoelastic filaments” International Polymer Processing Society 1999.

McKinley, G.H., Extensional Flow and Instabilities of Elastic Polymer Solutions, Dynamics of Complex Fluids; Proceedings of the Royal Society/ Unilever Indo-UK Forum, M. Adams (*ed.*), ICL Press, London, 1998

Miller, D. “Supercavitation: going to war in a bubble.” *Jane’s International Defense Review* 12 (1995): 61

Minnaert, M. “On musical air bubbles and the sounds of running water” *Phil. Mag.* 7 (1933): 235-248.

Narumi & Hasegawa ‘Experimental study on the squeezing flow of viscoelastic fluids. I: The effect of liquid properties on the flow between a spherical surface and a flat plate’ *JSME* 1986, vol. 29, pp. 3731-3736

Noltingk, B.E., Neppiras, E.A.. “Cavitation produced by ultrasonics.” *Proc. Phys. Soc.* B63 (1950): 674-685

Ouibrahim, A., Fruman, D.H. and Gaudemer, R. “Vapor cavitation in very confined spaces for Newtonian and non Newtonian fluids.” *Phys. of Fluids* 8 (1996): 1964-1971.

Pearson, G., Middleman, S. "Elongational flow behaviour of viscoelastic liquids: Part 1. Modelling of bubble collapse." *AIChE Journal* 23 (1977a): 714-721.

Petrie 'Elongational flows' Pitman, London 1979

Plessett, M.S., Prosperetti, A. "Bubble Dynamics and Cavitation." *Ann. Rev. Fluid Mech.* 9 (1977): 145-185.

Plesset, M.S., Hsieh, D.Y. "Theory of gas bubble dynamics in oscillating pressure fields." *Phys. Fluids* 3 (1960): 882-892

Plesset, M.S., Chapman, R.B. "Collapse of an initially spherical vapour cavity in the neighbourhood of a solid boundary." *J. Fluid Mech.* 47 (1971): 283-290.

Plesset, MS. "The dynamics of cavitation bubbles." *J. Appl. Mech.* 16 (1949): 277-282

Prosperetti A, in: JL Lumley, A Acrivos, LG Leal, S Leibovich (Eds.) 1996 *Research Trends in Fluid Dynamics*, AIP Press, New York.

Prosperetti, A. "Nonlinear oscillations of gas bubbles in liquids: transient solutions and the connection between subharmonic signal and cavitation." *J. Acoust. Soc. Am.* 57 (1975): 810-821

Prosperetti A, in: JL Lumley, A Acrivos, LG Leal, S Leibovich (Eds.) 1996 *Research Trends in Fluid Dynamics*, AIP Press, New York.

Prosperetti, A., Lezzi, A. "Bubble dynamics in a compressible liquid. Part 1. First-order theory." *J. Fluid Mech.* 168 (1986): 457-478

Rayleigh, Lord. "On the pressure developed in a liquid during the collapse of a spherical cavity." *Phil. Mag.* 34 (1917): 94-98.

B E Richards, D H Trevena and D H Edwards 'Cavitation experiments using a water shock tube ' *J. Phys. D: Appl. Phys.* 1980

Rodd, L.E, T.P Scott, D.V. Boger 'The inertio-elastic planar entry flow of low-viscosity elastic fluids in macro-fabricated geometries' *JNNFM* 129 (2005) 1-22

Roper III, P. Salminen, R. Urscheler and D.W. Bousfield 'Observations and proposed mechanisms of misting on high-speed metered size press coatings' *TAPPI Proceedings 1997 Coating Conference* pp1-14(1997)

Rosenschein U, Rassin T (1998) Ultrasound thrombolysis. *Sci Med.* 5:36-43. 4

Ryskin, G. "Dynamics and sound emission of a spherical cavitation bubble in a dilute polymer solution." *J. Fluid. Mech.* 218 (1990): 239-263.

Sedgewick and Trevena 'Limiting negative pressure of water under dynamic stressing' *J Phys. D: Appl. Phys.* 9 1983-1990 (1976)

Shima, A., Tsujino, T., and Nanjo, H., *Ultrasonics*, 24, 142, 1986

Skripov V P 1974 *Metastable Liquids* John Wiley and Sons

Smith, AM. "Negative pressure generated by octopus suckers: a study of the tensile strength of water in nature." *J. Exp. Biol.* 157 (1991): 257-271.

Spiegelberg, D.C. Ables & G.H. McKinley 'The role of end-effects on measurements end elastic decohesion of viscoelastic polymer solutions in extensional flow' *Journal of Non-Newtonian Fluid Mechanics* 64 (1996) p229-267

Speedy, R J. "Stability-Limit Conjecture. An interpretation of the properties of water." *J. Phys. Chem.* 86 (1982): 982-991.

Spikes 'The borderline of elastohydrodynamic and boundary lubrication' *Proc. Instn. Mech. Engrs.* 214 23 (2000)

Sridhar 'An overview of the project M'

Journal of Non-Newtonian Fluid Mechanics 35 pp85-92 (1990)

Strasburger, F. (1958) *F. Coll. Sci.* 13, 218

Szabo 'Transient filament stretching rheometer: Force balance analysis' *Rheologica acta* 36 277-284 (1997)

Temperley, H.N.V., Trevena, D.H. "Why is the tensile strength of water measured dynamically less than that measured statically." *J. Phys. D: Appl. Phys.* 20 (1987): 1080-1081.

Thompson, L. H., Doraiswamy, L. K. "Sonochemistry: Science and Engineering." *Ind. Eng. Chem. Res.* 38 (1999): 1215-1249.

Ting, R. Y. "Effect of polymer viscoelasticity on the initial growth of a vapour bubble from gas nuclei." *Phys. Fluids* 20 (1977): 1427-1431.

Tirtaatmadja and Sridhar 'A filament stretching device for measurement of extensional viscosity' *J Rheol* 37 (1993) 1081-1102

Thornycroft, J. I. and Barnaby, S.W. 'Torpedo-Boat Destroyers' *Institution of Civil Engineers Vol CXXII, Session 1894-95 Part IV (1895)*

Tomita, Y., Shima, A. "High-speed photographic observations of laser-induced cavitation bubbles in water." *Acustica* 71 (1990): 161-171.

Trevena D H 1987 *Cavitation and Tension in Liquids*, Adam Hilger, Bristol.

Trevena, D. H. 'Time effects in cavitation experiments'. *J. Phys. D* 15, 111-114 (1982)

- Tyree, M. T. "The Cohesion-Tension theory of sap ascent." *J. Exp.Bot.* 48, (1997): 1753-1765.
- Unsworth, A., Dowson, D. and Wright, V. "Cracking joints. A bioengineering study of cavitation in the metacarpophalangeal joint." *Ann. Rheum. Dis.* 30 (1971): 348-358.
- Vogel, A., Lauterborn, W. and Timm, R. "Optical and acoustic investigations of the dynamics of laser-produced cavitation bubbles near a solid boundary." *J. Fluid Mech.* 206 (1989): 299 – 338
- Vogel A, Busch, S and Parlitz, U. "Shock wave emission and cavitation bubble generation by picosecond and nanosecond optical breakdown in water." *J. Acoust. Soc. Am.* 100 (1996): 148-165.
- Vogel, A., Busch, S., Jungnickel, K, Birngruber, R. "Mechanisms of intraocular photodisruption with picosecond and nanosecond laser pulses." *Lasers Surg. Med.* 15 (1994): 32-43.
- Welsh R.D. 'Viscoelastic free surface Instabilities during exponential stretching'
Thesis 2001
- Willard, G.W. "Ultrasonically induced cavitation in water: A step by step process." *J. Acoust. Soc. Am.* 25 (1953): 669-686

Williams, P.R., Williams, R.L. "On anomalously low values of the tensile strength of water." *Proc. Roy. Soc. A* 456 (2000): 1321 – 1332

Williams, P. R., Williams, R. L. and Brown, S. W. J. "Tensile properties of liquid mercury under pulsed dynamic stressing." *J. Phys. D: Appl. Phys.* 31 (1998a): 1923-1926.

Williams P.R., Williams, P.M. and Brown, S.W.J. "A study of liquid jets formed by bubble collapse in elastic and Newtonian liquids." *J. Non-Newtonian Fluid Mech.* 76 (1998b): 307-325.

Williams, P. R., Williams, R. L. and Brown, S. W. 'An instrument for studying cavitation phenomena in liquids subjected to tension generated ab initio and by free-surface reflection of compressional waves' *Meas. Sci. Technol.* 9 (1998) 976-982

Williams, P. R., Williams, R. L. Cavitation of liquids under dynamic stressing by pulses of tension' *J Phys D* 35 (2002) 2222-2230

Williams, P. R., Williams, R. L. 'Measurements of the cavitation threshold of multigrade engine oils under dynamic stressing by pulses of negative pressure' *Int. J. Of Engine Research* vol 4 pp 269-282 (2003)

Williams, P R and Williams, R L 'Cavitation and the tensile strength of liquids under dynamic stressing', *Molecular Physics* 102, 2004, 2091-102.

Williams, P R and Williams, R L 'Measurements of the cavitation threshold of multigrade engine oils under dynamic stressing by pulses of negative pressure', *International Journal of Engine Research*, 4(4), 2004, 269-82

Williams, P. R., Williams, P. M. and Brown, S. W. 'Pressure waves arising from the oscillation of cavitation bubbles under dynamic stressing' *J. Phys. D: Appl. Phys.* 30 (1997): 1197-1206.

Wilson, D. A., Hoyt, J. W. and McKune, J. W. "Measurement of tensile strength of liquids by an explosion technique." *Nature* 253 (1975): 723-725.

Wunderlich et al. (2000) "Shear and Extensional Rheological Investigations in Solutions of Grafted and Ungrafted Polysaccharides," *J. Applied Polymer Science* 77:3200-3209.

Yau and G.H. McKinley 'Numerical simulation of extensional deformations of viscoelastic liquid bridges in filament stretching devices' *Journal of Non-Newtonian Fluid Mechanics* 74 pp47-88 (1998)

Yount, D.E. "On the elastic properties of the interfaces that stabilise gas cavitation nuclei." *J. Colloid and Interface Science* 193 (1997): 50 – 59.

Zang Y. H. , J. S. Aspler, M. Y. Boluk, and J. H. De Grace. "Direct measurement of tensile stress ("tack") in thin ink films." *J. Rheol.* 35 (1991): 345-361

Zheng, Q., Durben, D. J., Wolf, G. H. and Angell, C. A. "Liquids at large negative pressure: water at the homogeneous nucleation limit." *Science* 254 (1991):

Zosel, Int. J. Adhes. Adhesives, 1998, 18, 265

APPENDIX A

Additional pressure-tension records

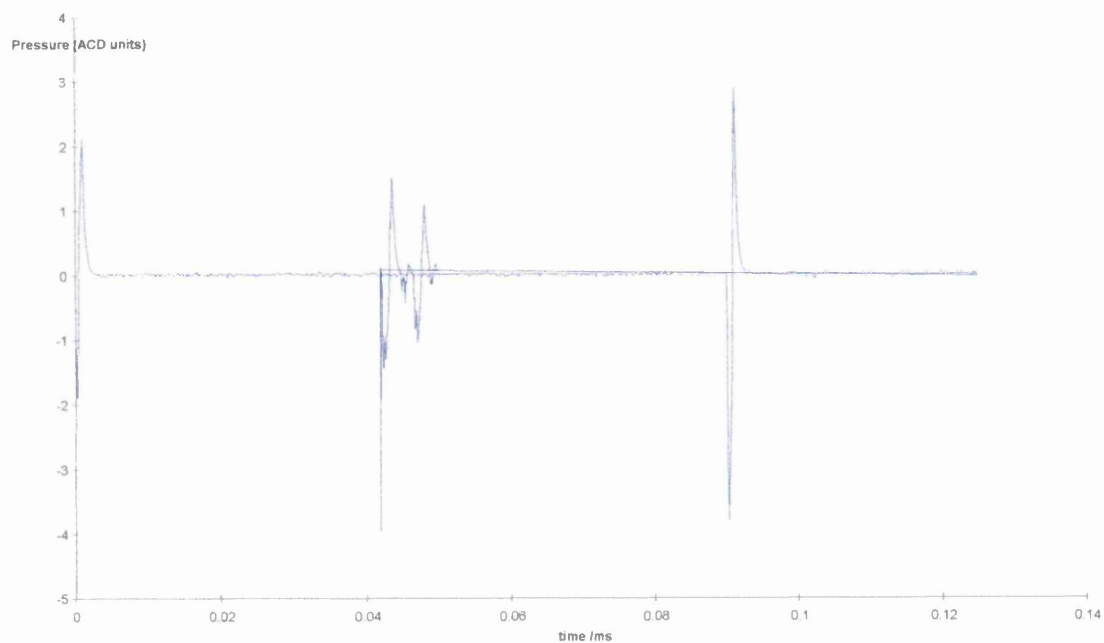


Figure A.1 Pressure-Tension cycle for a 0 psi static pulse for 1% 6000 Mw solution.

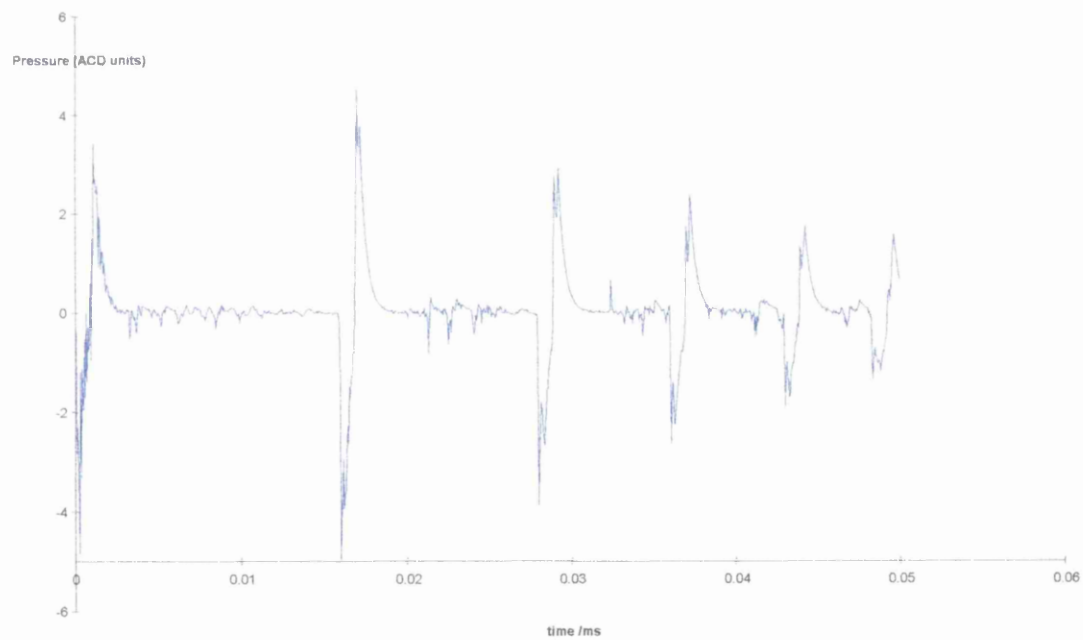


Figure A.2 Pressure-Tension cycle for a 100 psi static pulse for 1% 6000 Mw solution

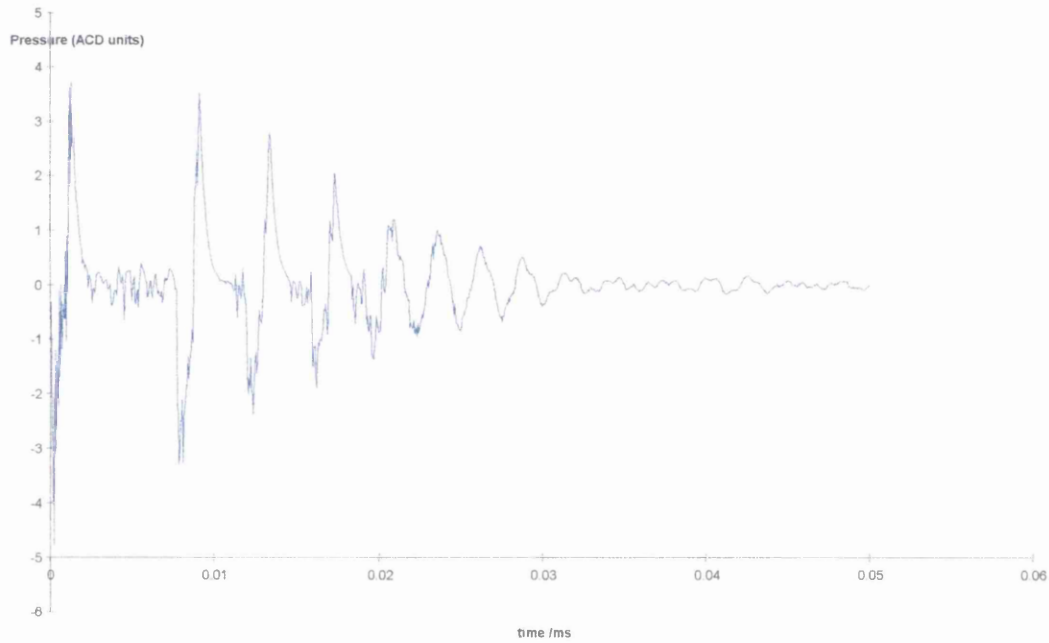


Figure A.3 Pressure-Tension cycle for a 200 psi static pulse for 1% 6000 Mw solution.

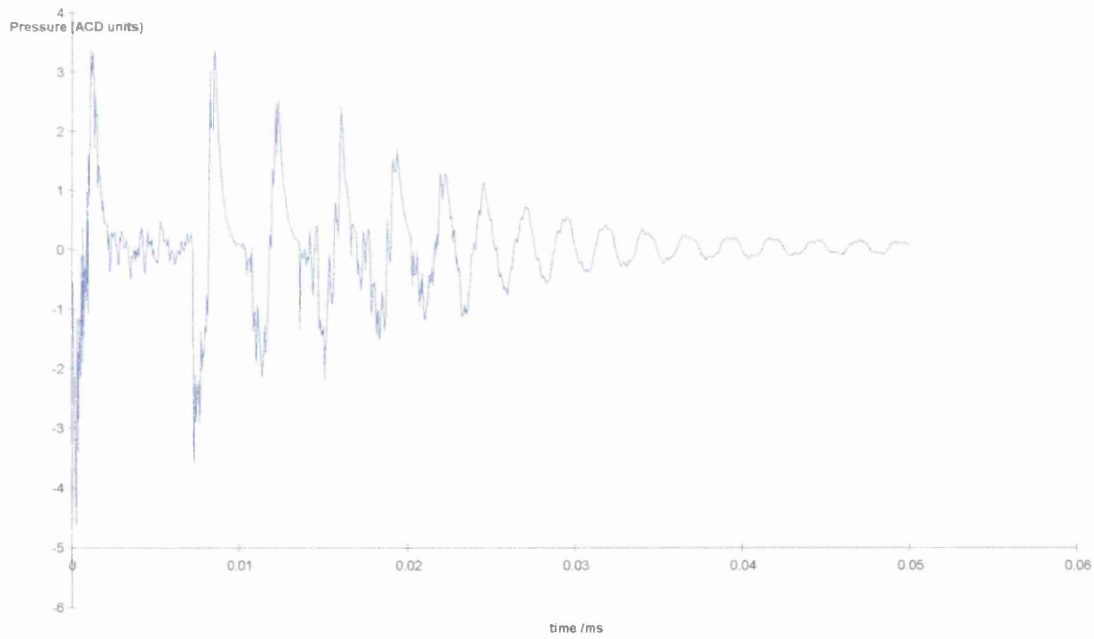


Figure A.4 Pressure-Tension cycle for a 250 psi static pulse for 1% 6000 Mw solution.

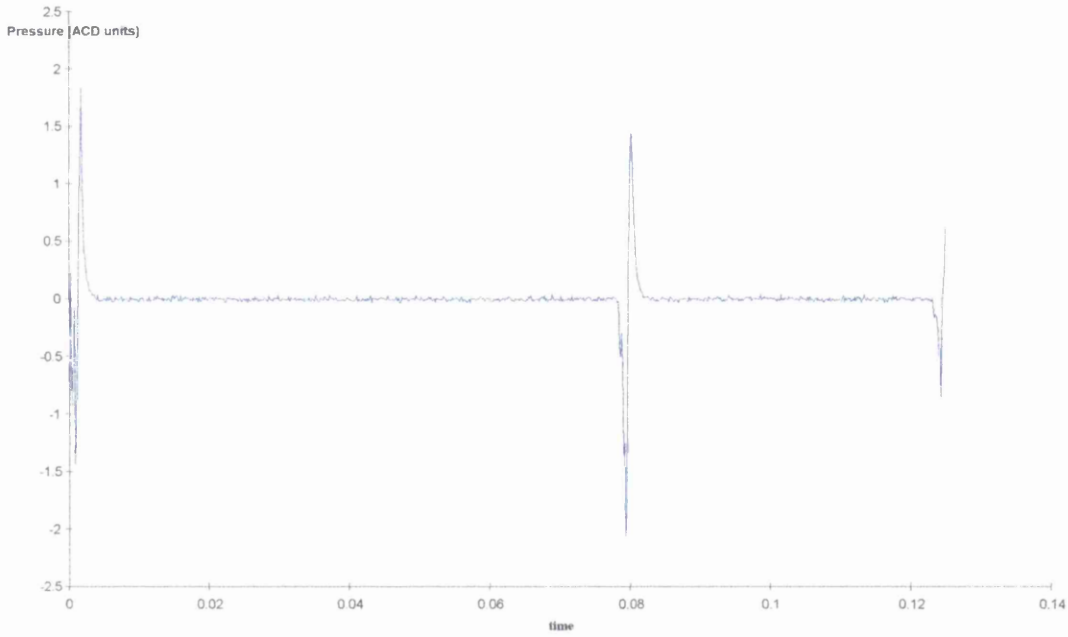


Figure A.5 Pressure-Tension cycle for a 0 psi static pulse for 5% 6000 Mw solution.

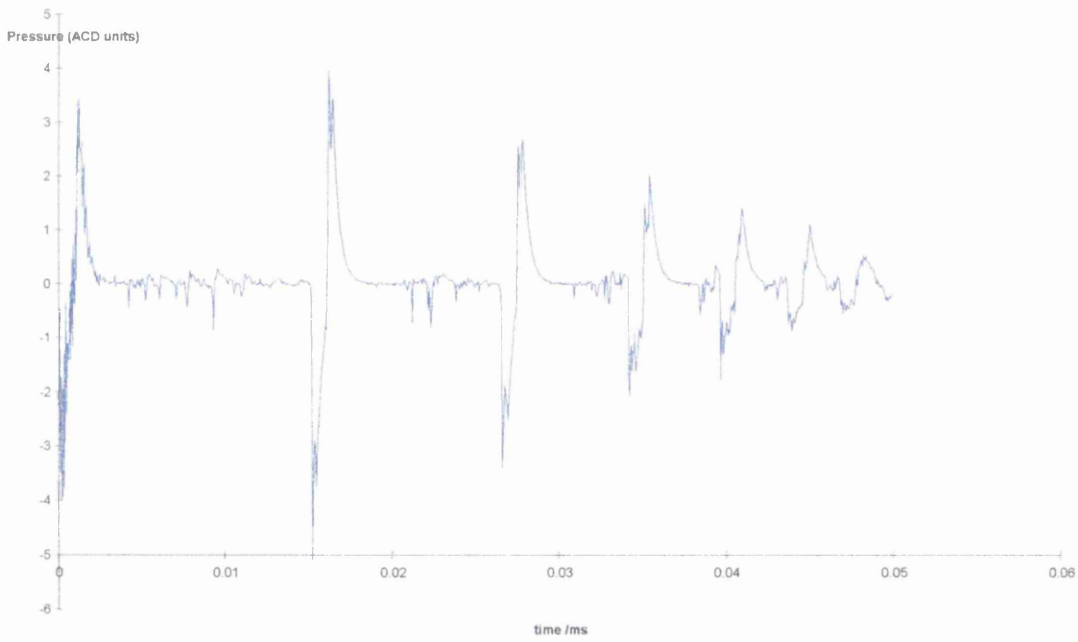


Figure A.6 Pressure-Tension cycle for a 100 psi static pulse for 5% 6000 Mw solution.

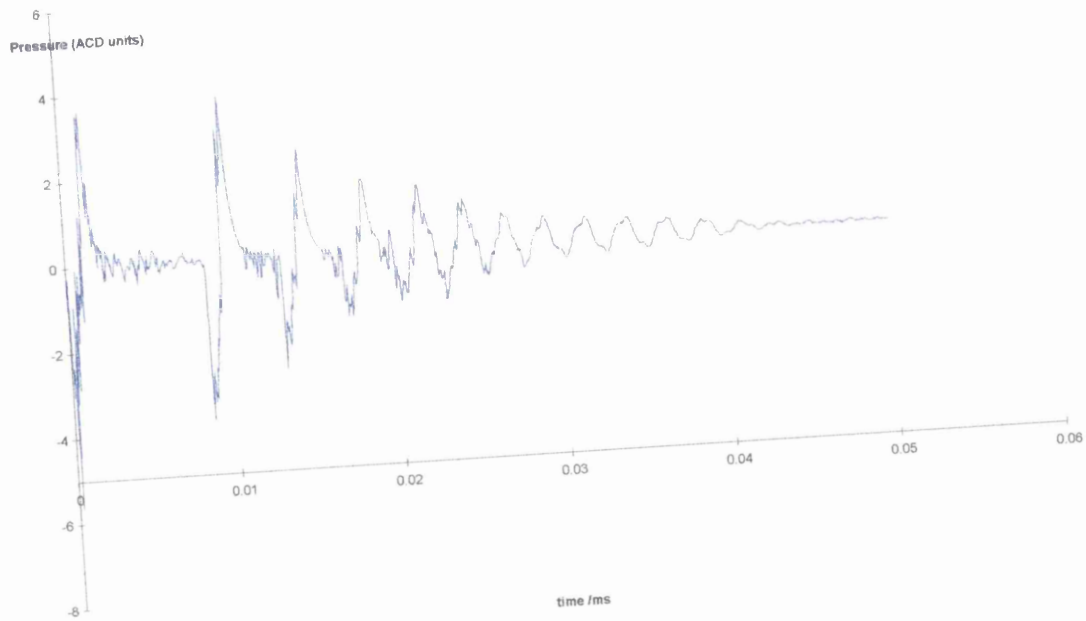


Figure A.7 Pressure-Tension cycle for a 200 psi static pulse for 5% 6000 Mw solution.

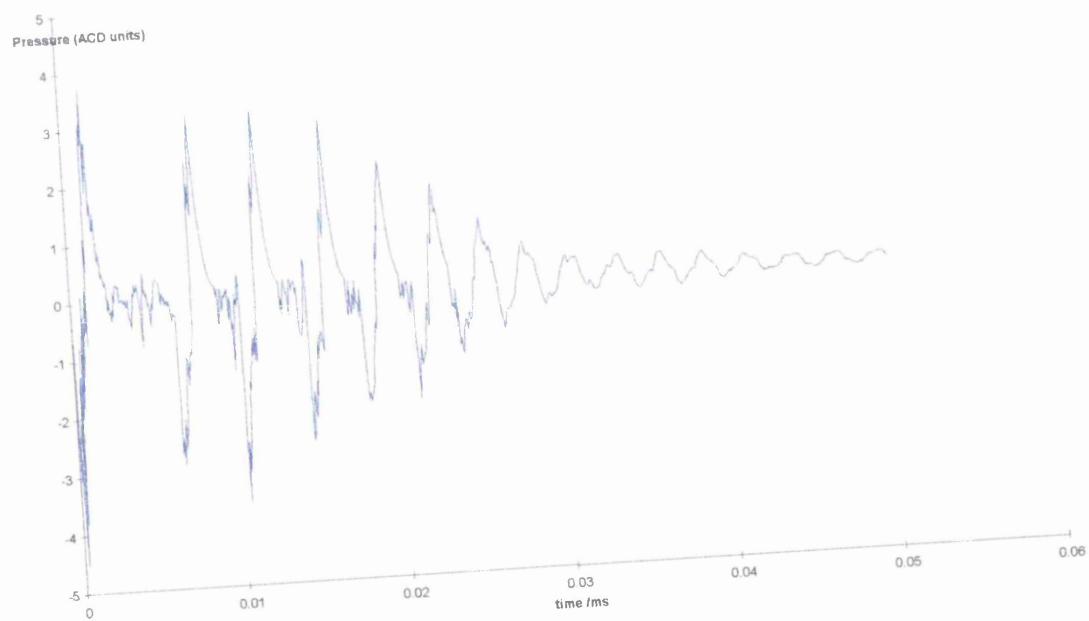


Figure A.8 Pressure-Tension cycle for a 250 psi static pulse for 5% 6000 Mw solution.

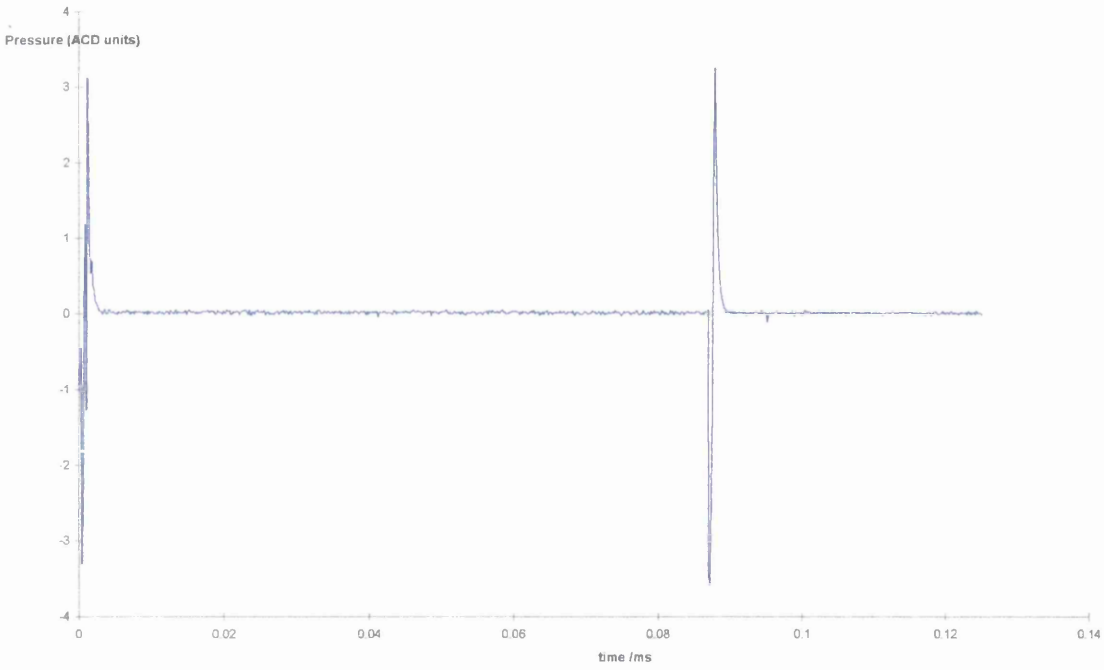


Figure A.9 Pressure-Tension cycle for a 0 psi static pulse for 10% 6000 Mw solution.

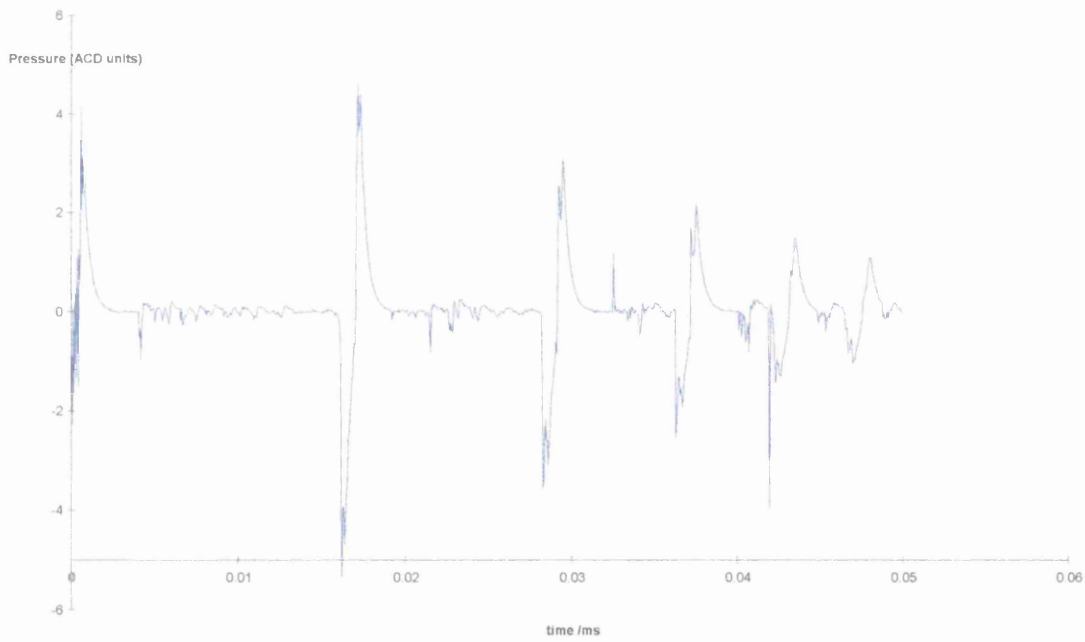


Figure A.10 Pressure-Tension cycle for a 100 psi static pulse for 10% 6000 Mw solution

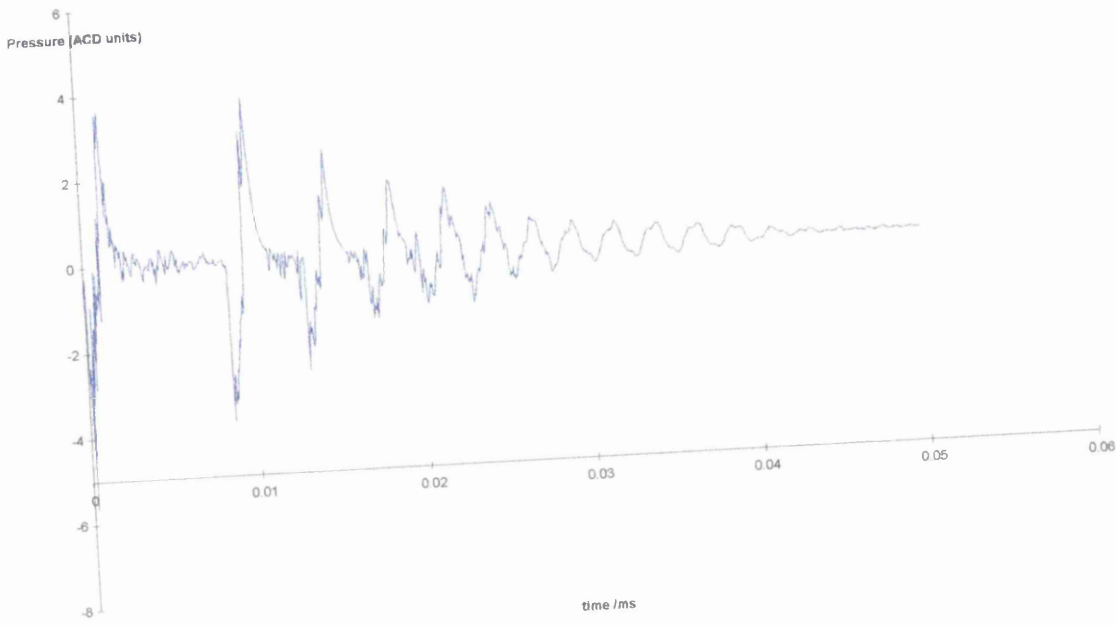


Figure A.11 Pressure-Tension cycle for a 200 psi static pulse for 10% 6000 Mw solution

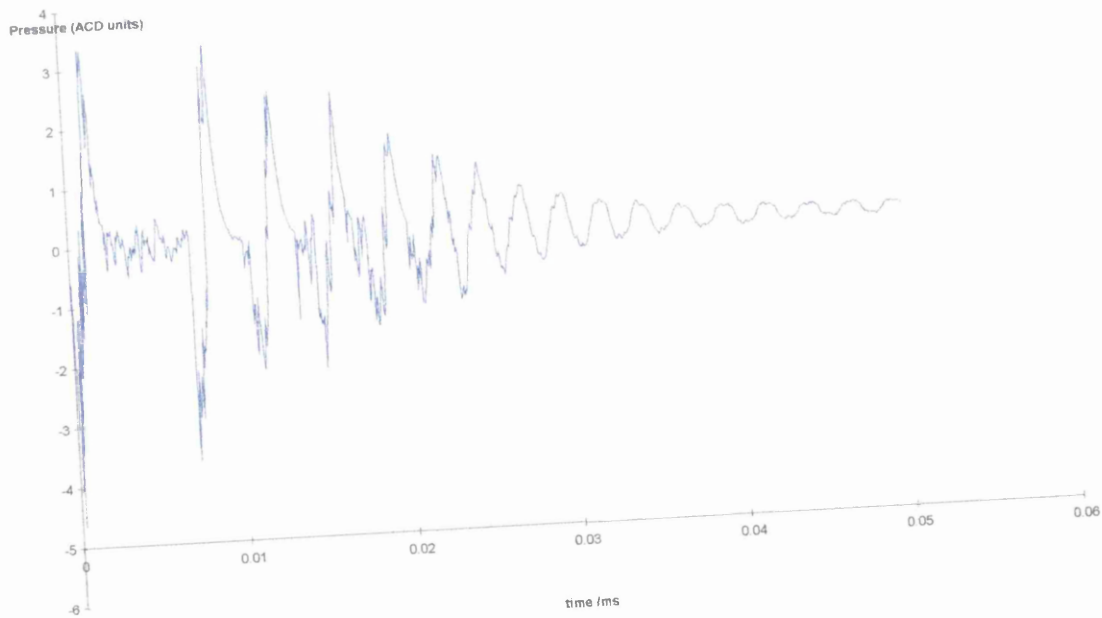


Figure A.12 Pressure-Tension cycle for a 250 psi static pulse for 10% 6000 Mw solution

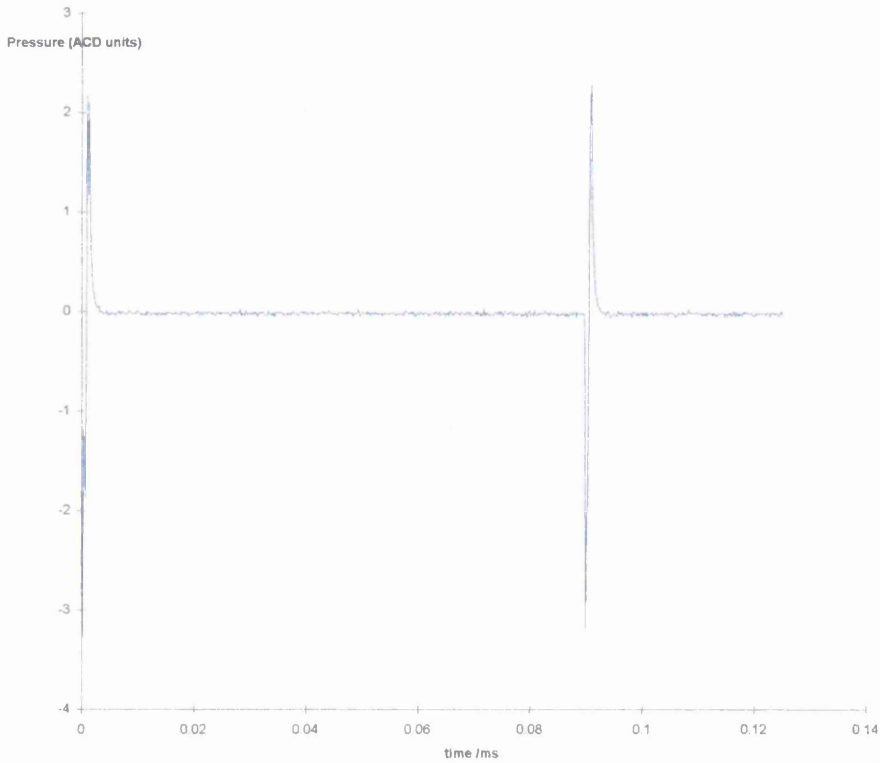


Figure A.13 Pressure-Tension cycle for a 0 psi static pulse for 1% 10000 Mw solution.

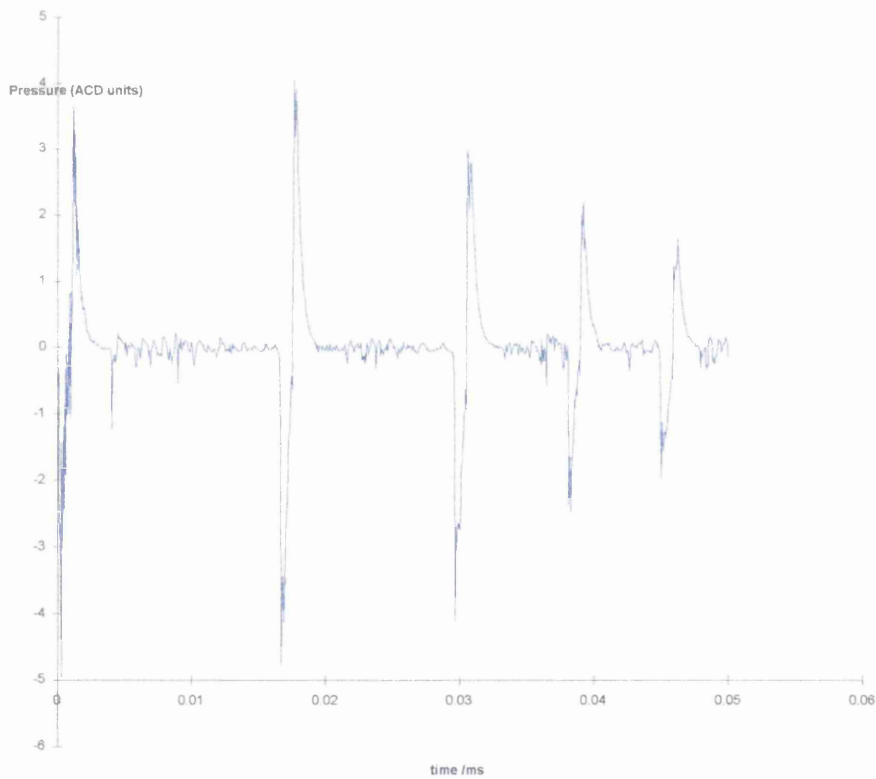


Figure A.14 Pressure-Tension cycle for a 100 psi static pulse for 1% 10000 Mw solution

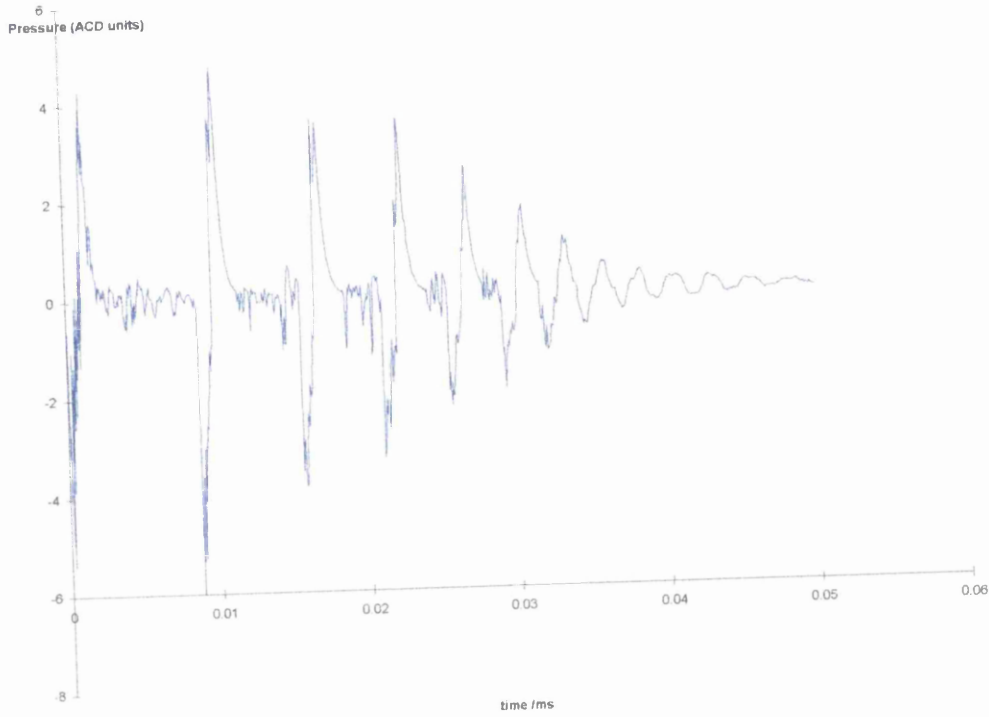


Figure A.15 Pressure-Tension cycle for a 200 psi static pulse for 1% 10000 Mw solution.

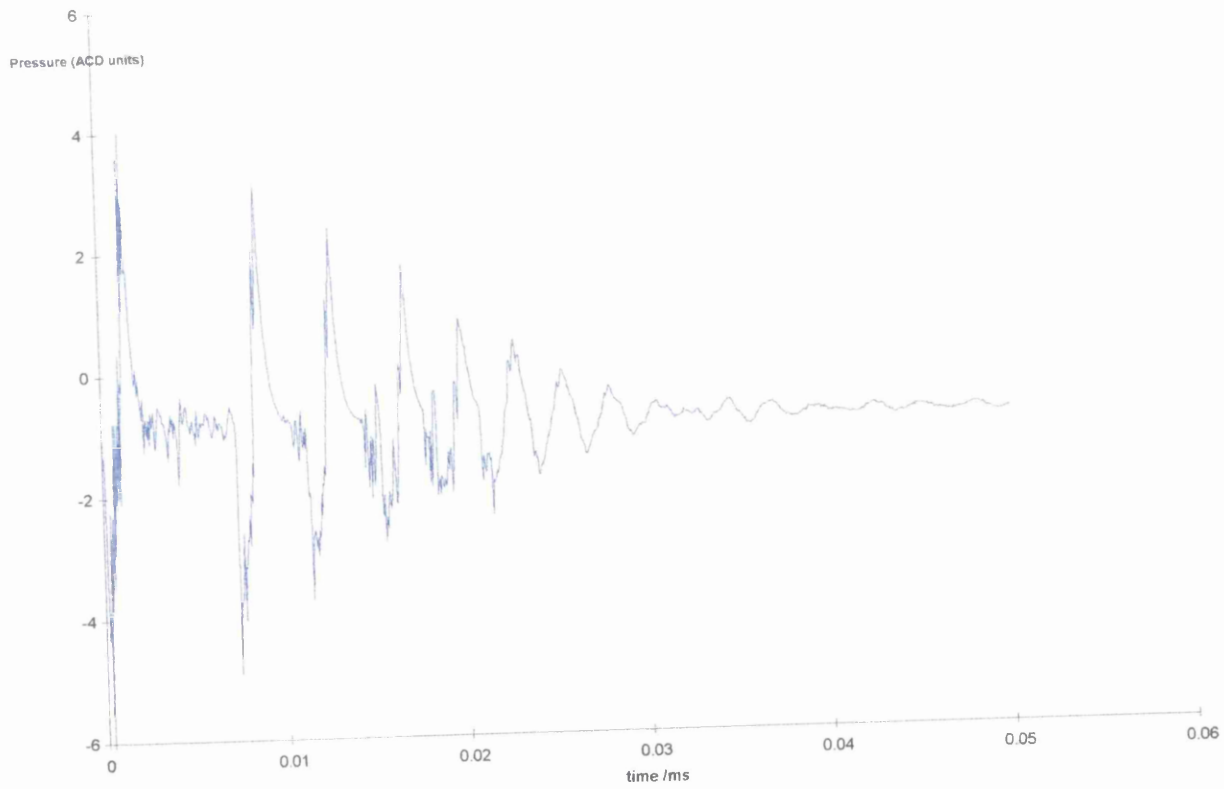


Figure A.16 Pressure-Tension cycle for a 250 psi static pulse for 1% 10000 Mw solution.

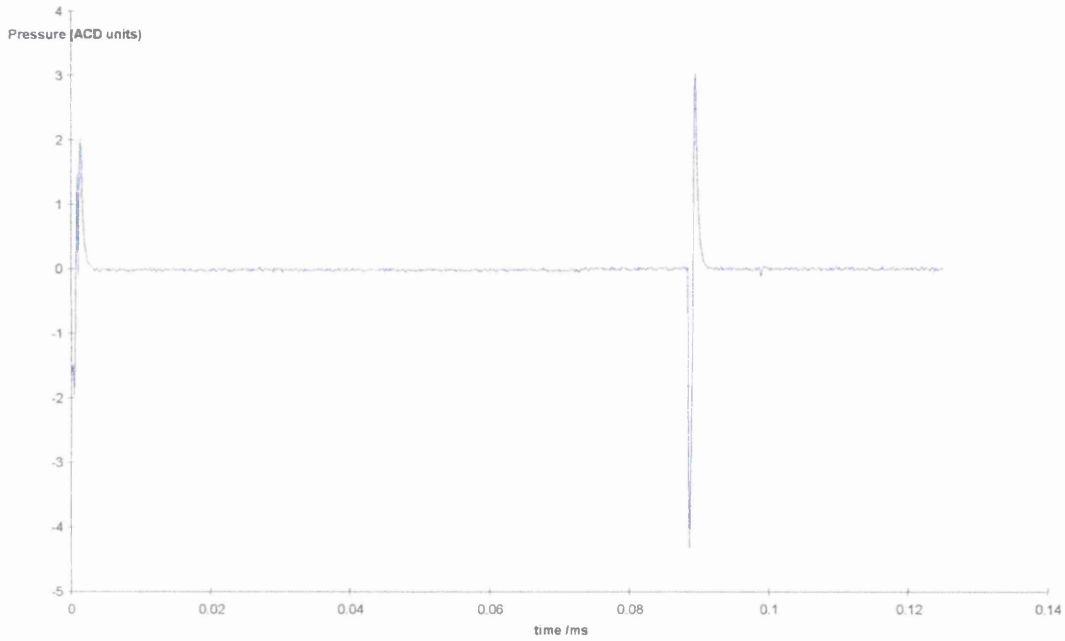


Figure A.17 Pressure-Tension cycle for a 0 psi static pulse for 5% 10000 Mw solution.

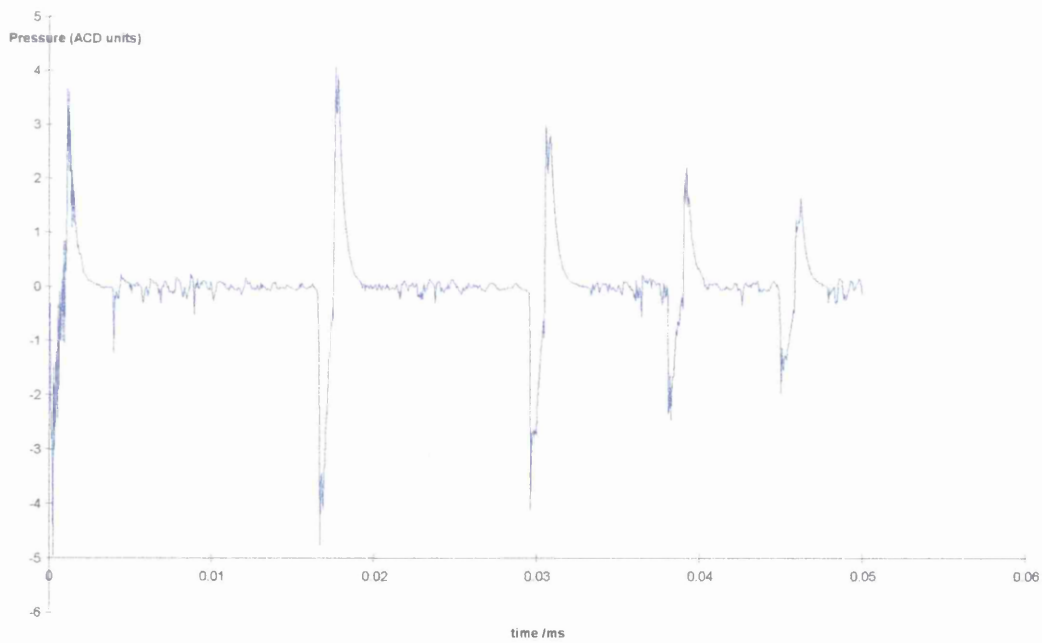


Figure A.18 Pressure-Tension cycle for a 100 psi static pulse for 5% 10000 Mw solution.

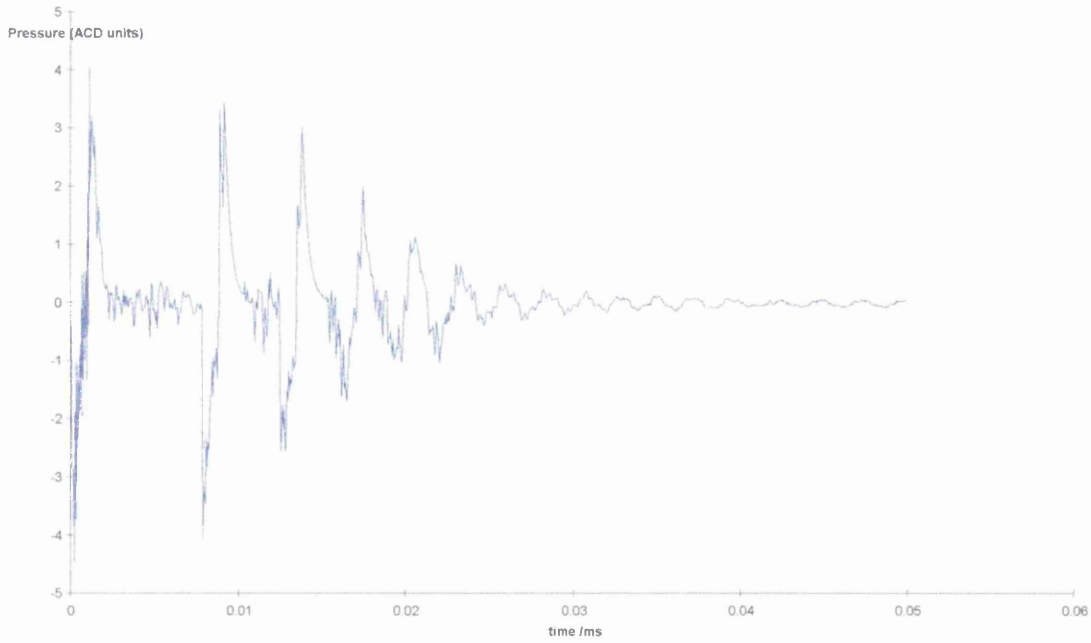


Figure A.19 Pressure-Tension cycle for a 200 psi static pulse for 5% 10000 Mw solution.

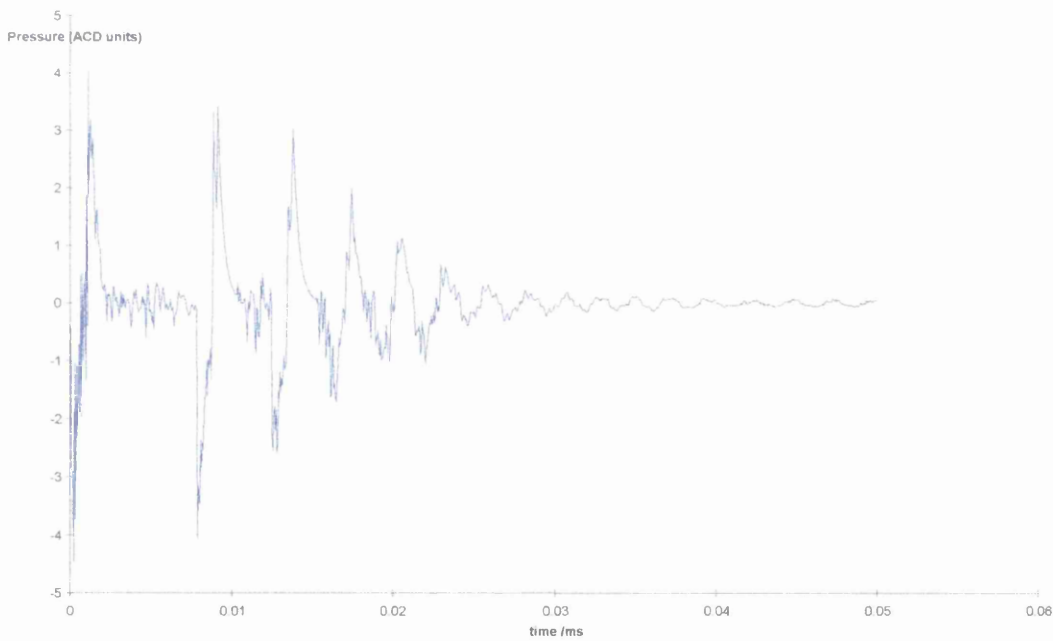


Figure A.20 Pressure-Tension cycle for a 250 psi static pulse for 5% 10000 Mw solution.

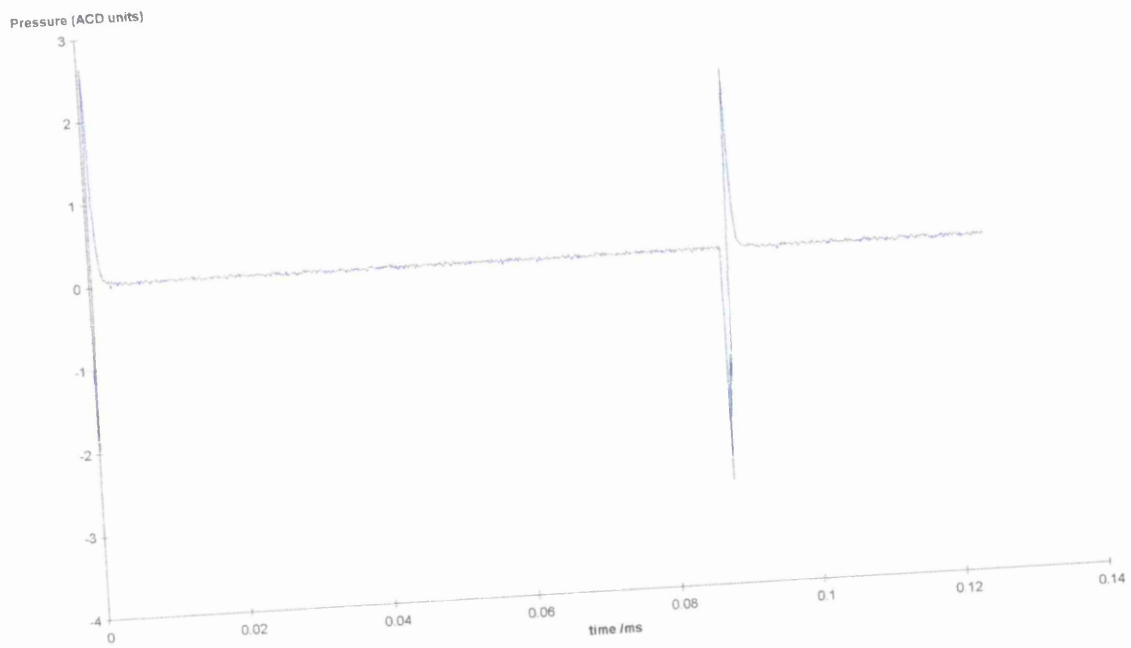


Figure A.21 Pressure-Tension cycle for a 0 psi static pulse for 10% 10000 Mw solution.

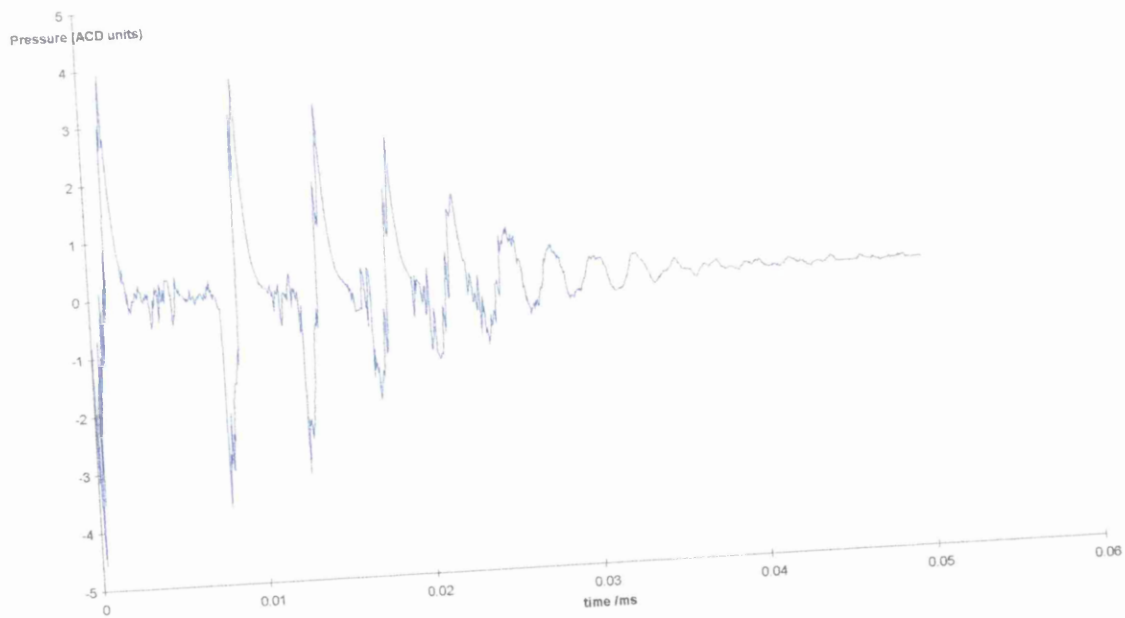


Figure A.22 Pressure-Tension cycle for a 100 psi static pulse for 10% 10000 Mw solution

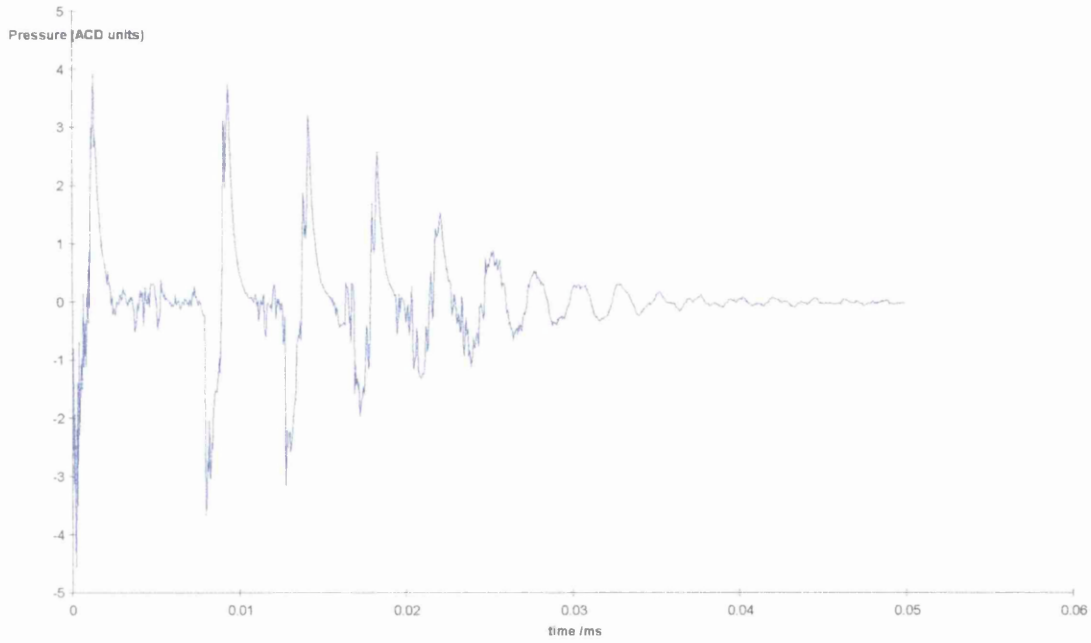


Figure A.23 Pressure-Tension cycle for a 200 psi static pulse for 10% 10000 Mw solution

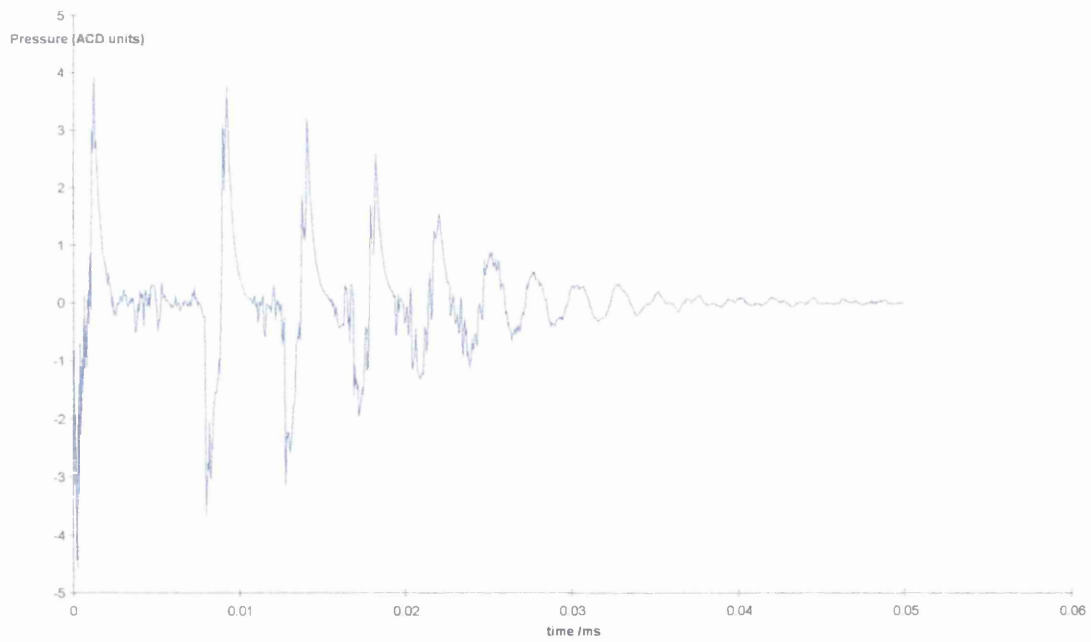


Figure A.24 Pressure-Tension cycle for a 250 psi static pulse for 10% 10000 Mw solution

APPENDIX B

Additional filament breakup images

Figures B.1 to B.6 are for 600 Mw PEG solutions.

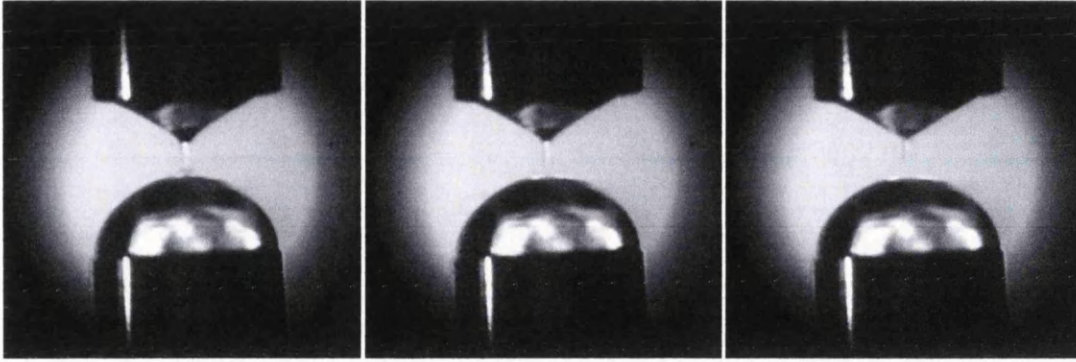


Figure B.1 600 Mw PEG solutions 0.5% concentration

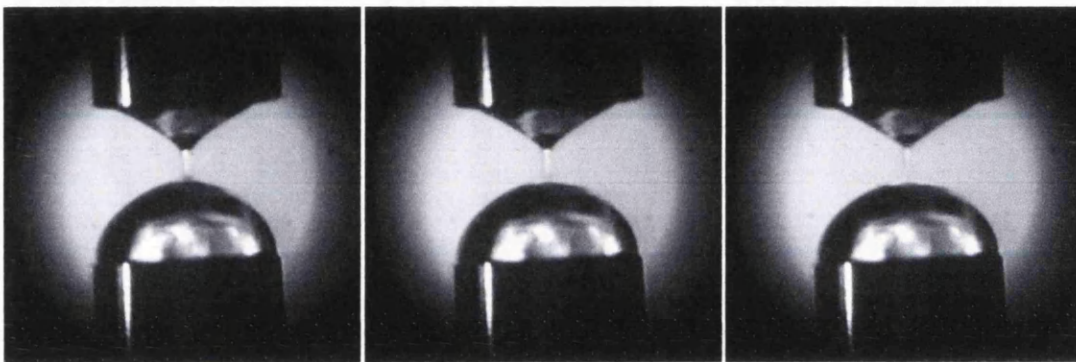


Figure B.2 600 Mw PEG solutions 1% concentration

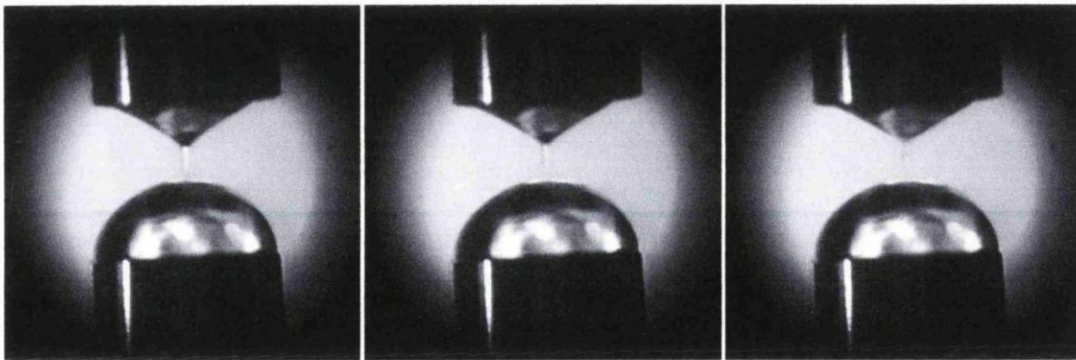


Figure B.3 600 Mw PEG solutions 2% concentration

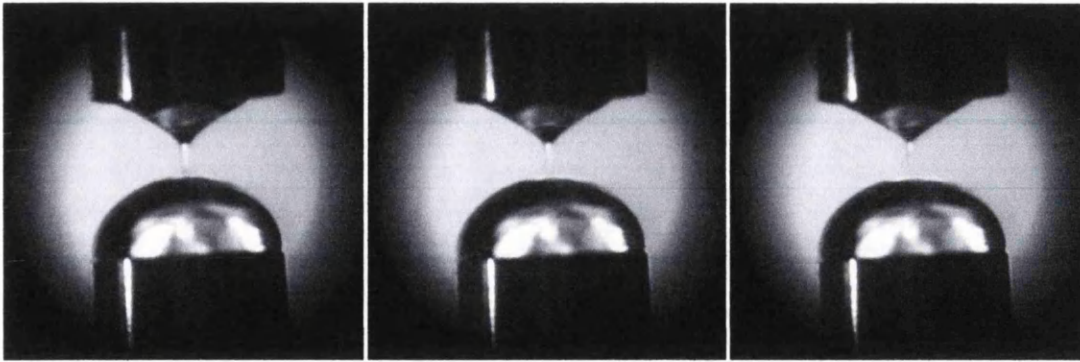


Figure B.4 600 Mw PEG solutions 4% concentration

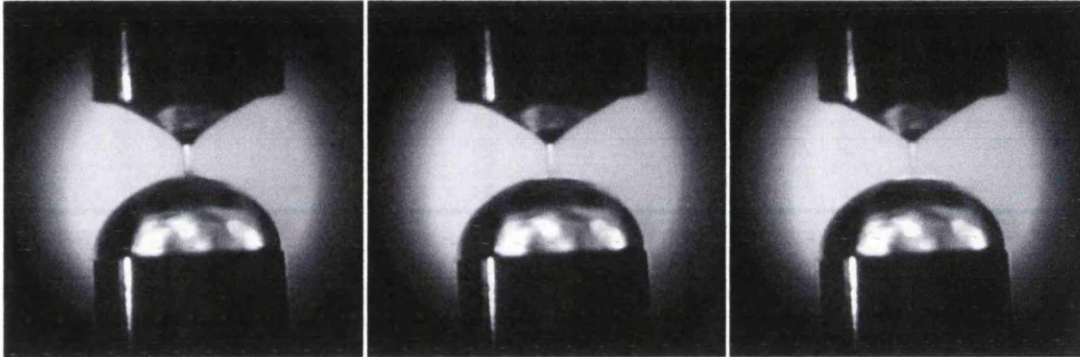


Figure B.5 600 Mw PEG solutions 8% concentration

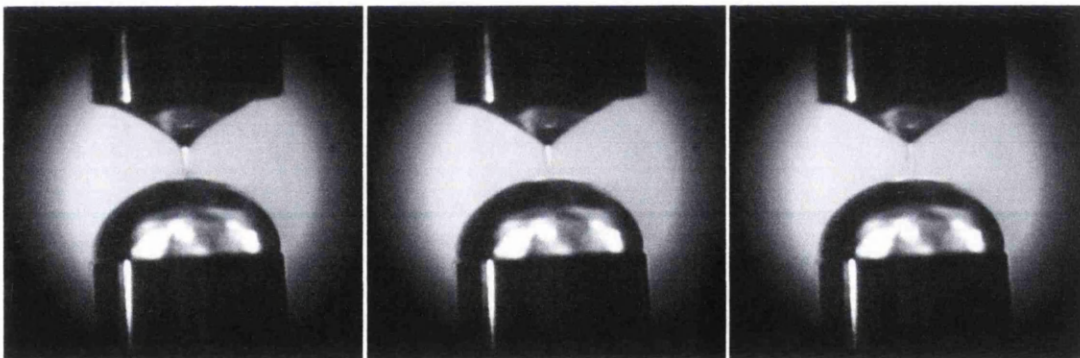


Figure B.6 600 Mw PEG solutions 16% concentration

Figures B.7 to B.12 are for 1500 Mw PEG solutions.

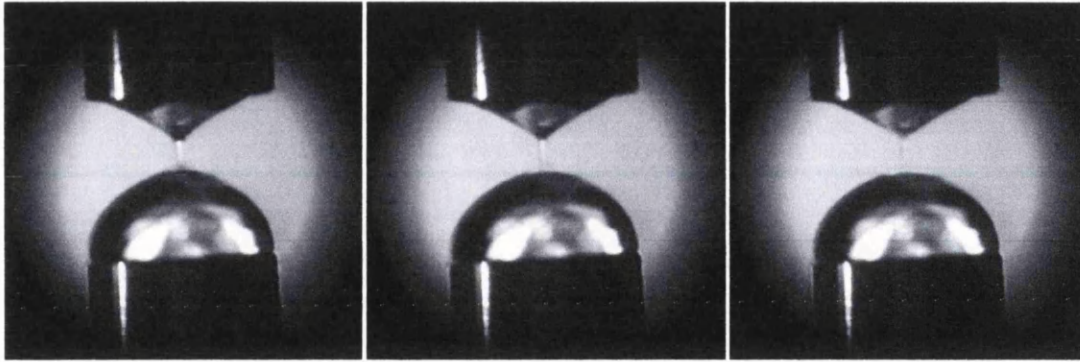


Figure B.7 1500 Mw PEG solutions 0.5% concentration

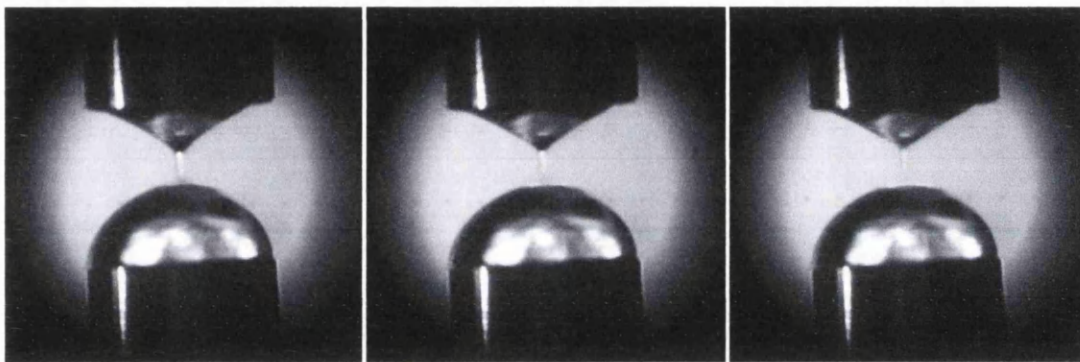


Figure B.8 1500 Mw PEG solutions 1% concentration

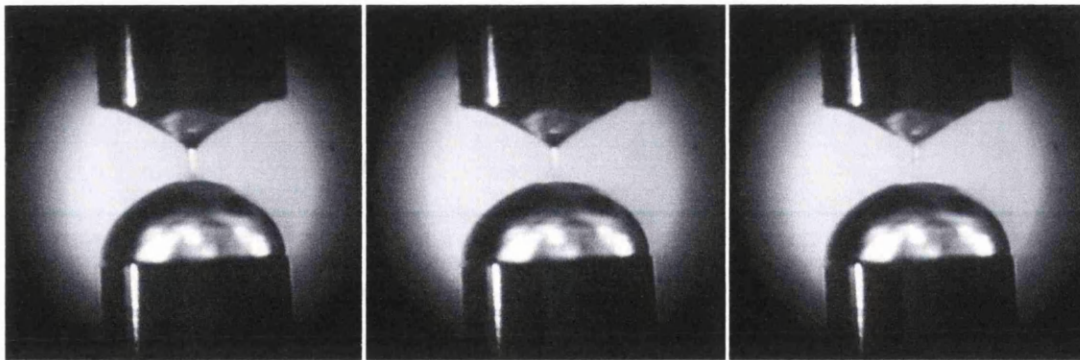


Figure B.9 1500 Mw PEG solutions 2% concentration

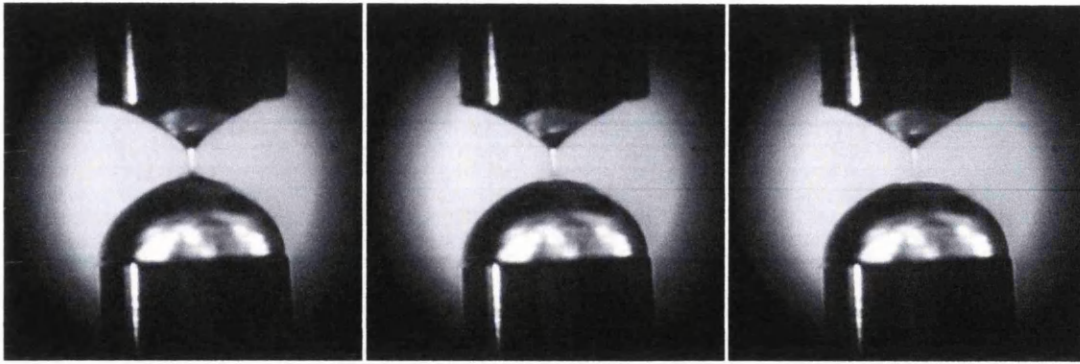


Figure B.10 1500 Mw PEG solutions 4% concentration

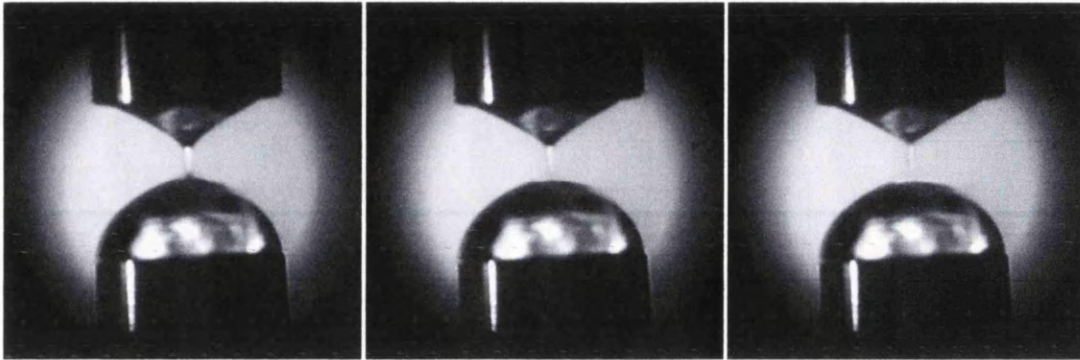


Figure B.11 1500 Mw PEG solutions 8% concentration

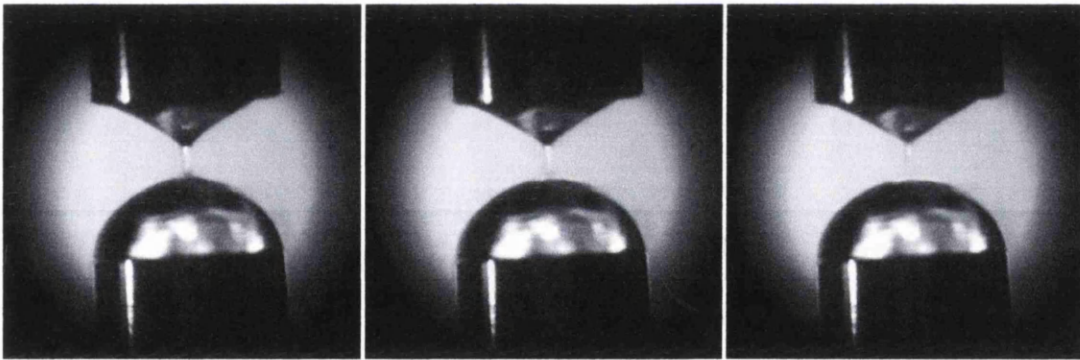


Figure B.12 1500 Mw PEG solutions 16% concentration

Figures B.13 to B.18 are for 6000 Mw PEG solutions.

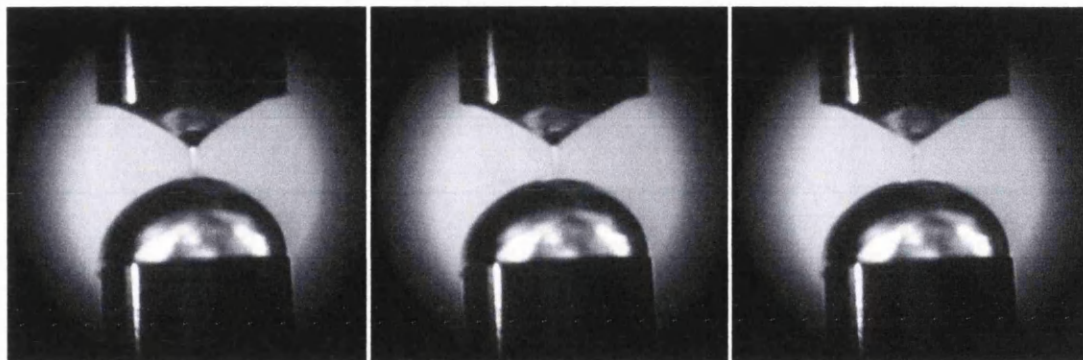


Figure B.13 6000 Mw PEG solutions 0.5% concentration

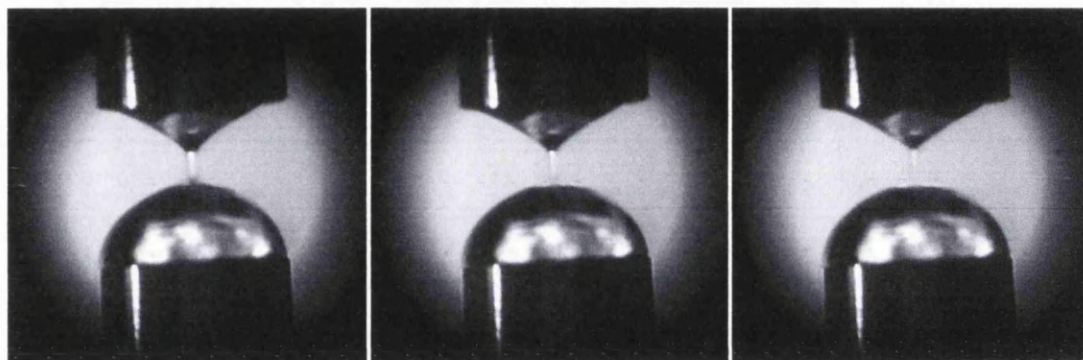


Figure B.14 6000 Mw PEG solutions 1% concentration

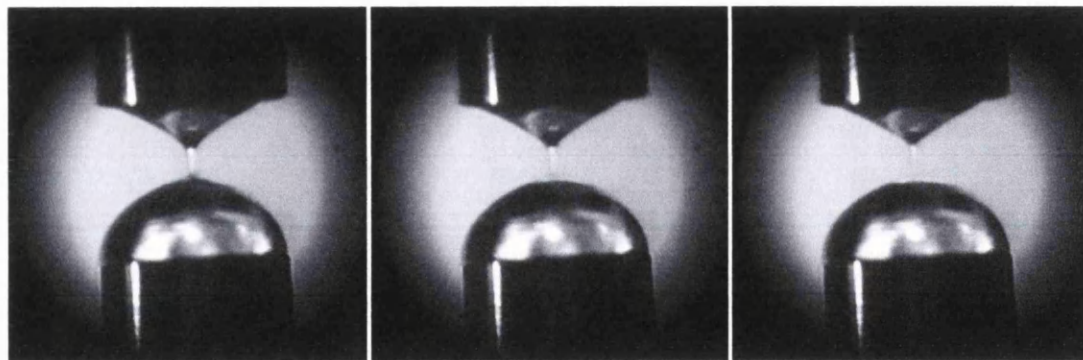


Figure B.15 6000 Mw PEG solutions 2% concentration

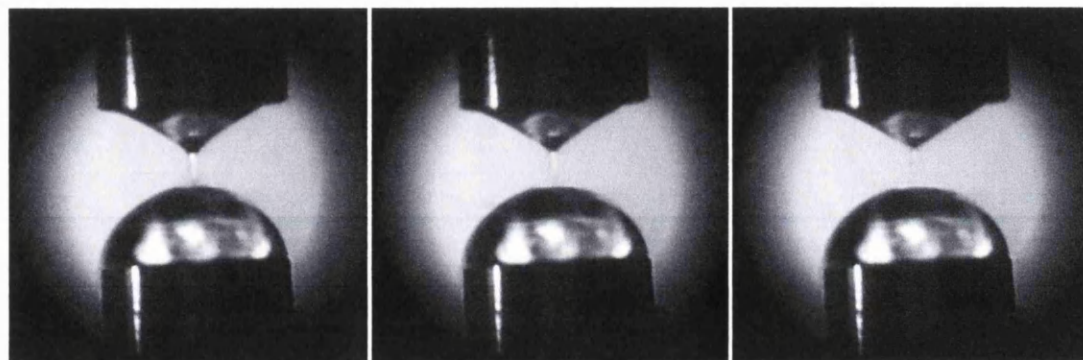


Figure B.16 6000 Mw PEG solutions 4% concentration

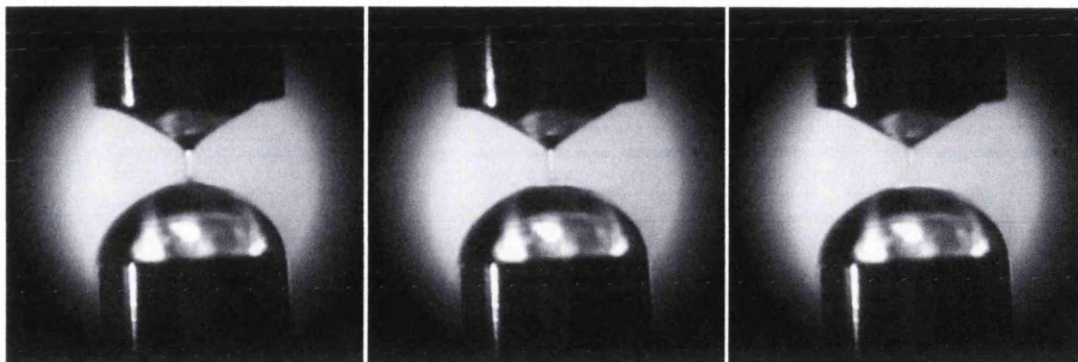


Figure B.17 6000 Mw PEG solutions 8% concentration

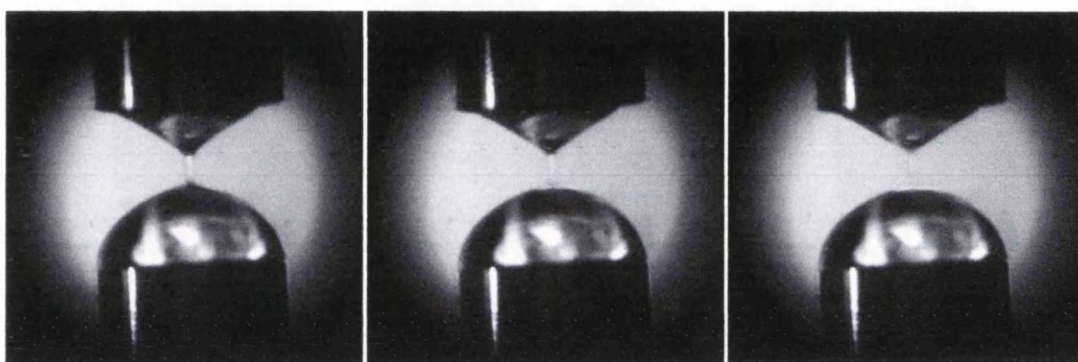


Figure B.18 6000 Mw PEG solutions 16% concentration

Figures B.19 to B.24 are for 10000 Mw PEG solutions.

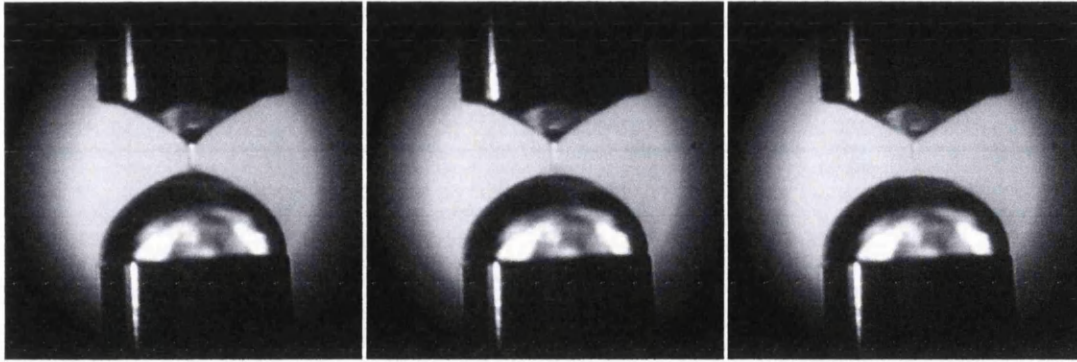


Figure B.19 10000 Mw PEG solutions 0.5% concentration

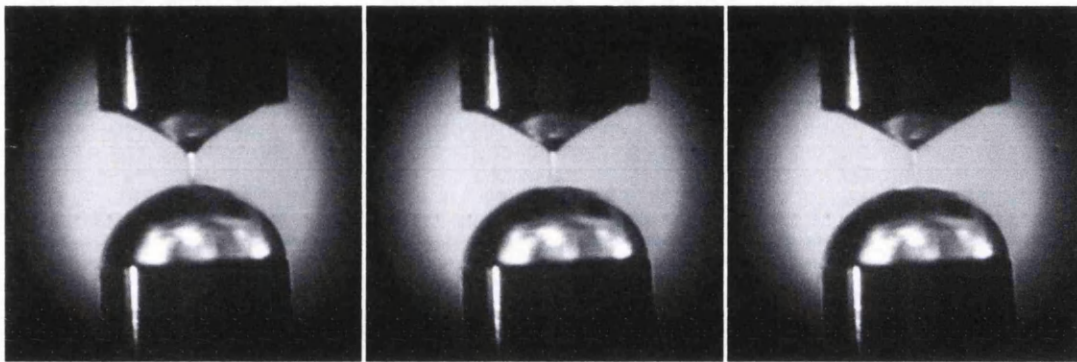


Figure B.20 10000 Mw PEG solutions 1% concentration

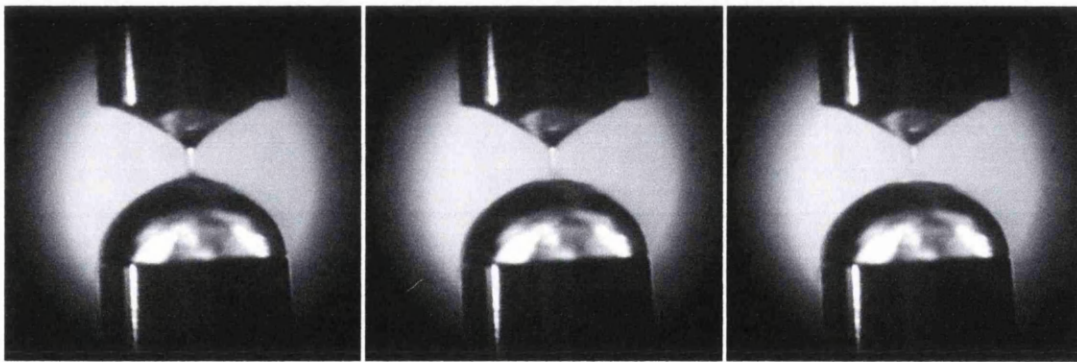


Figure B.21 10000 Mw PEG solutions 2% concentration

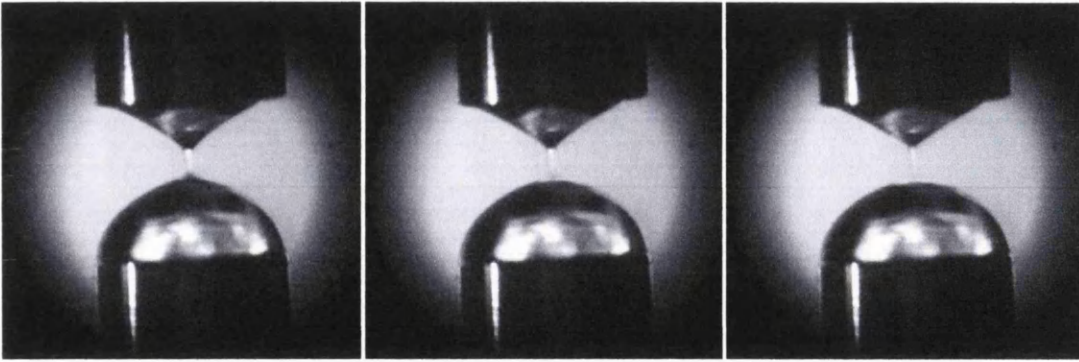


Figure B.22 10000 Mw PEG solutions 4% concentration

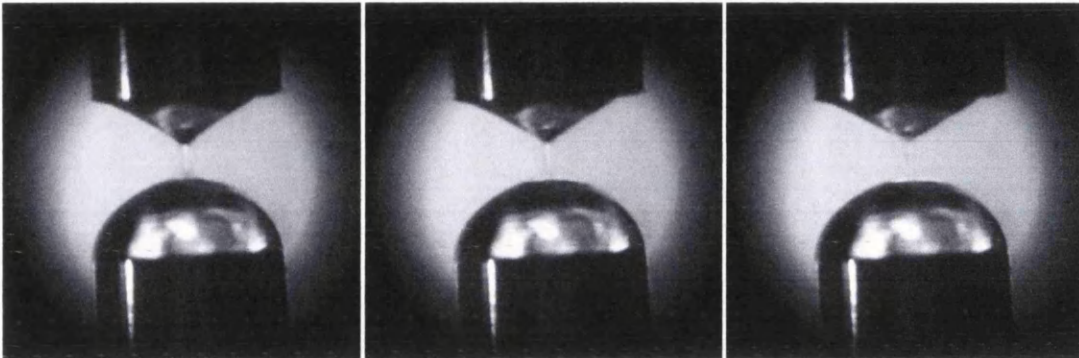


Figure B.23 10000 Mw PEG solutions 8% concentration

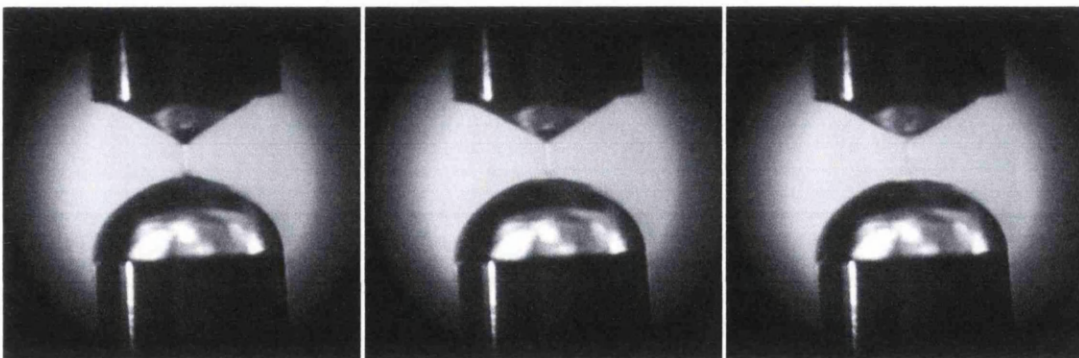


Figure B.24 10000 Mw PEG solutions 16% concentration

Figures B.25 to B.30 are for 20000 Mw PEG solutions.

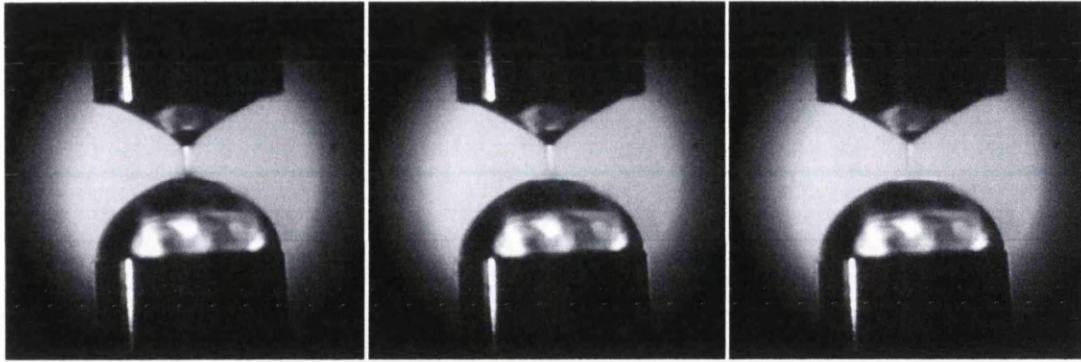


Figure B.25 20000 Mw PEG solutions 0.5% concentration

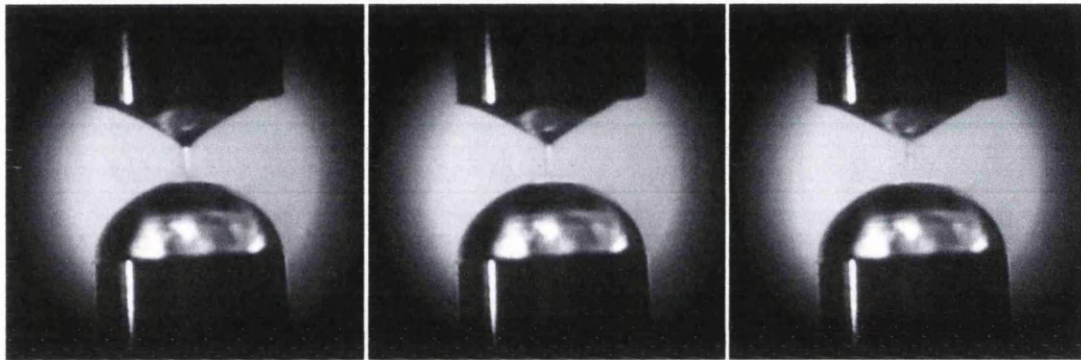


Figure B.26 20000 Mw PEG solutions 1% concentration

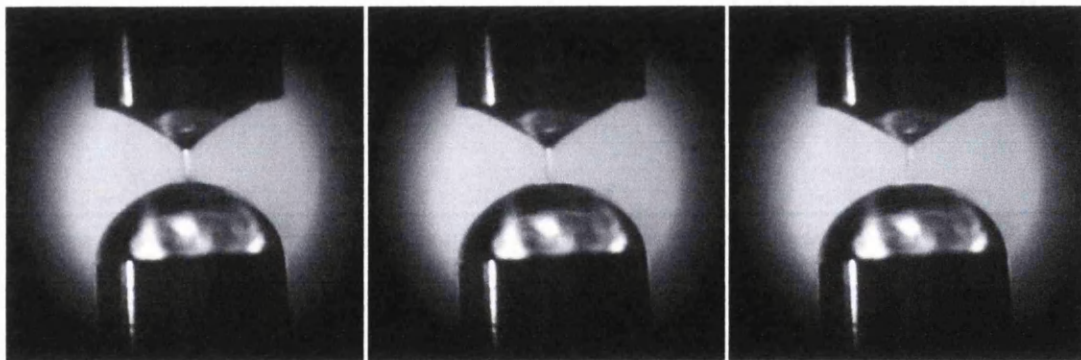


Figure B.27 20000 Mw PEG solutions 2% concentration

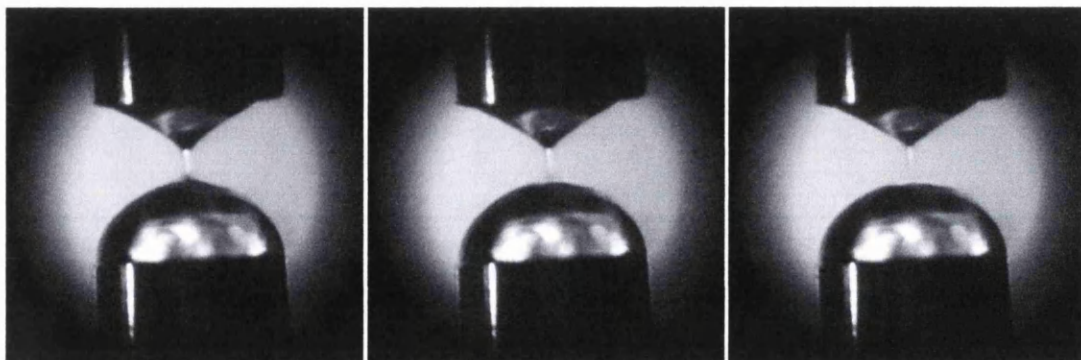


Figure B.28 20000 Mw PEG solutions 4% concentration

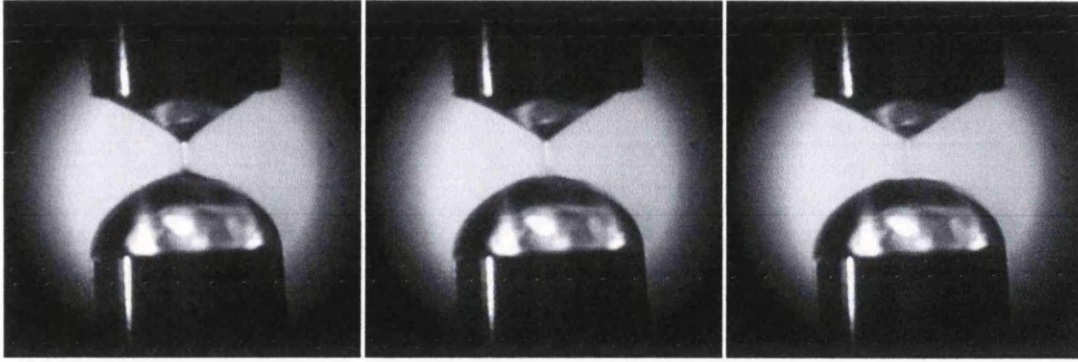


Figure B.29 20000 Mw PEG solutions 8% concentration

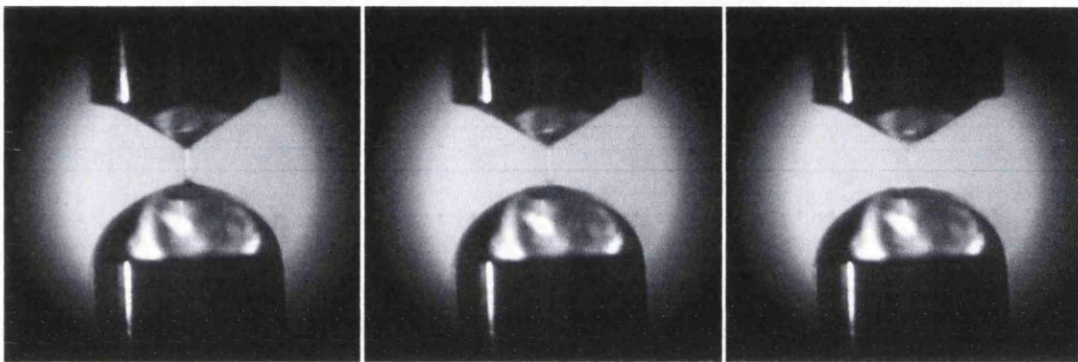


Figure B.30 20000 Mw PEG solutions 16% concentration